University of Naples Federico II

Impact of atmospheric emissions from ships in port on urban areas

by

Domenico Toscano

PhD Program in "Industrial Product and Process Engineering" – XXXIII Cycle

Department of Chemical, Materials and Production Engineering (DICMaPI)

Commitee

Prof. Fabio Murena

Prof. Pietro Salizzoni

Dr. Alberto Martilli

Coordinator

Prof. Andrea d'Anna

Abstract

Maritime transport, despite is one of the most efficient modes of transport, causes several major environmental problems, particularly about air pollution. Furthermore, due to the growth of the shipping activities, its environmental impact will be more relevant in the future. Because of the current environmental issues, the legislation on shipping emissions is frequently updated and becomes more and more stringent. Several policies were issued in the last decades, mainly focused on reducing the content of sulfur in marine fuels. The last international IMO-2020 regulation was enforced on 1 January 2020, it limits the sulfur content of any fuel oil used on board ships at a maximum of 0.50% m/m (mass by mass) outside emission control areas (ECAs) and 0.1% inside ECAs. Since 1 January 2021, in the Baltic and North Sea a nitrogen emission control area (NECA) was applied, requiring the ships built after 2021 operating in this area must respect a mandatory Tier 3 standard (80% reduction compare to Tier 1). The establishment of ECAs has become an important measure to reduce and control ship emissions. Even though, in-port emissions account for a relatively small proportion of the total emissions due to shipping, they can represent a significant impact on the health of population living in port cities and coastal areas. To accurately quantify the risk associated with atmospheric emissions of ships when in-port and the potential benefits of control measures, it is necessary to improve the state-of-art of both the estimation of emissions and the performance of atmospheric dispersion models.

The aim of this thesis is to assess the impact of ship emissions in the port of Naples in 2018 by the development of a bottom-up procedure improving the state-of-art of present methodologies. Pollutants considered are NOx, SO_2 and PM10. The developed methodology can be applied to any port.

The first issue analysed in this thesis is the validation and the optimization of CALPUFF model when used to simulate the dispersion of the ship emissions in a port. With this aim wind tunnel tests and Computational Fluid Dynamics (CFD) numerical simulations were used to model the dispersion of atmospheric emissions of cruise ships at hoteling in the port of Naples. A part of the Naples urban area large about 1.2 km^2 was reproduced at a scale of 1:500 for the wind tunnel experiments. The worst, but

very frequent, emission scenario with three cruise ships emitting at the same time and wind blowing from the south-east with a speed at funnel height of 3 m/s in neutral stability conditions of the atmospheric boundary layer was studied. Two different values UR=1 and UR=4 of the ratio funnel gas velocity/wind speed were considered. In the wind tunnel experiments, Ethane was used as the tracer gas and its concentration was measured at 35 receptor points inside the urban area and at different heights. The dispersion of ship emissions in the same area was also studied by CFD simulations using steady-state solutions of the RANS equations with a k-ω shear-stress transport (SST) turbulence model. A very good agreement between wind tunnel and CFD results is observed. The same simulations were then performed with CALPUFF. The results were used to analyse the accuracy of the predictions of the dispersion model CALPUFF. The effect of two CALPUFF model options was studied: the building downwash module and the parameterisation of the dispersion coefficients. The CALPUFF results are less accurate than the CFD simulations and show a general tendency to underestimate the experimental data. However, the optimization process improves the performance of CALPUFF. A more comprehensive analysis of the effect of a varying UR in the range 0.25 – 16 was also undertaken using numerical models.

The second step was the creation of a comprehensive global data base of all ships visiting the port of Naples in 2018. Using AIS data a data base containing the main information of more than 900 ships (category, name, IMO number, gross tonnage, deadweight; length, width, draft, total power installed onboard and the type of engines; maximum speed; the number of passengers, cars, containers) was created. All ships were lumped in 45 categories and five macro-categories (Commercial, Fishery, Passenger, Tanker, and Other). To fill the missing data, regressions based on real data for each category were adopted.

Once created this "static" database, AIS data were processed through a MATLAB code which is able to identify the phase of ships on the basis of the analysis of the temporal data, of the time delta between records, and of the speed data. The phases defined are as follows: entry to the port, navigation in the port, the start, stop, and end phases of mooring at the quay, exit from the port, and engine start and stop. In this way at each AIS record is associated a specific activity-phase of the ship.

Once all this information was completed, emission rates of NOx, SO_2, and PM were calculated. Great accuracy was applied to the evaluation of the real power of main engines starting from the average speeds when ships are moving in port with respect to that using the typical load factors corresponding to the cruise phase. Similar accuracy was also applied to the evaluation of the total power of auxiliary engines both during the navigation and hoteling phases. The reference adopted is the recent EMEP/EEA guideline using specific emission factors defined for each category of ships and activity phase.

AIS data were also used to identify in and out routes and mooring piers for each ship category. For the sake of simplicity piers and routes were merged when very close each other.

In parallel to this approach, typical of bottom-up procedures, a statistical study based on data from 38 ports all over the world in 45 annualities was performed with the aim to correlate emissions with traffic data per year. Traffic data considered are: number of passengers, hours spent in each phase, number of calls for passenger ships; and tons of good, hours spent in each phase and number of calls for commercial ships. The correlation with traffic data gives the possibility of an easy check of the emissions estimated but show, as expected, a certain degree of uncertainty.

Once verified and optimized the accuracy of CALPUFFF simulations, the complete emission inventory developed for the port of Naples was used as input to CALPUFF together with meteorological data. The results of simulations were compared with data from fixed monitoring stations in the urban area both as annual average and percentile. In this way the impact of ship emissions on air quality in Naples in 2018 was assessed.

The research provides at the same time useful insights on the contribution of ship emissions to air pollution in Naples and on an accurate procedure to assess the impact of ship emissions in port cities.

Acknowledgements

This thesis is the conclusion of a wonderful journey lasting three years that was the expression of a human and scientific experience by enriched by the encounter with many people. All the people I met during these years have enriched and inspired me. I cannot fail to thank them and all the people who have shared these years and this research project with me.

First, I would like to thank my supervisor Prof. Fabio Murena. He has been a great mentor to me. I want to thank him for encouraging my research and for allowing me to grow as a researcher. I am thankful to him for giving me constant inspiration and excellent guidance, which have immensely helped me in completing this research work.

I would like to express my sincere gratitude to Professor Pietro Salizzoni and Dr. Alberto Martilli, who kindly accepted role of examiner, and I 'm deeply indebted to them for the time spent reviewing the dissertation.

I would also like to say a thank you to Dr Benedetto Mele, for his insightful advice and much appreciated help with CFD model.

I want to thank ENEA members and in particular, Dr.ssa Grazia Fattoruso for enriched my passion for scientific research.

Very special thanks should go to my girlfriend, Roberta. She has always encouraged and supporting me spiritually throughout during these three years (and not only!). And a very special thanks to her family.

My appreciation also goes out to my family for their encouragement and support all through my studies.

At last, but not least, I want to thank myself.

Collaborations

During these three years I have collaborated with different teams, some of which are fundamental for the drafting of this thesis.

I wish to thank these people separately.

I want to acknowledge the very much appreciated help of the staff and researchers at LMFA. My sincere thanks goes to Professor Pietro Salizzoni, who provided me an opportunity to join their team during my research visit, and who gave access to the laboratory and research facilities. I would like to express my gratitude to Horacio Correia that helping me in the assembly the Naples port in Wind tunnel and I wish to thank Massimo Marro for his precious help and support of him during experimental measurements. Without they precious support it would not be possible to conduct the experimental part of this research.

I would like to thank Professor Franco Quaranta and Eng. Luigia Mocerino for their precious contribution and for their collaboration in the processing of AIS data and in the development of the part relating to the estimation of ship emissions.

Table of Contents

List of Figures

List of Tables

1 The aim and Outline of dissertation

The ultimate goal of the doctoral thesis is to provide an estimate of the impact of the emissions of ships in transit in the port on the quality of the air in the metropolitan area of Naples, with a calendar year as a reference time, in particular 2018.

Achieving this goal requires an advancement with respect to the current state of the art of scientific research regarding:

[1] reliability of the models to simulate the dispersion of atmospheric pollutants in an area characterized by the presence of buildings, which alter the field of motion of the wind and therefore the dispersion of pollutants.

[2] accurate estimation of the emissions into the atmosphere of the various types of ships, both passenger and commercial, during the various phases of activity in the port.

The work is structured in three phases.

The aim of the first phase is the validation of CALPUFF model that will be used for the impact study of ship emissions in the port of Naples in 2018. The experimental activity was carried out at the Ecole Centrale de Lyon (ECL) under the supervision of Prof. Pietro Salizzoni. Experimental tests of the atmospheric dispersion of ship emissions were carried out in the wind tunnel of the fluid mechanics and acoustics laboratory of ECL. A 1:500 scale model of the urban area of Naples was created and a significant emission scenario was selected. Then experimental results are compared with results of simulation obtained by a CFD model and CALPUFF. In this way the optimal CALPUFF configuration and its reliability are assessed.

The aim of the second phase is the development of a bottom-up methodology, starting from the AIS data of the year 2018, to evaluate the quantities of air pollutants emitted by ships in port. Great accuracy was dedicated to the minimization of missing data about ship traffic and on the identification of exact engine loads for the calculation of emission factors.

Finally, in the third phase, CALPUFF model was used to study the dispersion of pollutants in the atmosphere and the impact on the urban area of Naples. The results

obtained were compared with data from fixed monitoring stations to assess the contribution of ship emissions to air quality.

The thesis is structured into six chapters. The Chapter 2 provides an introduction of the maritime sector, the environmental regulation of this field, the main pollutants emitted by shipping sector, their impact on human health and the legislation of air quality. Finally, in this chapter a description of the area study was reported. In chapter 3 the validation and optimization of CALPUFF model by comparison with wind tunnel and CFD results is described. In chapter 4 a detailed global inventory of ship emissions of the Naples port in 2018 using AIS data and a statistical study based on data from literature review is presented. Chapter 5 shows the dispersion modelling outcomes using CALPUFF. Chapter 6 summarises the findings of this research. The future directions are also proposed.

2. Introduction

The maritime sector is becoming a more and more important role in the transport of goods and persons all over the world. In fact, over 80 per cent of global trade by volume and more than 70 per cent of its value being carried on board ships and handled by seaports worldwide (UNCTAD, 2017). On 1st January 2018, the world commercial fleet comprised 94,171 ships, with a combined tonnage of 1.92 billion dwt (dead weight tonnage). Dry bulk carriers represent the largest share in tons of dead weight and most of the total load capacity, at 42.5%, followed by tankers, which carry crude oil and its products (29.2%), and container ships (13.1%). Moreover, projections of world seaborne trade for the medium term also point to continued expansion, with volumes growing at an estimated compound annual growth rate of 3.2 per cent up to 2022 (UNCTAD, 2017). Therefore, the size of the ships for new deliveries continued to be greater than the existing fleet. A similar situation is also observed for passenger traffic recording maximum growth rate at 2.2% in 2017, (UNCTAD, 2018). In particular, cruise sector is characterized by a continuous growth for over three decades (Pallis and Vaggelas, 2018). In 2017, the number of passengers of cruise ships around the world were 24 million. This number will likely increase to 25 million by 2019, and 30 million by 2024 (Peisley, 2014). Together with the growth of maritime traffic the attention toward the effect of ships on the environment is rising. The impact of ship emissions on air quality has different aspects. It can be studied on a global or local scale. The effect on the global scale depends mainly on emissions during navigation between ports, while the local effects depend mainly on emission in ports or in their proximity. Emissions of CO_2 contribute significantly to the global warming effect while emissions of NOx, SOx, PM and VOCs impact mainly on human health of port cities. With respect to the global warming problem emissions of carbon dioxide due to maritime transport are estimated around 1 billion tons per year, and the contribution of global greenhouse gas emissions are about 2.5 per cent of the fuel combustion sector (UNCTAD, 2017; Smith et al., 2015). H. Liu et al. (2016a) estimate for East Asia that 16% of global CO_2 emissions are due to maritime transport. Very high is also the contribution of ship sector to anthropogenic emissions: NOx (15%) and SOx (5–8%) (Eyring et al., 2005; Corbett et al., 2007) on a global scale. With reference to East Asia the contribution is 9% (NOx) and 5% (SOx) (H. Liu et al., 2016a). About 70% of ship

emissions are estimated to occur within 400 km of land (Endresen et al., 2003). On local scale, Zhao et al. (2013) report that ship emissions are responsible for 4.23% of the total PM2.5 concentration in Shangai. For the same port Z. Liu et al. (2016) indicate that ships can contribute to 20–30% of the total PM2.5 but only during ship-plume-influenced periods, and about 11% at 10 km from the coastline. By 2050, depending on future economic growth and energy developments, shipping emissions may increase by between 50 and 250 per cent (Smith et al., 2015). By 2050, depending on future economic growth and energy developments, shipping emissions may increase by between 50 and 250 per cent (Smith et al., 2015). This increment is not compatible with the imperative in reducing worldwide emissions to limit the global average temperature increase. For this reason, environmental sustainability in maritime transport is an imperative of the 2030 Agenda for Sustainable Development (UNCTAD, 2017).

2.1 IMO Regulation

IMO was born in 1948 by a convention signed during an international conference in Geneva with the original name Inter-Governmental Maritime Consultative Organisation (IMCO), then modified definitively in 1982. The IMO Convention entered into force in 1958 and the new Organization met for the first time in the 1959. The purposes of the Organization are 5, as summarized by Article 1(a) of the Convention. The two most important are:

- to provide machinery for cooperation among Governments in the field of governmental regulation and practices relating to technical matters of all kinds affecting shipping engaged in international trade.
- to encourage and facilitate the general adoption of the highest practicable standards in matters concerning maritime safety, efficiency of navigation and prevention and control of marine pollution from ships.

The first task of IMO achieved in 1960 was to adopt a new version of the International Convention for the Safety of Life at Sea (SOLAS), the most important of all treaties dealing with maritime safety. Then IMO turned its attention to a new problem began to emerge - pollution. At this aim the first and most important of measures was the International Convention for the Prevention of Pollution from Ships, 1973, as modified by the Protocol of 1978 relating there to (MARPOL 73/78).

It covers not only accidental and operational oil pollution but also pollution by chemicals, goods in packaged form, sewage, garbage and air pollution. On 2 October 1983 the IMO adopted the International Convention for the Prevention of Pollution from Ships (MARPOL - MARine POLlution) initially with Annexes I and II, then adding a new Protocol (Annex VI) in 1997. It has been reviewed and updated by amendments over the years. At the present form, it includes six technical Annexes, among which Annex I and II are compulsory. Following the detailed list of the Annexes is reported:

- Annex I – Regulation for the Prevention of Pollution by Oil
- Annex II – Regulation for the Control of Pollution by Noxious Liquid Substances in Bulk

- Annex III – Prevention of Pollution by Harmful Substances Carried by Sea in Packaged Form
- Annex IV – Prevention of Pollution by Sewage from Ships
- Annex V – Prevention of Pollution by Garbage from Ships
- Annex VI – Prevention of Air Pollution from Ships.

The Annex VI entered in force 19th May 2005, ratified by 75 States and revised in July 2005. The revision of the Annex VI was adopted in October 2008 and entered in force in July 2010 focusing on modification of Regulation 12, 13 and 14. The current version of Annex VI comprises five chapters within which there are 26 regulations arranged that control and limit the following main areas (IMO, 2017):

- Emissions of ODS from refrigeration plants and firefighting equipment (regulation 12)
- NOx emissions from marine diesel engines (regulation 13)
- SOx emissions from ships (regulation 14)
- VOC emissions from oil tankers cargo tanks (regulation 15)
- Shipboard incinerators emissions (regulation 16)
- Marine fuels quality (regulation 18)
- Energy efficiency of ships (chapter 4)

Regulation 13 limits NOx emissions from all medium diesel engines (MDEs) which are installed on ships constructed, on or after the 1 January 2000. It also applies to engines of the same power which are subject to "major conversion" on or after 1 January 2000 (IMO, 2017). The Protocol of 1997 introduced initial NOx emission control levels in 2005 which were applicable to engines installed on the afore mentioned ships built before 1 January 2000. The revision of Annex VI in 2008 significantly tightened the NOx emissions allowed by introducing two additional limits of control which apply to MDEs installed on newer ships. These levels of control, known as Tiers, are based on a ship's construction date while the NOx emissions limits, expressed in g/kWh, depend on an engine's rated speed. The current IMO limits for all engines constructed on or after 2011 are expressed by Tier II, while Tier III standard is for new engines built since 2016 entering in any NECAs (NOx

Emission Control Areas). The latter standard reduces NOx emissions of 80% compared to Tier I limit. However, if a country proposes for an ECA, Tier III will be applied only to ships build after the date of the adoption of the ECA designation by IMO. Finally, NOx emissions from older engines (constructed before 2011) have to meet the Tier I standard. Therefore, the operation of each MDE to which regulation 13 applies is prohibited, except when the engine NOx emissions are within the Tier limits as presented in Table 1 which illustrates NOx emission limits at different engine speeds.

Table 1 . MARPOL Annex VI NOx emission limits value

Tier	**Date of construction of ships**	**NOx emission limit value (g/kWh)**		
		n < 130	n = 130 -1999	n ≥ 2000
I	1 January 2000	17.0	$45 \cdot n^{-0.2}$	9.8
II	1 January 2011	14.4	$44 \cdot n^{-0.23}$	7.7
III	1 January 2016* 1 January 2021**	3.4	$9 \cdot n^{-0.2}$	2.0

*ships operating in the North American or the US Caribbean ECA; ** ships operating in the Baltic Sea or the North Sea ECA

Regulation 14 of Annex VI controls the SOx and PM emissions from ships and apply to all MFOs used on board ships. The sulfur content limits allowed in MFOs, expressed as a percentage of the mass fraction (% m/m), have been progressively reduced over recent years. The current regulation 14 defines the maximum sulfur content allowed in MFOs used on board ships globally and further tightens these limits in designated ECAs, as shown in Table 2 which also includes the dates when the sulfur limit provisions came or are coming into force (IMO, 2017). The implementation day for the global 0.50% m/m sulfur limit will be 1 January 2020, as per the MEPC.280(70) resolution which was adopted on 28 October 2016.

Table 2. Evolution in IMO SOx limits in fuel oil

Global sulfur limits	**ECAs sulfur limits**
4.50% m/m *prior to* 1 January 2012	1.50% m/m *prior to* 1 July 2010
3.50% m/m *on and after* 1 January 2012	1.00% m/m *on and after* 1 July 2010
0.50% m/m *on and after* 1 January 2020	0.10% m/m *on and after* 1 January 2015

An ECA is a specific sea area, including port areas, designated by the IMO in accordance with criteria and procedures set forth in appendix III to Annex VI, in which more stringent emission regulations have been established. For the purpose of regulation 13 Tier III emission standards and regulation 14 requirements on SOx emissions limits, there are currently four designated ECAs, as presented in Table 3 and Figure 1 which includes adoption, enforcement and effective from dates. The Baltic Sea ECA is defined in MARPOL Annex I, while the North Sea ECA is defined in Annex V. The North American and US Caribbean Sea ECA are detailed in appendix VII to Annex VI. As is apparent from Table 3, the North American and US Caribbean Sea ECAs cover SOx and PM while European ECAs relate only to SOx emissions. While SOx restrictions are already applicable in all ECAs for all ships, a NOx ECA Tier III standard applies only on new ships built on or after Annex VI defined dates as indicated in Table 3. The latest resolution related to the ECAs was the MEPC.286(71) which was adopted on 7 July 2017 and which designated the Baltic Sea and the North Sea ECAs for NOx Tier III control.

Table 3. MARPOL Annex VI ECAs with indication of adoption, entry into force and date of taking effect (source: ww.imo.org).

ECAs	**Controlled pollutants**	**Adopted by IMO**	**Entry into force**	**Effective from**
Baltic Sea Area	SOx	26/09/1997	19/05/2005	19/05/2006
	NOx	07/07/2017	01/01/2019	01/01/2021*
North Sea area	SOx	22/07/2005	22/11/2006	22/11/2007
	NOx	07/07/2017	01/01/2019	01/01/2021*
	SOx; PM	26/03/2010	01/08/2011	01/08/2012

North American Sea area	NOx	26/03/2010	01/08/2011	01/01/2016*
US Caribbean Sea area	SOx; PM	26/07/2011	01/01/2013	01/01/2014
	NOx	26/07/2011	01/01/2013	01/01/2016*

*In effect for NOx Tier III compliant ships built on or after this date

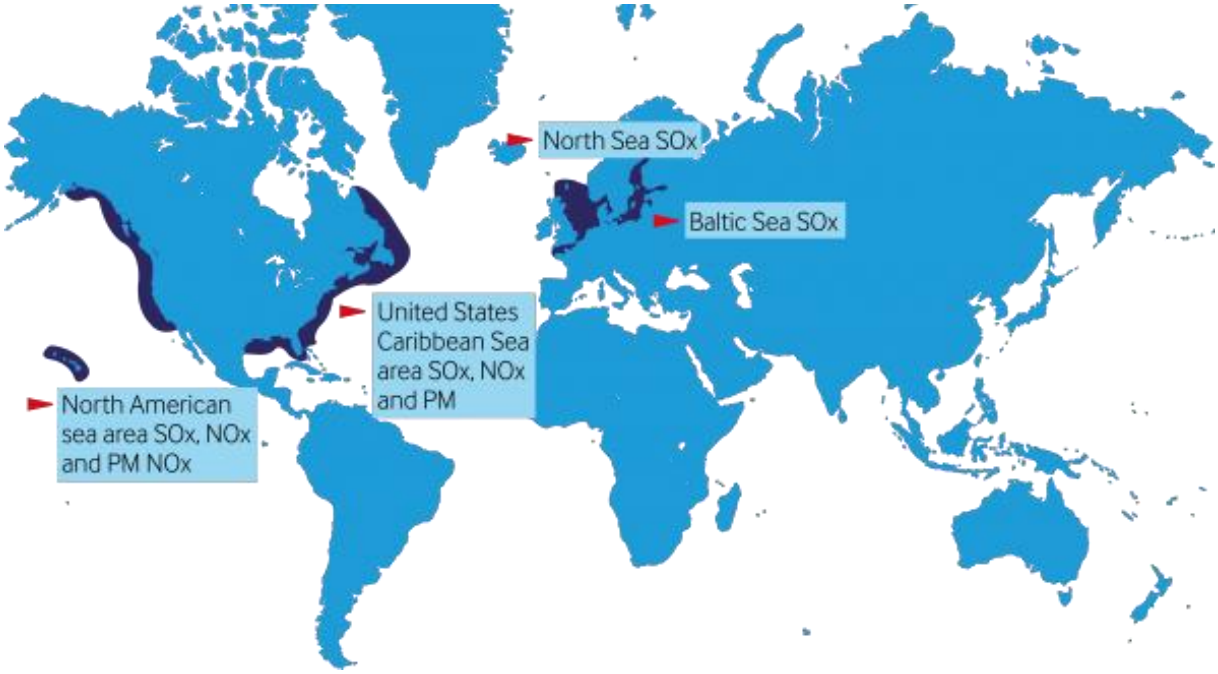

Figure 1. Geographical distribution of the ECAs in the world[1]

[1] (https://www.shipownersclub.com/louise-hall-sulphur-requirements-imo-emission-control-areas/).

2.2 Air pollutant

Air pollutants can be classified in several ways. A first classification method concerns their physical state and consists in dividing the pollutants into:

- gaseous substances (such as gases and vapours).
- substances in suspension or particulate in solid or liquid state.

With reference to the source of emission of pollutants, these can be:

- natural origin, emitted from sources not correlated by human activities (volcanoes, oceans, natural processes).
- anthropogenic origin, emitted by sources related to human activities (transport, industry, energy conversion, etc.).

Substances can also be classified according to their genesis:

- primary pollutants emitted directly from the sources.
- secondary pollutants, which are formed in the atmosphere as a result of chemical reactions between primary pollutants and other substances normally present in the air.

Shipping is a significant atmospheric source of aerosol particles (particulate matter, PM10, PM2.5) and gaseous pollutants (SO_2, NOx, VOCs, COx), especially near harbours and in coastal areas. In particular, NOx, PM and SO_2 are the common pollutants emitted by ships that determine an important impact on local air quality, close to harbours and downwind of them.

2.2.1 Nitrogen oxides

Nitrogen oxides are compounds generated by the oxidation of nitrogen and include different compounds, the most important are NO and NO_2. NOx formation mechanisms are closely related to combustion. There are 3 mechanisms that are responsible for NOx formation: i) Thermal NOx; ii) Prompt NOx and iv) Fuel NOx.

The Thermal NOx mechanism was developed by Zeldovich in 1946 and represents the NO formation mechanism that occurs in the combustion zone. Nitric oxide is formed by direct oxidation between oxygen and nitrogen both present directly from the air. This mechanism is activated when the Temperature is very high (T > 1800 K) and

depend on the residence time, that is, how long the nitrogen is in the reaction zone. The reaction occurs with the presence of intermediate reactions which therefore form intermediate products, which involve the presence of radicals. The radicals are O, N, OH and H, which are found in the combustion area. These radicals also attack nitrogen molecules.

The second mechanism is called NOx Prompt. According to this mechanism, NO is formed by oxidation of nitrogen in the air, therefore oxidation of N_2 by oxygen, but in this case, it is not a direct oxidation, but the reaction is activated by radical species that are generated by the presence of carbonaceous species present in the reaction environment. The mechanism starts from the interaction between a nitrogen molecule and the CH radical (formed by interaction of the carbonaceous fuel), this is a highly reactive radical that attacks N_2 forms hydrogen cyanide HCN which is a nitrogen radical and at this point the nitrogen radical, which is unstable, which attacks molecular oxygen and oxidizes forming NO and an O radical.

The third mechanism depends on the nitrogen chemically bonded to the fuel and is called Fuel NOx. When these fuels are fed into the combustion zone and are therefore brought to a high temperature, they begin to decompose forming nitrogenous substances. The intermediates can follow two reactive pathways, the first is oxidation i.e. react with O_2 and form NO (unwanted path), the second is a reduction reaction in the nitrogen compounds react with N to form N_2 this is a preferential path because this allows to form a molecule that is not harmful that can be safely released into the atmosphere.

2.2.2 Sulfur oxides

The sulfur oxides are product by the combustion of materials containing sulfur. This process will produce particular types oxides: sulfur dioxide (SO_2) and sulfur trioxide (SO_3). The main features of these two compounds indicated with general term of SOx are the absence of colour, the pungent smell and the high reactivity of SO_3. Basically, the equilibrium conditions for the formation are never reached, and the concentration of SO_3 remains low. Moreover, SO_3 gas may be present in the air only if the concentration of water vapor is low. Otherwise, the SO_3 tends to combine with water vapor leading to the formation of droplets of sulfuric acid. This conversion is

influenced by many factors including humidity, the intensity, duration and the spectral distribution of sunlight, the presence of larger or smaller amounts of catalyst materials, absorbent and alkaline.

2.2.3 Particulate matter

"Particulate matter" or PM is a complex mixture of particles and liquid droplets. According to their forming process, airborne particles can be classified as primary or secondary aerosols. Primary aerosols are emitted directly from the emission sources into the atmosphere in particulate form. Whereas secondary aerosols refer to particles generated in the atmosphere, formed by the conversion mode gas-particle due to the condensation of natural and anthropogenic vapours, or generated by the evolution of a primary particle. Primary PM sources are derived from both human (anthropogenic) and natural (nonanthropogenic or biogenic) activities. Secondary PM sources directly emit air contaminants into the atmosphere that form or help form PM. Natural sources are mainly sea salt, soil erosion, volcanic eruptions, wildfires and biogenic sources. Anthropogenic emissions of primary particles result mainly from the transportation sector (cars, trains, ships, and aircraft), industrial waste (metallurgy, foundries, refineries, and mining), petroleum products (housing, industrial, commercial), incineration sites and agricultural activities.

2.3. Impact on human health

In according to the World Health Organization air pollution is the largest environmental risk in Europe (WHO, 2014, 2018a; GBD, 2016). The World Health Organization (WHO) estimates that air pollution, both environmental and domestic, causes 7 million deaths per year, 5.6 million deaths from noncommunicable diseases and 1.5 million from pneumonia and 3% of cardiorespiratory mortality. Nine out of ten people in the world are exposed to levels of air pollution that are dangerous to health, and for this reason "in 2019, air pollution is considered by the WHO to be the greatest environmental risk to health". It is also estimated that 90% of premature deaths per year due to air pollution are concentrated in middle and low-income countries. The most common reasons for the premature deaths caused by air pollution are heart disease and stroke followed by lung diseases and lung cancer (WHO, 2018b). The assessment of the impact of air pollution on human health has been performed by many studies (Hoek et al., 2013, Cohen et al., 2017, Bloemsma et al., 2019; Dobaradaran et al., 2016; Hadei et al., 2020; Khaefi et al., 2017; Klepac et al., 2018; Sówka et al., 2019). The effects of air pollution on human health can be chronic (long-term) or acute (short-term). Chronic effects occur after prolonged exposure and they are: cardiovascular and pulmonary diseases, respiratory diseases, chronic changes in physiological functions, lung cancer, chronic cardiovascular diseases and intrauterine growth restrictions. Acute effects, due to short-term exposure (hours or days) to high concentrations of pollutants, are: respiratory and cardiovascular problems, physiological changes. Moreover, acute effects can induce oxidative stress, which in turn can damage the respiratory system and reducing resistance to viral and bacterial infections (Ciencewicki and Jaspers, 2007). Maternal exposure to ambient air pollution is associated with adverse impacts on fertility, pregnancy, new-borns and children (WHO, 2005, 2013a). There is also emerging evidence that exposure to air pollution is associated with diabetes in adults and it may be linked to obesity, systemic inflammation, Alzheimer's disease and dementia (RCP, 2016; WHO, 2016).

Many studies have demonstrated the correlation between ship emissions and health effects (Liu et al., 2016; Anderson et al., 2009; Broome et al., 2016; Corbett et al., 2007; Jonson et al., 2015; Winebrake et al., 2009). Corbett et al., (2007) have estimated about 60,000 annual premature deaths in 2010 and 90,000 annual premature deaths in

2012 due to cardiopulmonary diseases and lung cancer attributed to exposure to PM emissions in coastal regions of Europe, eastern Asia and southern Asia. In Europe and in the Baltic North Sea, Andersson et al. (2009) and Brandt et al. (2013) have estimated 50,000 and 14,000 annual premature deaths in 2011. In East Asia 24,000 premature deaths were estimated as due to PM2.5 related to shipping (Liu et al., 2016). In Mediterranean area, Viana et al., (2020) have conducted a health assessment study in eight coastal cities and they reported 430 premature death per year attributable to ship-related PM2.5 exposure.

As demonstrated by these studies the impact of ship emission on human health is not negligible. It is expected a reduction of the impact on the health effect consequently to the sticter IMO regulations. Contini and Merico (2021) reviewed some studies to evaluate the effectiveness of the stricter ECA regulation on the health effect. They found a globally reduction in premature death by 34% (range 18-49%) and in the morbidity of childhood asthma will be reduced by approximately of 54% (range 24-68%) (Sofiev et al., 2018). Furthermore, in the Baltic and North Sea areas, there will be a reduction in the impact of PM2.5 by 35% and 40% respectively (Jonson et al., 2015; Barregård et al., 2019). A 15% reduction in premature deaths attributable to PM2.5 (both primary and secondary PM2.5) will be observed for the Mediterranean region (Viana et al., 2020).

2.4 Italian air quality legislation

In order to protect human health, air quality legislation and guidelines should be developed. The first Italian law on air pollution, which identifies air as a legal asset to be protected, is the Law of 13 July 1966, no. 615 "Measures against atmospheric pollution". This law was replaced by the Decree of the President of the Republic (DPR) n. 203 of May 24, 1988, which implemented four European directives on pollution and air quality. The subsequent Presidential Decree 203/88 can be considered the basis of the Italian legislation on air pollution until the implementation in 1999 of the European framework directive on "Air quality assessment and management". The DPR introduced the concept of environmental protection alongside that of human health, absent in the previous legislation. In addition, it introduced limit values and guide values for air quality. In 1996, Directive 96/62/EC on the assessment and management of air quality was issued in Europe which aims to define a common strategy aimed at establishing air quality standards such as to prevent or reduce the harmful effects of pollutants on human health and the environment. The directive sets out general and common policies on air quality assessment and management, identifies the fundamental actions that member states must implement. It was followed by other directives that set the concentration limits in the air and the methods of measurement for the various pollutants. In Italy, the framework directive was implemented with Legislative Decree no. 351 "Implementation of Directive 96/62/EC on the assessment and management of ambient air quality". Legislative Decree 351/99 establishes the powers of the State and Regions. The Regions must deal with the assessment of air quality and the implementation of action plans (areas at risk of being exceeded), remediation plans (areas with levels higher than the limit values) and maintenance plans (areas with levels below the limit), while the State must establish the limit values and target quality values to be achieved, thus implementing air quality management through integrated planning throughout the national territory. The daughter directives of 96/62 / EC have been implemented by other regulations, such as:

- Ministerial Decree 2 April 2002, n. 60 of the Ministry of the Environment and Land Protection, for the transposition of the first daughter directive, relating to NOx, SO_2, Pb and PM10 in ambient air, and the second daughter directive, relating to benzene and carbon monoxide;

- Legislative Decree 21 May 2004, n. 183, for the transposition of the third daughter directive relating to ozone in the air.
- Legislative Decree 3 August 2007, n. 152 transposes the 4th daughter directive, concerning the presence of pollutants that pose a risk to human health (such as cadmium, mercury, nickel and polycyclic aromatic hydrocarbons).

Finally, the Legislative Decree 13 August 2010, n. 155 implements the "Directive 2008/50 / EC on ambient air quality and cleaner air in Europe". The decree reorganizes and repeals some previous regulations that governed the matter in a fragmented way and establishes a unitary regulatory framework for the evaluation and management of ambient air quality. Decree 155/2010 identifies four fundamental phases:

- zoning of the area based on emission density, orographic and weather-climatic characteristics, degree of urbanization.
- the detection and monitoring of the level of atmospheric pollution.
- the adoption, in case of exceeding of the limit values, of intervention measures on the emission sources.
- the general improvement of air quality.

Legislative Decree 155/10 establishes limits for the following pollutants: sulfur dioxide, nitrogen dioxide, benzene, carbon monoxide, lead and PM10 PM2.5, ozone, arsenic, cadmium, nickel and benzo (a) pyrene, polycyclic aromatic hydrocarbons.

The limits for sulfur dioxide, nitrogen dioxide, PM10, PM2.5 are summarized in the following table:

Table 4. Limit and target values of selected pollutants for the protection of human health

Pollutant	**Statistical indicator**	**Limit value**
SO_2	1h mean	350 μg/m^3 not to be exceeded more than 24 times a year
	24 h mean	125 μg/m^3 not to be exceeded more than 24 times a year
NO_2	1h mean	200 μg/m^3 not to be exceeded more than 18 times a year
	24h mean	40 μg/m^3
PM10	24 h mean	50 μg/m^3 not to be exceeded more than 35 times a year
	Annual mean	40 μg/m^3
PM2.5	Annual mean	25 μg/m^3

These air quality guidelines can be of vital importance for policy-makers to develop effective air quality strategies.

2.5 Area Description: Naples city

The city of Naples is the capital of Campania region located in the South of Italy (Figure 2). It was founded by the Cumans in the eighth century B.C. and was among the most important cities of Magna Graecia playing a notable commercial, cultural and religious role. After the collapse of the Roman Empire, in the 8th century the city formed an autonomous duchy independent of the Byzantine Empire; later, from the thirteenth century and for more than five hundred years, it was the capital of the Kingdom of Naples; with the Restoration it became the capital of the Kingdom of the Two Sicilies under the Bourbon Kings until the unification of Italy.

Figure 2. Map of Campania region with provinces

The extension of the municipality is 119.02 km^2 with 970.185 residents. With a density of 8.151 inhabitants/km^2 (www.ISTAT.it) Naples is the third most populated city in Italy. More than 3 million people live in the "Metropolitan Area" of Naples in an area of 1171 km^2 with a density of 2649 inhabitants/km^2.

The climate is a typical Mediterranean-type with a mean air temperature of about 17°C, a relative humidity equal to 60% and a mean precipitation equal to 900 mm, concentrated in the period from October to April. The bay of Naples faces the Tyrrhenian Sea and almost the 90% of the precipitation systems move directly from the sea within a sector from southeast to northwest. The summer climate of Naples

is influenced normally by the milder Azzorre anticyclone and, at times, by the hotter African anticyclone.

The city of Naples is the most industrialized area of the Campania region. Data on atmospheric emissions from the national inventory disaggregated at Naples level by ISPRA up to 2015 are reported in Table 5. As shown in Table 5 the main sectors with respect to NOx emissions were: "road transport" and "other mobile sources and machinery" especially maritime activity. The main source of SOx (as sum of SO_2 and SO_3) is the maritime activity. For PM10 and PM2.5 the main sector was "non-industrial combustion plants".

Table 5. Emission inventory of the main pollutant sources in Naples district in 2015 (ISPRA). The most relevant sectors are highlighted using bold characters

SNAP Code	SNAP Description	NOx	SOx	PM10	PM2.5
1	Combustion in the production and trasfrormation energy	0.4%	0.1%	0.0%	0.0%
2	Non- industrial combustion plants	9.2%	18.8%	**77.3%**	**80.0%**
3	Industrial combustion plants	1.5%	14.1%	1.3%	1.2%
4	Industrial processes without combustion	0.0%	0.0%	0.5%	0.3%
5	Extraction and distribution of fossil fuels and geothermal energy	0.0%	0.0%	0.0%	0.0%
6	Use of solvents and other products	0.0%	0.0%	0.0%	0.0%
7	Road transport	**47.8%**	1.1%	11.8%	10.0%
8	Other mobile sources and machinery 8.04 Maritime activity	**33.4%**	**54.9%**	5.2%	5.4%
	Other mobile sources and machinery 8.05 Aviation	5.1%	8.3%	0.2%	0.3%
	Other mobile sources and machinery (rest)	1.8%	0.5%	0.7%	0.8%
9	Waste treatment and disposal	0.1%	1.4%	0.1%	0.1%
10	Agriculture	0.3%	0.0%	0.7%	0.1%
11	Other sources and sinks (nature)	0.4%	0.8%	2.2%	1.9%

As evident, one of the most important sources in city of Naples is the maritime sector. The port of Naples occupies the northernmost natural inlet of the Gulf of Naples and extends for about 12 km, from the city centre towards its eastern part. It is one of the most important in Italy and the Mediterranean (Mocerino and Rizzuto, 2019a). In fact, in 2015 it ranked 12th among the busiest European ports

in terms of passenger numbers, while the 2017 figures place it in 35th place worldwide for tourist cruises. In 2019 the port was confirmed third in Italy (after Civitavecchia and Venice) for cruise traffic with 8 milions of passengers, while the commercial traffic was of about 2×10^7 tons of goods. While excluding the data up to May 2020, altered by the pandemic on a global scale, the statistics show how the role of the port has grown over the years. The data updated to 2019, compared to those of 2018, show for commercial traffic an increase of + 16.9% in the number of TEUs (681,929), + 4.39% in the tons of cargo transported by liquid bulk and a limited -2.63% for the tons of cargo transported by the solid bulk carriers; regarding passengers traffic + 26.90% (1,356,320) in the number of cruise passengers and + 1.25% (6,851,448) in the number of passengers arriving on ferries and small boats (< 20 nm).

Map of Naples and its port is reported in Figure 3 with the indication of docks for the various ship categories. From West to East there are terminals for hydrofoils and small ferries connecting the islands in the gulf of Naples (blue area in Figure 3), cruise ships (red area in Figure 3), ferry boats (yellow are in Figure 3), and finally commercial ships (green area in Figure 3).

Figure 3. Map of the port of Naples with berthing areas.

3. Validation of air quality models

In order to assess the impact on air quality of ship emissions in ports, studies have to date been performed using mainly Gaussian models. Among these Gaussian models, California Puff (CALPUFF) is one of the most used, notably in studies devoted to the assessment of the impact of ship emissions over long time periods (one year or more). Poplawski et al. 2011, estimated the impact of cruise ship emissions in James Bay (Victoria, Canada) and they showed that cruise ships could contribute up to 57% of the maximum 1-h concentration of NO_2 and up to 84% of the maximum daily concentration of SO_2 at about 500 m downwind of the mooring. Murena et al., 2018, focused on the port of Naples and showed that ship emissions contributed significantly to hourly peak concentrations. In fact, the contribution to the 99th percentile of 1-hour NO_2 concentrations can reach 86.2% during the high season (June-September). Lonati et al., 2010, instead evaluated the impact on local air quality due to the atmospheric emissions of a new port in the Mediterranean Sea.

A major limitation in the use of Gaussian models in the built environment near a port is related to their failure to properly model the influence of buildings on the dispersion process. In fact, dispersion in urban areas is strongly influenced by interactions between the atmospheric flow and the buildings, which gives rise to a wide variety of dispersion patterns, i.e. enhanced dispersion in the wake of a building, the trapping of pollutants in street canyons, the channelling of pollutants along canyon axes, and mixing and dispersion within street intersections.

As is well known, all these phenomena are not properly taken into account within Gaussian dispersion models such as CALPUFF and evaluating their role in the dispersion process requires the adoption of a more complex modelling approach using Computational Fluid Dynamics (CFD). However, each modelling approach has distinct features and advantages and should be properly used. Current consensus is that both physical and numerical approaches are useful; they should be complementary in their advantages and limitations, thereby reducing the inaccuracy in the results of a single-approach method (Tominaga and Stathopoulos, 2016).

A suitable assessment of ship emissions on urban air quality has to be performed over a time period covering at least a whole year. Despite enhanced computer

performance, this kind of analysis cannot be reasonably performed by means of CFD numerical simulations; therefore, the only practical solution is to use operational Gaussian models or lagrangian particle models. But to overcome the limits of operational models some specific CFD simulations, performed in significant operating conditions, can be run to optimize the use of the operational models.

The aim of this chapter is a detailed analysis of the reliability of an operational dispersion model (CALPUFF) as a tool to assess the impact of ship emissions on the air quality of port cities. To that end, wind tunnel and CFD simulations have been performed to obtain a rich dataset of (time-averaged) concentration fields, as induced in specific scenarios of ship emissions. The comparison of the results of these two models have admitted us to validate the CFD model. Then CALPUFF results were validated in the same emissive scenarios. Once CFD model was validated, it is possible to extend the validation of CALPUFF not only at emissive scenarios tested with both WT and CFD models but also in other emissive scenarios simulated only with CFD.

3.1. Urban area model

Cruise ships make port at "Stazione Marittima" terminal including several berths; the terminal is only within 200 m of the nearest residential buildings (Figure 5). To define the emissive scenario in this study, the year 2016 have been considered. In this year, the fleet of cruise ships visiting the port of Naples is composed of 73 ships. The cruise ships arrive/departure calendar was examined with the aim to evaluate the number of hours during which one or more cruise ships were at berth. The most frequent figure (1184 hours in the year) corresponds to the presence of a single cruise ship at berth C (Murena et al., 2018a), however the simultaneous presence of three cruise ships (A+B+C) is also quite frequent (284 hours per year). A wind rose graph (Figure 4) shows the frequency of wind direction and speed in 2016.

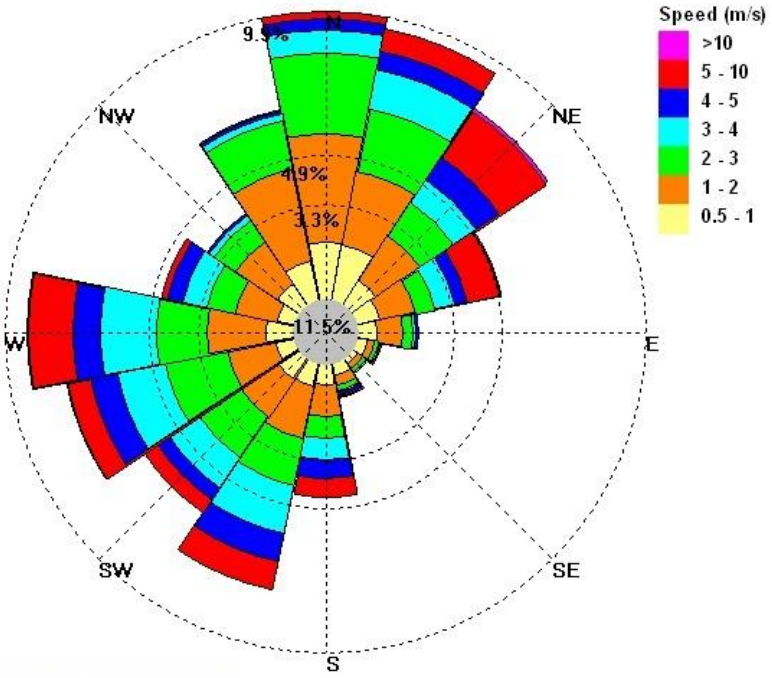

Figure 4. Wind rose of meteorological file at h = 10 m in 2016

The most critical emissive scenario was then selected: presence of three cruise ships at berths A, B and C; wind blowing from SE (the urban area is downwind in NW direction to the cruise berths). To evaluate emission rates of atmospheric pollutants the three cruise ships simultaneously present at berth have been selected among those with the most frequent simultaneous presence in the port of Naples. The SO_2

emission rates Q_{SO_2} (Table 1) have been calculated as the product of emission factors multiplied for the power applied in the hoteling phase by each ship (EEA, 2017). The Sulfur content in fuel was assumed at 0.1% weight in consequence of a deliberation of the Port Authority of Naples.

Figure 5. Map of Naples with the locations of sampling points in the wind tunnel experiments

3.2. Wind tunnel experiments and numerical simulation by CFD and CALPUFF models

The approach relies on performing reduced scale experiments of the pollutant dispersion in the port of Naples which are then used as a reference to evaluate the accuracy of the output of two different numerical models, i.e. Reynolds Averaged Navier Stokes (RANS) simulations and CALPUFF.

The wind tunnel experiments be assumed as representative of the 'real' dispersion phenomena occurring at the full scale, as far as flow field reproduced in the wind tunnel is similar to that driving the dispersion in the real-world scenarios we aim at simulating.

The similarity between the wind tunnel flows and the real atmospheric flows in the port of Naples relies on two conditions. Firstly, the flow in the wind tunnel experiments is fully turbulent, with a Reynolds number $Re \propto 10^5$, i.e. so large that the dynamics of the flow can be assumed to be in the asymptotic condition $Re \to \infty$ (and therefore similar to the real flows for which we have $Re \propto 10^7$). Secondly, the approaching wind field is shaped as a neutral atmospheric boundary layer, having a depth which is an order of magnitude larger than the size of the buildings. This allows us to reproduce the separations of scales, between the larger atmospheric eddies and the shear induced eddies produced by building wakes, that characterises urban atmospheric flows.

Once set these conditions ensuring the dynamical similarity, the wind tunnel can be simply transposed at the real scale by adopting proper scales length and velocity scales.

Concerning the results of the numerical models, it is worth remembering that the parametrisations adopted in both RANS and CALPUFF simulation do assume that the flow is fully turbulent ($Re \to \infty$) and therefore any possible influence of Reynolds number variation on the model outputs is precluded.

3.2.1 Wind tunnel

Wind tunnel experiments using a reduced-scale physical model of the port of Naples were performed, within which three cruise ships, and the surrounding urban district have been placed. The urban area modelled covers approximately 1.2 km^2 and the model scale is 1/500. The geometric parameters for each cruise ship, namely the funnel height from sea level H_f and the funnel diameter D_f, were therefore scaled by a factor of 1/500 in the wind tunnel test (see Figure 6). The ratio wind velocities in the reduced scale model are instead assumed to be the same as those at the real scale.

The experiments were performed in the atmospheric wind tunnel of the Laboratoire de Mécanique des Fluides et d'Acoustique at the Ecole Centrale de Lyon in France. This is a recirculating wind tunnel with a working section measuring 14 m long, 3.7 m wide, and 2.2 m high. The air temperature in the wind tunnel is regulated so that any variation can be kept in the range ±0.5°C.

A neutrally stratified boundary layer was generated by combining the effect of roughness elements on the ground and a row of spires (with a height H = 0.5 m, spaced by a distance H/2) placed at the beginning of the test section (Irwin, 1981; Nironi et al., 2015). The wind tunnel floor was overlain with metal nuts of height h = 0.005 m to simulate the effect of sea waves on the wind as a distributed surface roughness. The nuts were placed in a staggered array and covered approximately 1.8 % of the tunnel floor surface. This experimental set-up allowed us to reproduce a boundary layer of depth $\delta = 0.8$ m. Imposing a free-stream velocity $U_\infty = 5$ m s^{-1}, the Reynolds number $Re = \delta U_\infty/\nu \approx 2.6 \times 10^5$ ($\nu=1.5x10^{-5}$ m^2/s^2 is the kinematic viscosity of air) was sufficiently high to ensure the simulation of a fully turbulent flow (Jiménez, 2004). The resulting flow field is similar to that well documented by Nironi et al. (2015) and represents a neutral atmospheric boundary layer.

Ethane (C_2H_6), used as a passive tracer as its density is similar to that of air, was continuously released from the funnels of the ships. The flow control system at the source was composed of two lines, ethane and air, each of them equipped with a mass flow controller. The two lines then converged through a valve and the ethane-air mixture was directed to the source. The volume flow Q_{tot} was kept constant in

order that the ratio of the emission velocity and the wind velocity at the funnel height was equal to 1 or 4 (depending on the experimental set-up). The ethane-air mixture was released at ambient temperature. Therefore, in this study we do not consider the buoyancy effect that is considered a minor one in ship emissions dispersion (Menter and Egorov, 2010).

The comparison between wind tunnel and real operating condition of cruise ships A, B, C (Figure 1) in terms of emission flow rate (Q_r), funnel height (H_r), funnel diameter (D_r) and emission velocities at funnel height (U_r) are reported in Table 6.

To study the effect of the ratio of UR (funnel gas velocity/wind speed at funnel height) two different exit gas speed at funnel height were imposed (both in wind tunnel and simulation models) to obtain as operating condition UR = 1 or UR = 4. Correspondingly, the emission rate was varied in wind tunnel experiments. This is the reason of the double values reported in Table 6 in the columns of Q_{WT} and U_r.

Table 6. Main parameters of the wind tunnel experiments and the real scenarios.

	Wind tunnel				**Real case**			
Cruise ship	Q_{WT} (L/s) UR1/UR4	H_{WT} (mm)	D_{WT} (mm)	U_{WT} (m/s)	Q_r (L/s) UR1/UR4	H_r (m)	D_r (m)	U_r (m/s)
A	$1.23 \cdot 10^{-2}$/$4.92 \cdot 10^{-2}$	60	2.2	3.2	0.28/1.12	30	1.1 m	3.2
B	$1.30 \cdot 10^{-2}$/$5.17 \cdot 10^{-2}$	80	2.2	3.4	0.73/2.92	40	1.1 m	3.4
C	$1.30 \cdot 10^{-2}$/$5.17 \cdot 10^{-2}$	80	2.2	3.4	0.75/3.00	40	1.1 m	3.4

For clarity, in the rest of the chapter pollutant concertation at the real full scale, i.e. as induced by SO_2 ship emission will be compared. To perform this conversion, it has been taken into account that i) a 1/500 ratio between the length scales and that ii) all concentrations are directly proportional to the flux of pollutant imposed at the source due to the linearity of the advection-diffusion equation. The real scale SO_2 concentrations C_r, expressed in parts per million [ppm], are then computed as:

$$C_r = C_{WT} * \frac{Q_r}{Q_{WT}} * \left(\frac{D_{WT}}{D_r}\right)^2 * \frac{U_{WT}}{U_r} \quad (1)$$

where $C_{WT}[ppm]$ are wind tunnel (Ethane) concentrations, Q_r is the real emission rate [l/s] of SO_2 emitted by cruise ships, Q_{WT} is the Ethane emission rate [l/s] in the wind tunnel experiments, D_{WT}/D_r = 1/500 is the ratio of funnel diameters (wind tunnel/ real funnel) and U_{WT}/U_r = 1 is the ratio of emission velocities at funnel height.

A hot wire constant temperature anemometer equipped with an X-wire probe with a velocity-vector acceptance angle of 45°, allowing for the simultaneous measurements of two velocity components has been used. Calibration was carried out in the wind tunnel using a Pitot tube to measure a reference velocity. The probe was not calibrated in yaw. In order to decompose the calibration velocities from the X-probe into the longitudinal and transversal velocity components (Jorgensen, 2002), a yaw correction with constant coefficients $k_{12}=k_{22}=0.0225$ has been adopted. The sampling frequency was 5000 Hz and the experimental error, estimated by repeating the measurements in a fixed reference location, was approximately ±2 % for the mean and the standard deviation (Nironi et al., 2015).

Concentration measurements were performed with a Flame Ionization Detector (FID) (Fackrell, 1980) with a sampling tube 0.3 m long, permitting a frequency response of the instrument to about 400 Hz. The vertical profiles of the mean concentration at various positions were collected and an averaging time of about 60 seconds allowing stable values to be obtained was imposed.

The calibration was carried out using ethane-air mixtures with concentrations equal to 0, 500, 1000 and 5000 ppm. Calibration was performed twice a day, as long as the flame temperature of the FID (which was continuously monitored) was constant. When the flame temperature showed variations of more than 2°C (from its value at the beginning of the experiment), calibration was repeated. The relationship between ethane concentration and tension response was linear, with a

slope (representing the sensitivity of the instrument) whose variations could reach ±3 %, depending on the ambient conditions (Nironi et al., 2015).

Recirculation of air in the wind tunnel implies background concentration increasing with time. To take into account the contribution of this drift, the background concentrations were recorded before and after acquiring any of the concentration time series. The background concentration, which was assumed to evolve linearly with time from its initial to its final value, was then subtracted from the signals (Nironi et al., 2015).

Figure 6. The reduced-scale physical model of the port of Naples realized in the wind tunnel at the Ecole Centrale de Lyon.

3.2.2 CFD model

A CFD model reproducing the shape of the three cruise ships and buildings for a large part of the wind tunnel model was realized. At full scale, the computational domain is 7 km^2 wide and 1 km in height. A multi-block mapped mesh of about 10 million hexahedral cells with refinements at the walls was generated (Figure 7) through an optimization process; indeed, the grid was initially generated by adopting an unstructured approach with tetrahedral cells and prism refinement at the walls. Such an approach is particularly useful in the case of complex geometries because it strongly reduces the mesh generation time, however the grid must have a large number of grid points to reach a satisfactory quality. To optimize the number of grid points, the final grid was generated following a structured approach consisting of a fine partitioning of the domain in hexahedral blocks that can be meshed with a mapped scheme.

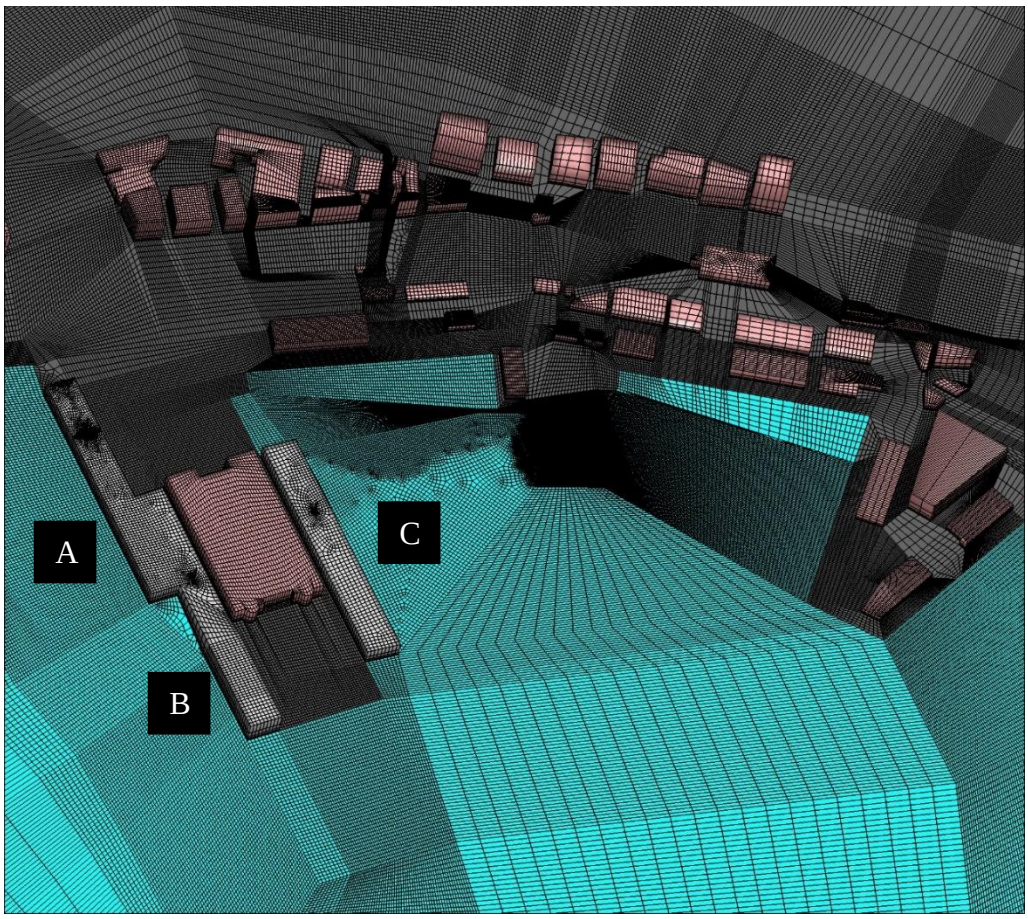

Figure 7. Surface mesh in the buildings and ships zone of the computational domain. A, B, C indicate the three cruise ships (with volumes) at berth.

The computational domain adopted herein is the same as that adopted by Murena et al. (2018a) and Toscano et al. (2019), where the unsteady incompressible formulation of Navier-Stokes equations with species transport (air-SO_2 mixture neglecting chemical reactions) were solved with the Scale Adaptive Simulation (SAS) turbulence closure model (Menter and Egorov, 2010; Murena and Mele, 2014; Murena and Mele, 2016). In this study, instead the steady RANS equations, with a k-ω SST turbulence model were solved. As shown Kulkarni et al., (2006) this approach is well suited to simulate flows induced by smoke emissions from ships. A similar study enlightening the reliability of numerical simulation in reproducing the downwash effect of ship emission was performed using the MITRAS model (Badeke et al., 2020).

The numerical method adopted is pressure-velocity coupled with second-order accurate numerical schemes and Green-Gauss node-based gradient computation, in particular the second-order upwind scheme has been used for the momentum and concentration equations these settings return a highly accurate resolution of the flow field together with an optimal numerical stability and they have been chosen after an optimization phase of the numerical schemes.

A grid convergence study was initially performed using three mesh sizes of 5 million, 10 million and 15 million grid points). Results obtained using the grid with 10 million cells did not show any significant variation compared to those provided by the 15 million grid point mesh. The procedure adopted follows best practice guidelines for the CFD simulations as reported by Tominaga et al., (2008).

In setting the boundary conditions a velocity inlet with a 135° wind direction at the side faces of the computational domain and a pressure outlet at the top were imposed. The inlet vertical profile of the mean longitudinal velocity, imposed with a User Defined Function (UDF), was set to be equal to the income velocity profile measured in the wind tunnel experiments. The boundary condition at the wall for ω is $\omega = \frac{u_\tau^2}{\nu} S_R(k_s^+)$, where u_τ^2 is the friction velocity, ν the kinematic viscosity and S_R is a function of k_s^+ the average height of the sand-grain roughness elements (the equivalent roughness) in wall units. k_s^+ has been set to match the roughness elements of the wind tunnel. Also, the free stream boundary conditions for

turbulence (turbulence intensity and turbulence viscosity ratio) have been set to match the wind tunnel conditions.

3.2.3 CALPUFF model

The CALPUFF modelling system includes three components: a meteorological model (CALMET), the main model that predicts concentrations for a specified average time of at least 1 h (CALPUFF) and a post-processor (CALPOST). CALMET is the diagnostic meteorological model that generates an hourly three-dimensional meteorological field in the gridded modelling domain. The input for the CALMET model includes gridded geophysical parameters, and surface and upper air meteorological and precipitation data. The CALPUFF model is a multi-layer, multi-species non-steady-state puff dispersion model that simulates the effects of time- and space-varying meteorological conditions on pollutant dispersion. CALPUFF simulates a continuous plume as a superposition of puffs of pollutant and evaluates the contribution of a puff to the concentration at a receptor using a "snapshot" approach. Each puff is "frozen" at each sampling step and the concentration due to the puff at that time is computed (or sampled). The puff is then allowed to move, evolving in size, strength, etc., until the next sampling step. The details of the model are given in Scire et al., (2000).

The CALPUFF model calculates the evolution of the puff spread (usually referred to as σ_y and σ_z) as a function of the standard deviations of the lateral and vertical component of the wind velocities, referred to here as σ_v and σ_w, of approximated horizontal and vertical Lagrangian time scales (parameterized). Estimates of horizontal and vertical plume dispersion are provided from turbulence-based dispersion coefficients based on measured or computed coefficients. The model includes several options to compute σ_y and σ_z based on the adoption of: i) direct turbulence measurements, ii) similarity theory, and iii) Pasquill-Gifford (rural) and McElroy-Pooler (urban) coefficients.

In this study how the model results compare to the wind tunnel measurements, adopting options i) and ii) were analysed. With regard to option i), σ_y and σ_z were estimated based on the measurements of σ_v and σ_w in experiments and for option ii), σ_y and σ_z were computed using the relationship presented in Scire et al. (2000).

It is important to note that the CALPUFF procedure internally calculates the surface layer scales based on the mean meteorological fields input, by means of a micrometeorological model (Scire et al., 2000). The well-known Hanna (1984) parameterisation calculates the values of wind standard deviations and Lagrangian time scales as functions of the surface layer scales. These relationships are based on the analysis of data from field experiments (Hanna, 1968; Hanna, 1981), theoretical considerations (Panofsky et al., 1977) and a second-order closure model (Wyngaard et al., 1974). The Hanna (1981) and the CALPUFF parameterisations are similar and differ only in the empirical curves used to estimate the wind velocity standard deviations. Notably, CALPUFF recalculates internally the surface layer scales from the mean fields, thus introducing additional parameterisations.

3.2.4 Statistical analysis for the evaluation of model performance

As customary Chang and Hanna (2004), the agreement between numerical models and experimental data has been evaluated by means of statistical indices: the normalized mean square error (NMSE), the fractional bias (FB), the correlation factor (R) and the fraction of predictions within a factor of two (FAC2). These are defined as:

$$\mathrm{NMSE} = \frac{\overline{\left(C_o - C_p\right)^2}}{\overline{C_o}\,\overline{C_p}}$$

$$\mathrm{FB} = \frac{\left(\overline{C_o} - \overline{C_p}\right)}{0.5\left(\overline{C_o} + \overline{C_p}\right)}$$

$$\mathrm{R} = \frac{\overline{\left(C_o - \overline{C_o}\right)\left(C_p - \overline{C_p}\right)}}{\sigma_o \sigma_p}$$

$$\mathrm{FAC2} = \text{ fraction of data that satisfy } 0.5 \leq \frac{C_p}{C_o} \leq 2$$

where C_p and σ_p are concentration results and the standard deviation of the model, while C_o and σ_o are concentration values and the standard deviation of the experimental results. A perfect model would have a value of 1 for R and FAC2, and a value of 0 for FB and NMSE. FB quantifies the systematic bias while NMSE measures systematic bias and random scatter, providing a balance in evaluating the

quality of numerical results. The FAC2 is highly robust as the effect that outliers have on it is limited. Box and scatter plots are used as tools to analyse the resulting datasets. Chang and Hanna (2004) recommended that the minimum number of observation prediction pairs had to be around 20 for the interpretation of confidence limits to be statistically meaningful. In an urban area the criteria for « good » model performance as reported in Hanna and Chang (2012) are: $\mathrm{NMSE} \leq 6; \mathrm{FAC2} \geq 0.3; |\mathrm{FB}| \leq 0.67$.

3.3. Model validation

In WT experiments 35 receptor points are sited in the port area and inside the urban area (Figure 5). At each receptor point passive scalar concentrations are measured at different heights (from 0 to 320 mm) corresponding to 0-150 m in the real scale.

Figure 8 shows vertical profiles of the non-dimensional mean stream-wise velocity u(z) and of the standard deviations σ_v and σ_w. The measurements were carried out upstream of the port model and represent the flow field that hits the urban area. The vertical profiles show that over the sea the flow is homogeneous in the horizontal planes. According to the similarity theory (Tennekes and Lumley, 1972), in the lower part of the velocity field, in the so-call 'surface layer' the mean velocity profile is well modelled by logarithmic law of the form,

$$\frac{\bar{u}(z)}{u_*} = \frac{1}{k} \ln\left(\frac{z}{z_0}\right) \qquad (1)$$

where k = 0.4 is the Von Kármán constant, with u* = 0.13 ms^{-1} the friction velocity and z_0 = $2 \cdot 10^{-3}$ m the roughness length. These two latter parameters were determined by fitting (1) to the experimental data for $z < 0.2\ \delta$.

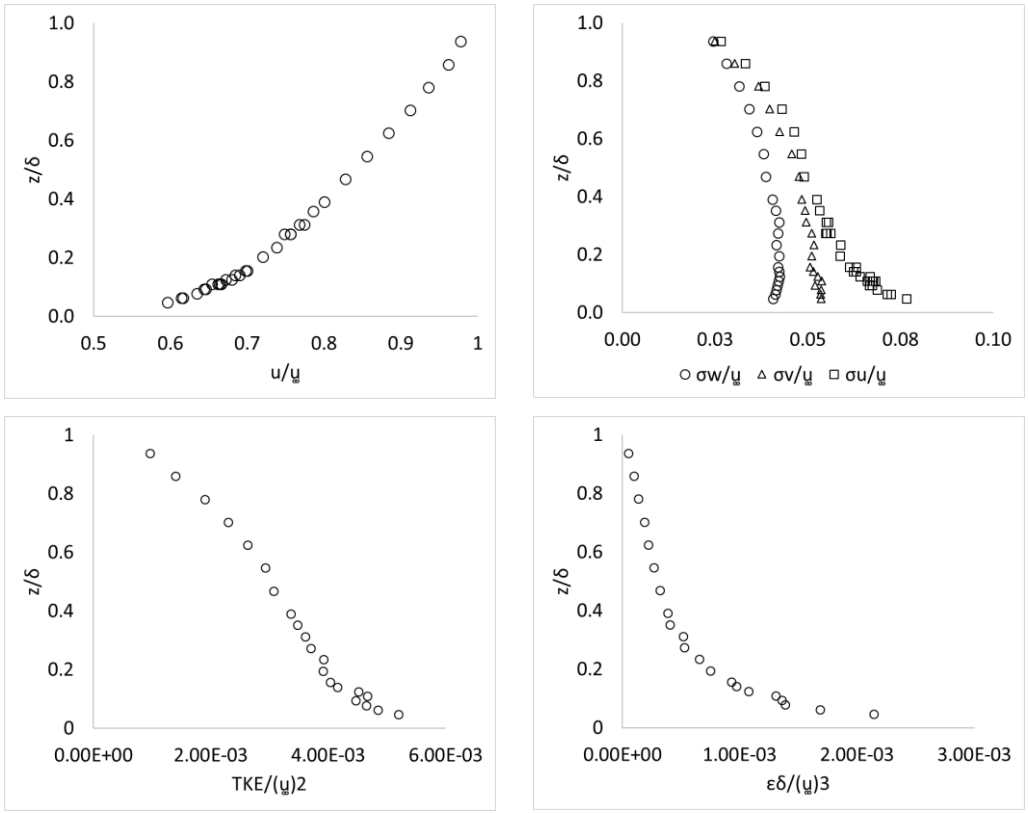

Figure 8. Mean velocity, turbulence intensity, TKE and ε profiles from WT experiments

In what follows, concentration will be expressed in terms of SO_2 concentration, as induced by realistic flow rates Q_r emitted by the cruises. To that purpose ethane concentrations from WT experiments are converted to SO_2 concentrations in real case scenarios adopting the following formula:

$$C_{SO_2}[ppm] = C_{eth}[ppm] * \frac{Q_r}{Q_{eth}} * \left(\frac{H_{WT}}{H_r}\right)^2 * \frac{U_{WT}}{U_r} \qquad (2)$$

where $C_{SO_2}[ppm]$ and $C_{eth}[ppm]$ are respectively the SO_2 and ethane concentration, expressed in part per million, Q_{eth} is the emission rate in the wind tunnel experiments, the ratio of funnels height H_{WT}/H_r = 1/500 and is the ratio of stack velocities (wind tunnel/ real funnel) U_{WT}/U_r = 1.

Then vertical concentration profiles obtained in correspondence of each receptor point are compared with results obtained in CFD simulations.

Figure 9 shows vertical SO_2 concentration profiles in correspondence of some sampling points (Figure 5), for both values of the velocity ratio (air funnel/wind) UR=1 and UR=4.

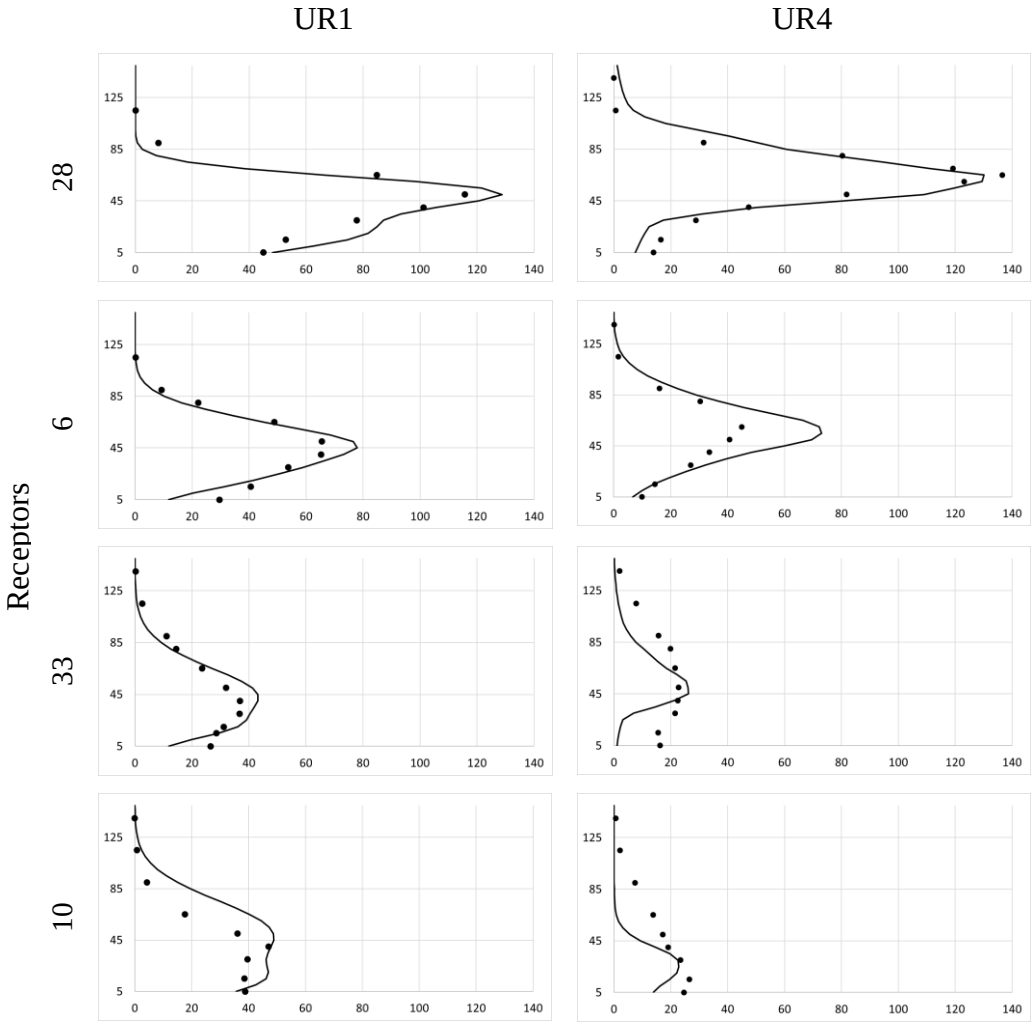

Figure 9. Comparison of vertical profiles of SO_2 concentration from WT (black dots) and CFD model (solid line). On the left UR=1, on the right UR=4

As shown by the scatter plots presented in Figure 10, the two sets of data agree reasonably well.

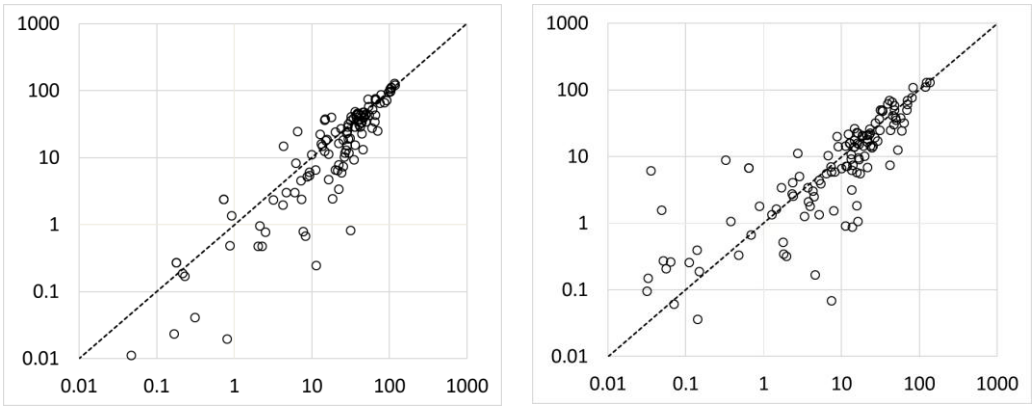

Figure 10. Scatter plots of SO_2 concentrations: CFD model (y axis) vs. WT (x axis) for UR=1 (left) and UR=4 (right).

To quantify the correspondence between the results of the two models (WT and CFD), the values of statistical parameters BIAS, NMSE, CORR, FAC2 and FB are reported in Table 7. The agreement is good. In fact, the criteria ($NMSE \leq 6$; $FAC2 \geq 0.3$; $|FB| \leq 0.67$), reported in Hanna and Chang (2012), are all satisfied.

Generally, the results obtained when UR=1 are better than those for UR=4, NMSE =0.17 (UR=1) against 0.29 (UR=4) and CORR coefficient = 0.931 (UR=1) against 0.920 (UR=4). These findings confirm the results in Toscano et al. (2020) for this same case study and are in agreement with the results of Ergin and Dobrucalı (2014) and Ünlügençoğlu et al. (2020).

Table 7. Comparison between the results of Wind tunnel and CFD models

Velocity ratio	BIAS	NMSE	CORR	FAC2	FB
UR = 1	3.40	0.17	0.931	0.625	0.122
UR = 4	1.82	0.29	0.920	0.651	0.097

A sensitivity analysis of CALPUFF model was performed analysing the effect of two options of the model, namely:

- the building downwash module (to include the interaction between the plume emitted by the emitting cruise ships and/or by the nearby buildings);
- the parameterisation of the plume spread;

For this reason, simulations were performed using three different model set-ups.

In the base case (referred to as Case 1) dispersion coefficients are estimated as a function of the standard deviations of the wind velocity and of the parameterisations of the horizontal and vertical Lagrangian time scales. Giving in input to the CALMET meteorological pre-processor the vertical profile of wind velocity evaluated in wind tunnel, CALMET has been calculated the standard deviations of the wind velocities based on the SL scales using the equations reported in Scire et al. (2000).

In the second (Case 2) the building downwash module was adopted. A proper estimate of the effect of the downwash is crucial because the exhaust gases are pulled into the wake of the funnel and coming down on the deck as they mix with the vortices behind the funnel. Many studies are devoted to the design of funnels to minimize this phenomenon (P.R.Kulkarni et al., 2007, Dobrucalı and Ergin 2012), that can also occurs at hotelling (depending on the wind speed) despite the lower funnel gas velocity (engines works at low loud). At hotelling, the occurrence of downwash due to funnel and ship shape can result in higher ground level concentrations immediately downwind of the ship.

In the third set-up (Case 3) the building downwash option was activated, and the dispersion coefficients were directly estimated using the wind tunnel measurements of the velocity standard deviation as input data.

The performances of CALPUFF model in the three cases were evaluated by comparing results of simulations with experimental data obtained in wind tunnel tests. The comparisons include: i) ground level concentrations; ii) vertical profiles; iii) the evaluation of statistical performance parameters reported in section 2.5.

Contour maps at ground level obtained with CALPUFF (case 1, 2 and 3) and WT are reported in Figure 11. The main findings are: i) CALPUFF underestimates ground level concentrations; ii) results in case 3 are better than in the other cases.

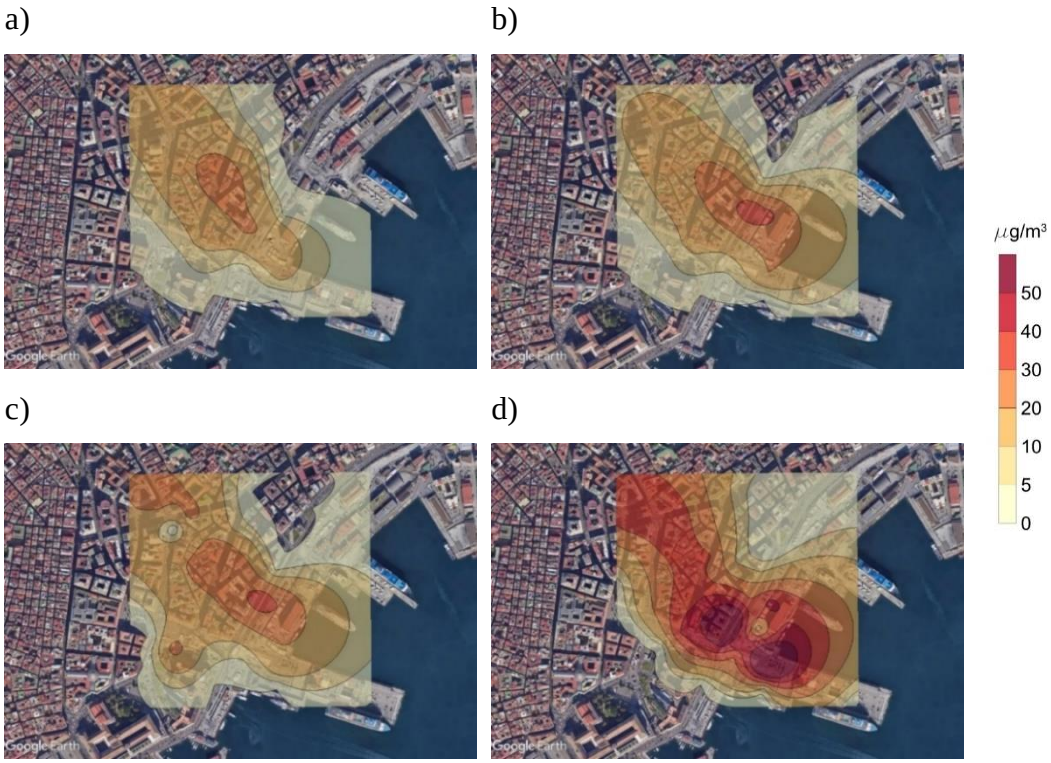

Figure 11. Ground level contour maps of SO_2 concentration: a) CALPUFF case 1; b) CALPUFF case 2; c) CALPUFF case 3; d) Wind Tunnel

The same findings are observed considering ground level concentrations only (Table 8), for which the better performances of CALPUFF also occur in case 3.

Table 8. Correlation between CALPUFF and WT at ground level: statistical parameters

Model	BIAS	NMSE	CORR	FAC2	FB
WT – CALPUFF (Case 1)	12.99	2.93	0.515	0.222	0.880
WT – CALPUFF (Case 2)	11.57	2.15	0.581	0.250	0.748
WT – CALPUFF (Case 3)	9.62	1.68	0.539	0.389	0.584

To extend the comparison between WT and CALPUFF results to all heights of the domain, scatter plots are reported in Figure 12. This figure provides an overview of the general performances of the CALPUFF model in predicting the wind tunnel concentrations. The calculation domain is divided in three different subdomains:

1. The port area (limited to the first line of buildings, (blue square receptors in Figure 5).

2. The open area (Municipio square, red circle receptors in Figure 5).
3. Street canyons (green rhombus receptors in Figure 5).

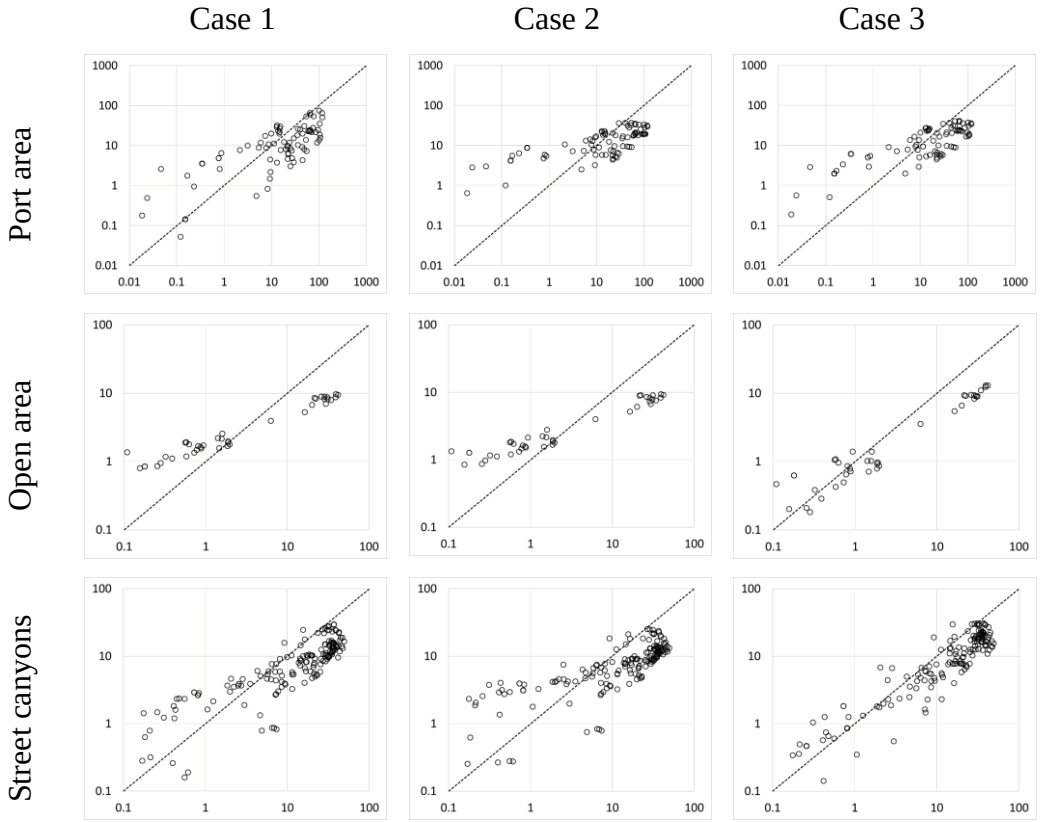

Figure 12. Scatter plots of SO_2 concentration: CALPUFF simulations (y axis) vs. WT (x axis) measurements.

Figure 12 shows that CALPUFF case 3 provide the best fit of WT results, especially inside the open area (Municipio square) and in street canyons. In the port area the difference between the three cases is less evident, as confirmed by the statistical parameters (Table 9).

Table 9. Statistical Parameters of correlation between WT and CALPUFF: cases 1-2-3 and areas: Port area, Open area and street canyons.

Areas	Case	NMSE	CORR	FAC2	FB
Port	1	2.24	0.716	0.230	0.689
	2	2.86	0.732	0.280	0.770
	3	2.53	0.731	0.250	0.717
Open area	1	5.39	0.962	0.264	0.912
	2	5.57	0.953	0.245	0.919
	3	4.73	0.990	0.434	0.935
Street canyons	1	1.15	0.791	0.376	0.688
	2	1.46	0.761	0.289	0.760
	3	0.69	0.839	0.555	0.532

To better analyse the behaviour of CALPUFF model in function of the height of the receptor, the results obtained by wind tunnel and CALPUFF are divided in two groups: i) measurement below the average roof top level ($z < 30$ m); ii) measurement points above the roof top level ($z > 30$ m). The corresponding scatter plots are reported in Figure 13. When $z < 30$ m SO_2 concentrations are generally high (range 10 – 100 $\mu g/m^3$) and difference among the three different configurations of CALPUFF are not relevant. Moreover, it is quite evident the tendency of CALPUFF to underestimates concentration levels. Instead, for $H > 30$ m, SO_2 concentrations are lower and case 3 formulation of CALPUFF shows the best performance. The corresponding values of statistical parameters are reported in Table 10.

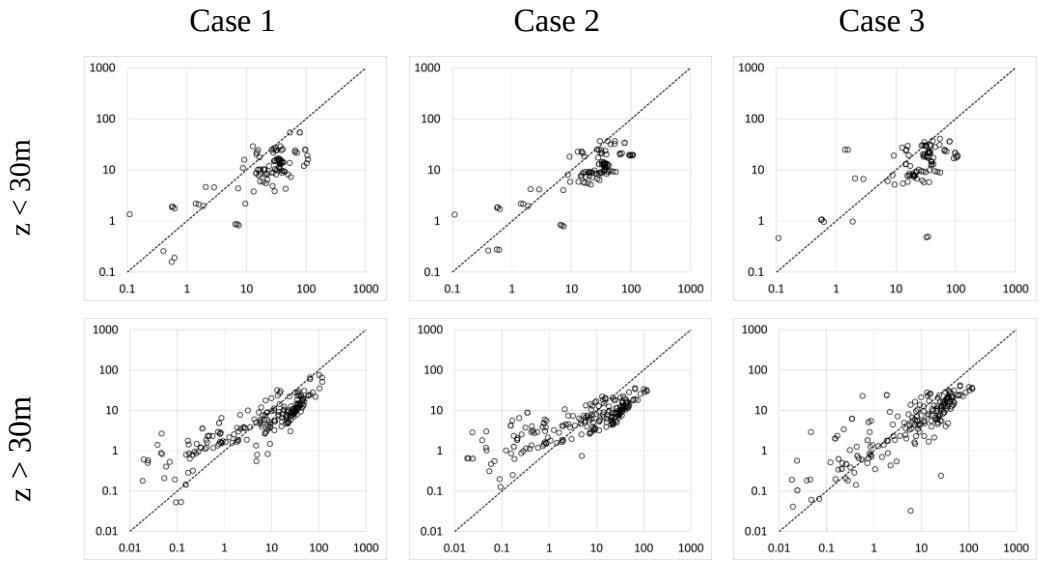

Figure 13. Scatter plots for SO_2 concentration: CALPUFF (y axis) vs. WT (x axis) below and above the roof-top level (H=30 m).

Table 10. Statistical Parameters of WT vs. CALPUFF below and above the roof top level

	Case	NMSE	CORR	FAC2	FB
z < 30m	1	2.17	0.613	0.302	0.806
	2	2.19	0.662	0.267	0.823
	3	1.69	0.578	0.388	0.658
z> 30m	1	1.75	0.838	0.319	0.620
	2	2.75	0.833	0.286	0.734
	3	2.08	0.800	0.400	0.619

The sensitivity analysis has shown that case 3 provides overall the best performances compared to case 1 and case 2. Therefore, we assess the model performances adopting this configuration of the model for both velocity ratios at the pollutant source, i.e. UR=1 and UR=4.

Contour maps at ground level for UR=4 are reported in Figure 14 in addition to contour maps for UR=1 reported in Figure 11. Scatter plots are reported in Figure 15 and statistical parameters in Table 11. Vertical profiles at some representative receptor points are instead reported in Figure 16.

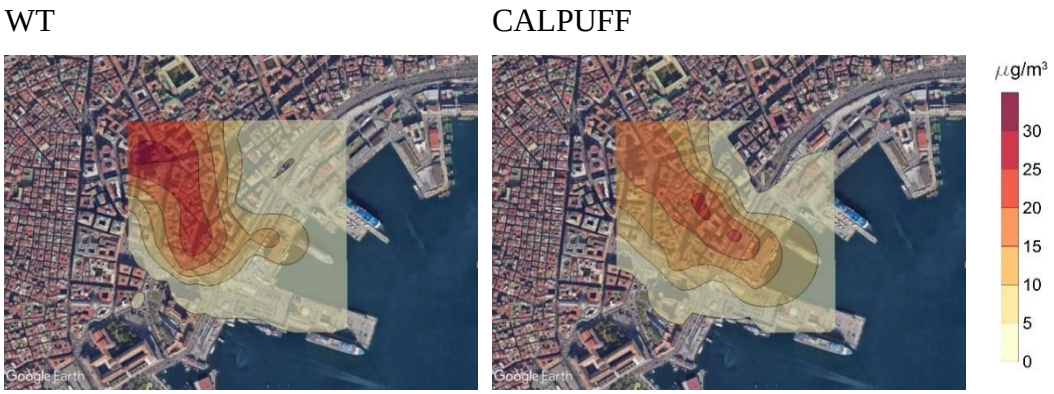

Figure 14. concentration at ground level for WT and CALPUFF (case 3) for UR=4

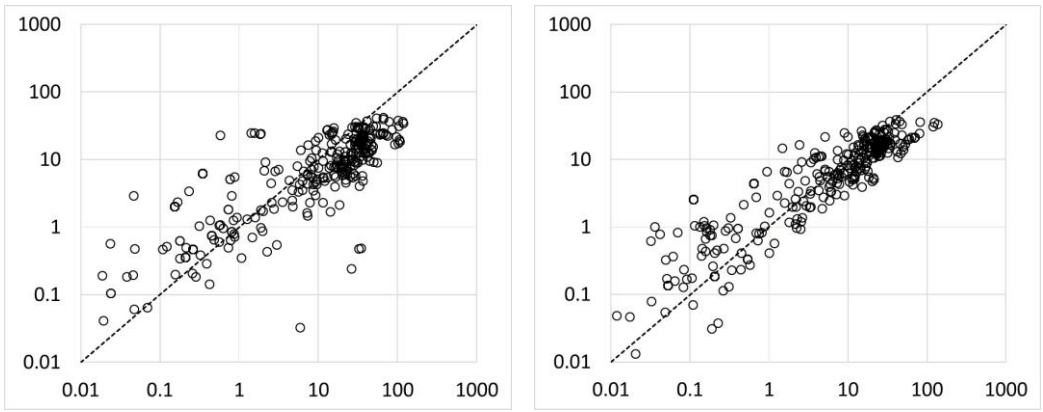

Figure 15. Scatter Plots for SO_2 concentrations: CALPUFF (Case 3) (y axis) vs. WT (x axis) for UR=1 and UR=4

Table 11. Statistical Parameters of correlation WT vs CALPUFF (case 3) for UR=1 and UR=4

UR	NMSE	CORR	FAC2	FB
1	1.95	0.720	0.396	0.636
4	1.57	0.780	0.515	0.413

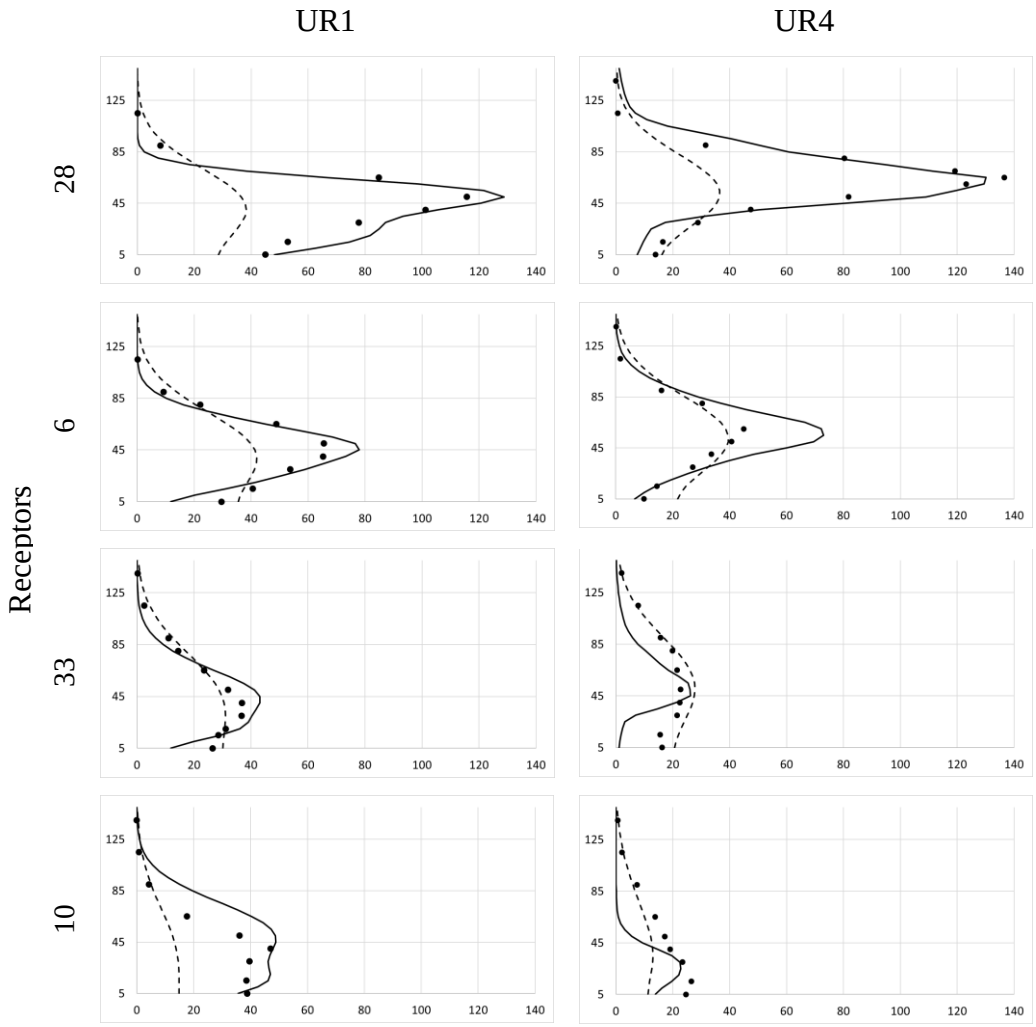

Figure 16. SO_2 vertical profiles of WT (black dots), CFD (solid line) and CALPUFF (dashed line) UR=1 and UR=4 at selected receptor points.

The evaluation of concentration at ground level is of primary importance in the assessment of the impact of ship emissions. We therefore focus on these (Table 12) analysing the main statistical parameters (mean, 95th and 98th percentile) related to the comparison between wind tunnel experiments and CALPUFF simulations (the comparison with CFD is not reported, as we previously showed that results of CFD are very similar to WT data).

Table 12. Statistical values and Absolute difference ($C_{CALPUFF} - C_{WT}$) and Percentage variation ($^{(C_{CALPUFF} - C_{WT})}/_{C_{WT}} * 100$) at ground level for WT and CALPUFF UR=1 and UR=4

	UR= 1			**UR= 4**		
	CALPUFF (Case 3) (µg/m^3)	WT (µg/m^3)	Difference (µg/m^3)	CALPUFF (Case 3) (µg/m^3)	WT (µg/m^3)	Difference (µg/m^3)
Mean	11.65	21.26	-9.62 (-45%)	8.43	8.58	-0.15 (-2%)
95th	29.73	57.76	-28.04 (-49%)	20.72	25.01	-4.28 (-17%)
98th	31.63	75.94	-44.31 (-58%)	21.24	25.70	-4.46 (-17%)

Data in Table 12 show that, in general, CALPUFF tends to systematically underestimate the concentrations measured in wind tunnel experiments. Notably, the difference between WT and CALPUFF for UR1 are -45% (mean), -49% (95% percentile) and -58% (98th percentile). The difference between the two models is lower when considering UR4, for which the percentage variations are -2% for mean and -17% both for 95th and 98th percentile. This finding is also confirmed considering vertical profiles of concentrations. A better agreement between wind tunnel and CALPUFF in UR4 (compared to the UR1) was indeed expected. Increasing the momentum flux of the exhaust gases induces an enhancement of rise of the plume whose dispersion will be then less affected by the presence of buildings, whose influence is not explicitly modelled in CALPUFF (except in the very near field through the building downwash module).

3.4 Effect of funnel air gas velocity

Having assessed the performance of CFD and CALPUFF models, their use to analyse configurations that were not studied experimentally were extended. In particular, the effect of the funnel air gas velocity on the dispersion of SO_2 which implies a variation on the plume rise in the near-source region was focused. Four different values of UR: 0.25, 1, 4 and 16 were considered. In Figure 17, box and whisker plots show the distribution of plume height for all receptor points expressed as the height of the maximum concentration in the vertical profiles obtained by CFD simulations. As can be observed, increases in the velocity ratio UR result in increases in the height of the SO_2 maximum concentration (plume height).

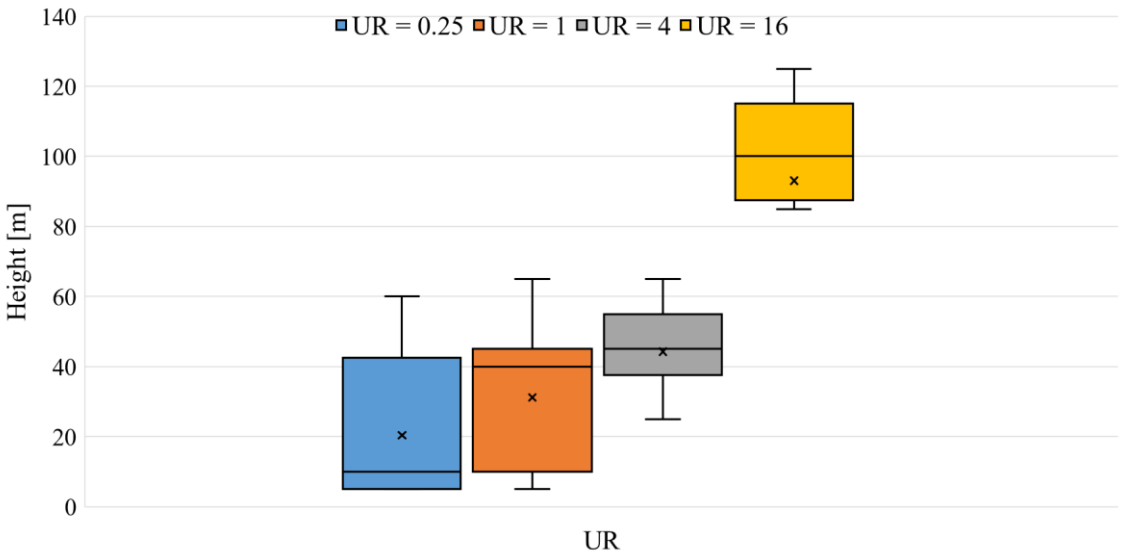

Figure 17. Box and whiskers plots of plume height distribution at all the receptor points as a function of the velocity ratio UR.

This effect is confirmed in Figure 18 which shows the contour map of SO_2 concentration at ground level. As can be seen as the UR increases, the concentration on the ground level decreases and the point of maximum concentration moves away from the sources. This effect may be a consequence of increasing the height of the maximum concentration. Both Figure 17 and Figure 18 show a limited difference between results for UR=0.25 and UR=1. The difference is more evident when UR=4 and becomes dramatic when UR=16. In this last case (see Figure 18), the pollutants are mainly transported outside the domain and do not induce relevant ground-level concentrations.

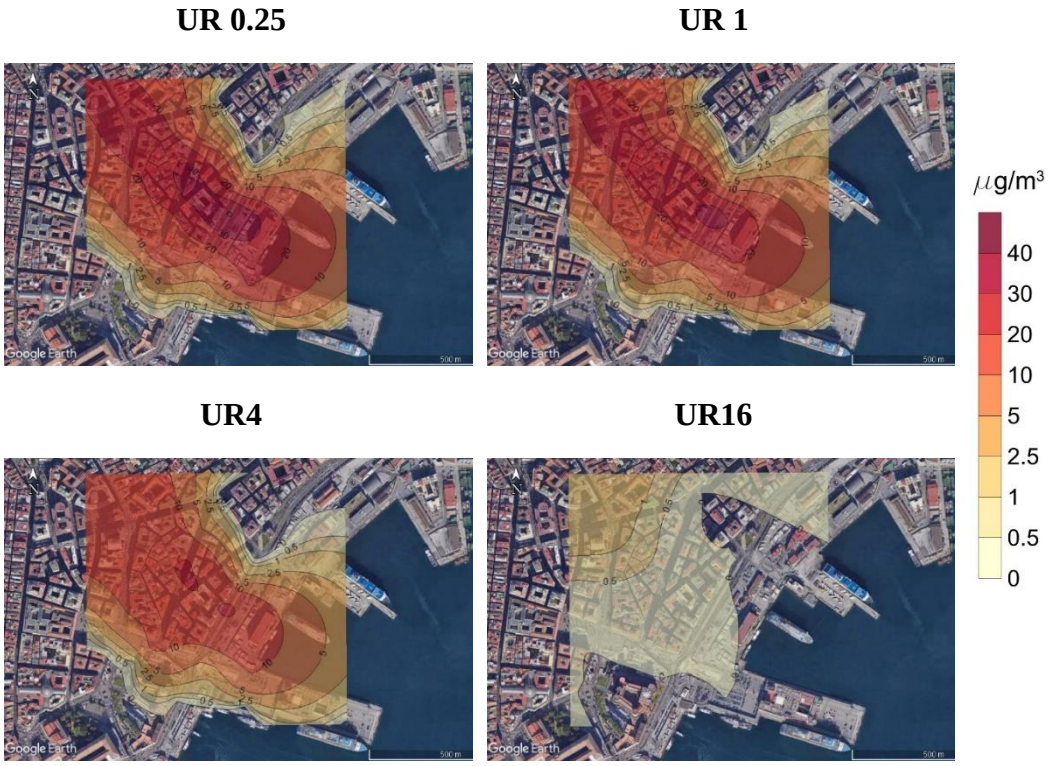

Figure 18. CALPUFF: contour maps of SO2 concentration at ground level as a function of the velocity ratio UR.

3.5 Conclusion of model validation

In this chapter a detailed analysis of the reliability of the CALPUFF operational dispersion model as a tool to assess the impact of cruise ship emissions on air quality was performed comparing results with those of wind tunnel and CFD models. The port of Naples was used as the case study. To this end it has been realised a reduced-scale model of the port of Naples and surrounding urban area and performed wind tunnel simulations of the dispersion of pollutants released by cruise ships while moored. Two different values of the velocity ratio UR=1 and UR=4 (funnel gas velocity/wind speed) were studied. Firstly, the wind tunnel measurements and CFD simulations were compared. Then three different configurations of CALPUFF were used to analyse the effect of the building downwash module and parameterisation of the plume spread. The performance of the CALPUFF model in the three cases was evaluated.

The main findings of this study are:

- CFD simulation results are in very good agreement with wind tunnel measurements.
- the best agreement between CALPUFF, wind tunnel measurements and CFD data is obtained when adopting the building downwash module and using direct velocity wind tunnel measurements as input data for the dispersion coefficients.
- even adopting this model set-up, CALPUFF shows a systematic tendency to underestimate the time-averaged concentration at ground level. At a low value of the velocity ratio (funnel gas velocity/wind speed) UR=1, the percentage of underestimation is about 54%. When UR=4, the percentage of underestimation decreases to 17%;
- a sensitivity study on the effect of the air velocity ratio (UR) shows its effect on plume height and on the distance from the source of the area of impact on ground level.

For an accurate assessment of the impact on the urban area of atmospheric pollutants emitted by ship funnels when cruise ships are moored, the use of a Gaussian model such as CALPUFF can be conveniently coupled with wind tunnel or CFD simulations. This approach improves the performance of the operational Gaussian model and reduces the uncertainty in the numerical predictions. Moreover, the exit velocity of the fume play, a parameter which is usually poorly documented, play a key rule.

4. Emission study

In this chapter the focus is on the estimation of the emissions of noxious gases from ships in port. The main goal of this chapter is to develop a highly detailed bottom-up emissions inventory for port activities over the Naples port case study. For this purpose, a comprehensive global data base of all ships visiting the port of Naples in 2018 using AIS data was created. At same time, a thoroughly review and assess the current status of ship emissions was developed. From which a statistical study based on literature review was performed in order to correlate emissions with traffic data per year.

4.1. Literature review of emission studies

A reliable and up-to-date ship emission inventory is a fundamental input in assessing maritime emissions and the effectiveness of emission control options. Methodologies for the assessment of ship emissions goes from: full top-down approach to full bottom-up approach (Miola and Ciuffo, 2011). In the full top-down approach total emissions are calculated at a large scale, generally national, and then geographically reduced at a smaller scale (regional or urban) using proxy variables. In the full bottom-up approach, air pollutants emitted by each ship in its specific position and during a specific activity is estimated. Then data are aggregated over the time and the space. The full top-down approach is applied in several studies (Corbett and Fischbeck, 1997; Corbett et al., 1999; Skjølsvik et al., 2000 and Endresen et al., 2007) and by national agencies (ISPRA, 2018; MINENV, 2009; Kentair, 2013; MEIC, http://www.meicmodel.otg). Common opinion is that top-down approach can be very useful to obtain a preliminary estimation of local emissions, but results must be confirmed by bottom-up studies (Eyring et al., 2009; Miola and Ciuffo, 2011; Perez et al., 2009; Saxe and Larsen, 2004; Tzannatos, 2010; Jalkanen et al., 2012; Ng et al., 2013). Due to the increase in the ships data availability and particularly following the introduction of the Automatic Identification System (AIS), bottom-up studies are nowadays generally more popular than top-down. AIS was introduced by the IMO International Convention of Safety of Life at Sea (SOLAS) to improve safety and efficiency of navigation (Tichavska and Tovar, 2015a), (Tichavska and Tovar, 2015b). But is now often

used to estimate ship emissions because it transmits for each ship useful information: i) IMO identification number; ii) size; iii) weight; iv) name; v) type; vi) position; vii) heading; and viii) speed (Coello et al., 2015); (Tichavska and Tovar, 2015b); (Winther et al., 2014). Bottom-up methods estimate the emission rates during each specific activity (hotelling, manoeuvring and navigation) as the product of an emission factor (EF) multiplied by the energy output of the engine or the fuel consumption (EEA, 2016). Energy output is generally estimated using the maximum continuous rated engine power multiplied by a load factor. The Emission Factors are expressed in terms of mass of pollutant per power unit [g/kWh] or mass of pollutant per mass of fuel [g/g fuel]. EFs depend on various parameters: vessel category, type of fuel, type and load factor of engine (main and auxiliary), speed (Corbett and Koehler, 2004) and ambient conditions, in particular wind speed and wave heights and the mean wave direction (Jalkanen et al., 2009). In the literature there are many bottom-up studies. The majority of them use activity-based methodologies and emission factors derived from literature (Tichavska and Tovar, 2015a; Tichavska et al., 2017; Maragkogianni and Papaefthimiou, 2015; Papaefthimiou et al., 2016; Dragovic et al., 2018; Saraçoglu et al., 2013; Kilic and Tzannatos, 2014; CAIMANs, 2015; APICE, 2013; Nunes et al., 2017a; Alver et al., 2018; Deniz and Kilic, 2009; Kiliç and Deniz, 2010; Berechman and Tseng, 2012; Yau et al., 2012; Ng et al., 2013; Song, 2014; Chen et al., 2016; Chen et al., 2017; Saxe and Larsen, 2004). De Melo Rodriguez et al. (2017) use EFs from literature but a fuel-consumption based methodology. Some studies modify EFs reported in literature on the basis of different considerations (Tzannatos, 2010; Murena et al., 2018). Other studies measure emissions on board (F. Zhang et al., 2016; Zetterdahl et al., 2016) or on land using DOAS or LIDAR technologies (Merico et al., 2016; Boselli et al., 2019). Even though bottom-up methodology would be more accurate than top-down, uncertainties still exist due to the quality of numerous input parameters like engine load factors, fuel type and consumption rate which are generally known only as average values depending on the vessel classes (Eyring et al., 2009; ICF, 2005; Maragkogianni et al., 2016). Therefore, uncertainties on emission factors are generally between 20% and 50% for the different pollutants (Cooper and Gustafsson, 2004). Other uncertainties are related to ship traffic

details. Considering that errors are random, some underestimations could be balanced by other overestimations so that a reasonable value of 30% could be assumed as uncertainty on estimated emissions (Broome et al., 2016; Merico et al., 2016). Several reviews have been published on the survey of ship emissions. Miola and Ciuffo (2011) provided a meta-analysis for both bottom-up and top-down modelling approaches and available data sources to estimate emissions from shipping. The authors demonstrated the uncertainties associated to different methods and attributed the level of uncertainty to the different sources of the input information used. A comparative analysis of current methods for estimating energy consumptions and shipping emissions during navigation mode is reported by Moreno-Gutierrez et al. (2015). They use several methodologies (Corbett and Koehler, 2003; Environmental Protection Agency (EPA, 2000); Entec, 2005 (Environmental Engineering Consultancy); Endresen et al., 2007; Eyring et al., 2005; IMO, 2010 (International Maritime Organization); STEAM (Ship Traffic Emission Assessment Model) by Jalkanen et al., 2009; and TNO (Netherlands Organisation for Applied Scientific Research) by van der Gon and Hulskotte (2010) to calculate fuel consumption of ships crossing the Strait of Gibraltar and corresponding emissions in the atmosphere. A difference among the results up to 27% is observed, mainly due to the relationship between engine use (from main to auxiliary) and engine loads. However, they conclude that the most reliable model of emissions assessment is the STEAM model by Jalkanen et al. (2009, 2012). Nunes et al. (2017b) analysed 26 articles published since 2010 that used activity-based methodologies to estimate ship emissions. The study provides a summary of the main sources and procedures used to obtain the parameters necessary to calculate ship emissions. The main conclusions are: i) most of the emissions are emitted during the mooring phase; ii) container vessels are responsible for 60% of total emissions; iii) cruise ship emissions are higher in the summer. Y. Zhang et al. (2017) reviewed and summarized the studies reporting all relevant aspects of maritime emissions and their impact on air quality in China. Many papers give data or information on emission factors. The most adopted reference is Entec (2002). The emission factors of ENTEC are relative to NOx, SOx, CO2, VOCs and PM for five kind of engine (slow speed diesel - SSD, medium speed diesel - MSD, stream

turbine - ST and gas turbine - GT) and three type of fuels (residual oil - RO, marine diesel oil - MDO and marine gas oil - MGO). These EFs are adopted by European Environment Agency (EEA) in chapter 1.A.3.d. namely Navigation (Shipping) of air pollutant emission inventory guidebook. Tzannatos (2010) adopts emission factors of ENTEC opportunely modified using different load factors for both main and auxiliary engines. Yau et al. (2012) and Ng et al. (2013) adopted EFs by Entec (2002) implemented with correction factors by Starcrest Consulting Group (2005a), Starcrest Consulting Group (2005b) reports. Different emission factors for NOx, PM, SOx, CO_2 and CO are used in STEAM model. (Jalkanen et al., 2009, 2012, 2014). The NOx EF in STEAM is estimated by the rotation data of the motor shaft (rpm, revolutions per minute) (Jalkanen et al., 2009). The emission factors change according to the engine load and can be higher for engines that operate at low loads, which is particularly true during manoeuvres in port (Jalkanen et al., 2012). Unfortunately, not always papers report both data of emissions and of ships traffic in port. Data on ships traffic are generally published by port authorities in terms of number of passengers, number of calls, tons of good, TEU depending on if they are referred to passenger or commercial ships. Typically, data of passenger ships are divided in cruise and "other than cruise" ships; while data on commercial ships are often only given as global. To assess PM10 emission factor information about the composition of particulate matter in function of the engine load and the sulfur content in the fuel are used (Jalkanen et al., 2014). SOx and CO2 EFs are modelled (Jalkanen et al., 2014) in function of the combustion conditions and specific fuel consumption. Finally, the CO EF is estimated (Jalkanen et al., 2014) following the procedure reported by Sarvi et al. (2008a, 2008b).

4.2 Estimation of ship emissions

A bottom-up methodology was used in order to estimate ship emissions. In fact, it starts from the activity of individual ships in the port and leads to the creation of a complete inventory of emissions relating to the entire port for the year 2018.

This inventory, including:

- an hourly calendar of the ship activities classified as navigation during arrival or departure and hoteling at berth.

- NOx, SO_2, and PM emission rates.
- the individuation of typical routes for each pier of the port.
- heights and diameters of the funnels and the speed of the fumes for ship macro-categories.

4.2.1 AIS data

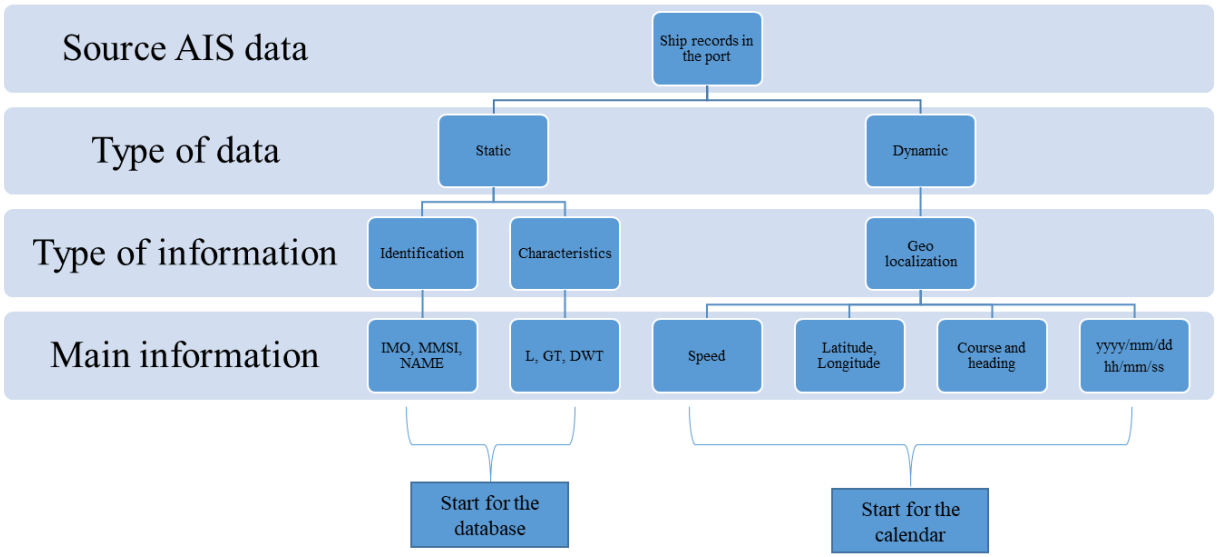

Figure 19. Flowsheet of the use of AIS data

The rates of emission have been calculated using a bottom-up activity-based methodology, using AIS data. AIS messages provide static information (MMSI number, type, and length) and dynamic information (the ship's position, i.e. latitude and longitude, course over ground (COG), speed over ground (SOG), and UTC. AIS transmits signals in a period from 3 s to a few minutes depending on the ship's operation (Yang et al. 2019). The flowsheet describing the use of the AIS data is reported in Figure 19.

The AIS data used include more than one million records associated with 922 objects, identified by their MMSI (Maritime Mobile Service Identity) numbers and grouped in categories. Among them, those belonging to seven categories have been eliminated because they correspond to stationary objects or to ships lacking adequate information and are not relevant for the purpose of the analysis. In this way, sailing vessels, law enforcers, military OPS, SAR aircraft, the null category containing ships without data, pleasure craft, and port tender were excluded from

the analysis because their contribution to emissions is null or not relevant. Overall, 141 elements were deleted (84,965 records, equal to 7.95% of the total records).

Table 13 reports the main average data (max speed, power, GT, and the number of ships) of the fleet visiting the port of Naples in 2018, subdivided into 45 categories. The first column in Table 13, represents the initial of five macro-categories Commercial, Fishery, Passenger, Tanker, and Other in which all ships have been lumped for the successive dispersion study. The last column of the same table counts the number of calls for each category and is one of the results of the MATLAB Code explained in the next paragraph.

Table 13. Main data of the fleet arriving at the port of Naples in 2018 sub-divided in 45 ship categories.

Macro-categories	Category	speed [kn]	power [kW] mean	GT mean	Number of ships	Calls
O	Aggregates Carrier	11.6	1790.0	995.0	1	1
O	Anchor Handling Vessel	12.0	4050.0	1471.0	1	2
T	Asphalt/Bitumen Tanker	14.0	2981.3	5774.3	3	17
C	Bulk Carrier	16.2	6830.5	22045.8	32	36
T	Bunkering Tanker	8.5	892.0	775.3	3	94
O	Cable Layer	12.0	6005.0	9024.0	2	3
C	Cargo	10.0	625.5	311.0	1	5
C	Cargo/Containership	16.7	6728.2	8017.2	5	11
T	Chemical Tanker	15.0	8179.3	24996.0	1	40
C	Container Ship	22.2	33811.9	45043.4	131	503
O	Crane Ship	7.5	526	505	5	7
C	Deck Cargo Ship	10.0	3180.0	2770.5	2	2
F	Fish Carrier	8.5	1600.0	206.0	1	1
F	Fish Factory	12.0	1194.0	1085.0	1	1
F	Fishery Research Vessel	12.0	1600.0	398.0	1	1
F	Fishing Vessel	13.5	666.5	170.4	13	17
C	General Cargo	15.0	4826.3	11427.8	153	270
O	Grab Hopper Dredger	10.0	1102.0	481.0	1	2
O	Heavy Load Carrier	17.3	4300.0	6295.3	3	4
O	Hopper barge	8.0	882.0	1192.0	1	2
P	HSC	32.3	5864.0	1006.8	9	2960
P	Hydrofoil	38.0	4000.0	196.0	1	8
P	Inland	18.5	34241.0	62750.7	3	30

T	LPG Tanker	17.8	6093.6	11135.4	23	118
T	LPG-Chemical Tanker	15.5	6000.0	9835.0	1	7
O	Motor Hopper	12.0	2388.0	1469.0	1	39
O	Offshore power Supply Ship	13.2	4457.1	1973.3	8	415
T	Oil Products Tanker	14.0	6145.0	17794.3	4	78
T	Oil-Chemical Tanker	16.2	6269.9	15250.8	100	230
O	Other	19.5	28151.7	113216.0	3	38
P	Passenger Ship	23.8	22178.6	38916.3	130	12798
P	Passenger-Cargo Ship	13.0	648.0	196.0	1	90
O	Patrol Vessel	32.0	9440.0	550.0	1	1
O	Research-Survey Vessel	14.2	5616.0	2442.0	2	4
C	Ro-Ro-Cargo	19.2	16150.3	29773.4	14	62
C	Ro-Ro-Container	20.3	18251.4	33718.0	7	37
P	Ro-Ro-pax	20.1	15013.1	15653.7	54	8133
O	Salvage-Rescue	13.6	2942.5	1204.0	4	58
O	Special Vessel	16.0	8000.0	4201.0	1	1
F	Trawler	14.0	665.6	177.3	6	12
O	Tug	12.6	3110.5	344.1	14	89
O	Unspecified	19.5	1333.8	367.0	5	61
T	Water Tanker	11.9	1219.7	1200.1	7	174
T	Wine Tanker	11.9	1219.7	1200.1	3	71
P	Yacht	18.7	3152.7	470.0	8	6

The dataset was handled in order to generate an annual calendar using a MATLAB code based on the following main steps: the import of AIS data, the definition of code suitable for identifying phases, spike, warnings, and the generation of a calendar and the export of results. Figure 20 shows a synthetic block diagram showing how AIS data are used by the MATLAB code.

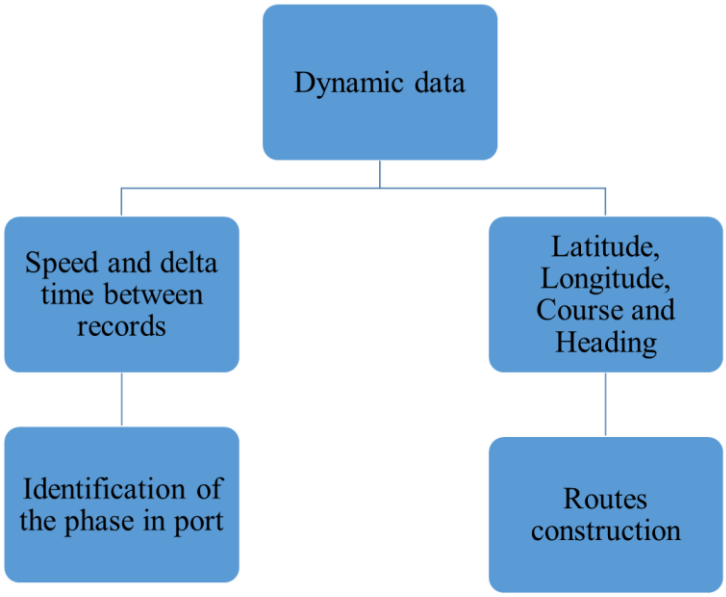

Figure 20. Scheme of the MATLAB code

The MATLAB code is able to identify the phase of ships on the basis of the analysis of the temporal data, of the time delta between records, and of the speed data. The phases defined are as follows: entry to the port, navigation in the port, the start, stop, and end phases of mooring at the quay, exit from the port, and engine start and stop. Each of these phases is characterized by a unique combination of speed and time delta with respect to the neighboring records. To better understand the results of the code, Table 14 shows the result obtained for a particular container ship. As can be observed in Table 14, each record is marked with a particular wording. The detailed articulation of the AIS data allowed the subsequent accurate estimation of emissions. Obviously, the lines corresponding to mooring records between ”mooring start” and “mooring end” are not reported in Table 14.

Table 14. Example of MATLAB results

Ship name	**Latitude**	**Longitude**	**Course**	**Heading**	**Timestamp (UTC)**	**Speed [kn]**	**Phases**
Ship 1	4083307	1427542	319	346	21/04/2018 10:51	5.7	In
Ship 1	4083563	1427474	16	39	21/04/2018 10:53	4.0	navigation in port
Ship 1	4083763	1427673	50	74	21/04/2018 10:55	4.3	navigation in port

Ship 1	4083834	1427959	86	108	21/04/2018 10:57	3.7	navigation in port
Ship 1	408381	1428215	86	134	21/04/2018 11:00	1.3	navigation in port
Ship 1	4083906	1428272	4	169	21/04/2018 11:03	1.9	mooring phase (start)
Ship 1	4084019	1428288	220	187	21/04/2018 11:07	0.0	…… ……
Ship 1	4083978	1428305	164	195	21/04/2018 20:27	1.8	mooring phase (end)
Ship 1	4083817	1428196	258	270	21/04/2018 20:30	2.5	navigation in port
Ship 1	408383	1427936	273	257	21/04/2018 20:33	3.7	navigation in port
Ship 1	4083791	1427637	242	214	21/04/2018 20:35	3.7	navigation in port
Ship 1	4083615	1427466	199	176	21/04/2018 20:37	3.8	navigation in port
Ship 1	4083568	1427453	188	170	21/04/2018 20:37	3.9	navigation in port
Ship 1	4083355	1427491	160	149	21/04/2018 20:39	5.3	out

4.2.2 Estimation of emission rates

For an accurate estimation of the emission rates, a database of all the ships visiting the port of Naples in 2018 was created. The database contains all the information necessary for the estimation of emission rates:

- category, name, IMO number, gross tonnage (GT), and deadweight (DWT) from static AIS data (Yang et al., 2019).
- length (L), width (B), and draft (T) [m].
- total power installed onboard (P) [kW] and the type of engines.
- maximum speed (v) [kn].
- the number of passengers, cars, containers, etc. as a function of the type of vessel.

Unfortunately, not all the records contain all the mandatory information for the calculation of emission rates. The percentage of missing data was 10.55% for power

installed onboard and 5.72% for maximum speed. Table 15 shows the categories for which the per-centage of missing data is different from zero.

Table 15. Percentage of missing data for each ship category. Categories without missing data are not reported.

Category	Depth (%)	Power (%)	Max speed (%)
Bulk Carrier	21.88	12.50	12.50
Cargo	100.0	0.0	100.0
Cargo/Containership	20.0	0.0	0.0
Chemical Tanker	0.0	100.0	0.0
Container Ship	36.6	3.8	0.0
Deck Cargo Ship	100.0	50.0	0.0
Fish Carrier	100.0	100.0	0.0
Fish Factory	100.0	0.0	100.0
Fishing Vessel	38.5	69.2	15.4
General Cargo	1.96	5.23	0.0
Grab Hopper Dredger	0.0	0.0	100.0
Inland	33.3	0.0	33.3
LPG Tanker	8.7	4.3	0.0
Oil Products Tanker	25.0	0.0	0.0
Oil-Chemical Tanker	13.0	15.0	3.0
Other	46.2	46.2	46.2
Passenger Ship	12.3	6.9	5.4
Ro-Ro-Cargo	21.4	14.3	14.3
Ro-Ro-Container	0.0	28.6	0.0
Salvage-Rescue	0.0	25.0	0.0
Special Vessel	0.0	100.0	0.0
Trawler	50.0	83.3	50.0
Tug	14.3	21.4	21.4
Unspecified	20.0	0.0	20.0
Yacht	12.5	12.5	12.5

In order to fill the missing data, regressions based on real data for each category were adopted. Regressions (almost all linear) are structured as a function of LBP (length be-tween perpendicular) [m] or GT. In fact, the database thus constructed consists of as many columns as indicated by the specific characteristics of each ship. The regressions for the categories of ships with only one ship were grouped with a category of similar mission profiles; for example, fish factories, fishing vessels, and fish carriers were lumped together. Table 16 and Table 17 show the main

characteristics of the regressions obtained, respectively, for power and max speed. In each table, the category, the type of regression, m and q ($y= mx+q$ or $y = mx^q$), the predictor used, and the determination coefficient obtained are reported.

Table 16. Main parameters of regressions for total power in kW

Category	Type of regression	Coefficient		Predictor	R^2
		m	q		
Bulk	linear	$6.48 \cdot 10^{1}$	$-4.53 \cdot 10^{3}$	L [m]	0.78
Container Ship	linear	$3.14 \cdot 10^{2}$	$-3.85 \cdot 10^{4}$	L [m]	0.90
Crane ship	linear	$1.40 \cdot 10^{1}$	$3.54 \cdot 10^{1}$	L [m]	1.00
Deck cargo	power	$4.95 \cdot 10^{-1}$	2.32	L [m]	0.82
Fishing vessel	linear	-3.04	$1.33 \cdot 10^{3}$	GT	0.87
General cargo	linear	$7.80 \cdot 10^{1}$	$-5.50 \cdot 10^{3}$	L [m]	0.82
LPG Tanker	linear	$1.04 \cdot 10^{2}$	$-7.64 \cdot 10^{3}$	L [m]	0.92
Oil Chemical tanker	linear	$6.44 \cdot 10^{1}$	$-3.16 \cdot 10^{3}$	L [m]	0.76
RoRo cargo	linear	$3.69 \cdot 10^{-1}$	$5.16 \cdot 10^{3}$	GT	0.75
Passenger (L<50m)	power	$2.93 \cdot 10^{-2}$	3.14	L [m]	0.54
Passenger (L>50m)	power	$5.80 \cdot 10^{-3}$	2.84	L [m]	0.94
RoRo container	linear	$2.38 \cdot 10^{-1}$	$1.21 \cdot 10^{4}$	DWT	0.41
Salvage rescue	linear	$-7.29 \cdot 10^{1}$	$4.63 \cdot 10^{3}$	L [m]	1.00
Trawler	linear	-3.04	$1.33 \cdot 10^{3}$	GT	0.87
Tug	linear	6.34	$9.30 \cdot 10^{2}$	GT	0.74
Yacht	linear	2.76	$7.72 \cdot 10^{2}$	GT	0.70

Table 17. Main parameters of regressions for max speed in kn

Category	Type of regression	Coefficient		Predictor	R^2
		m	q		
Bulk	constant	13kn for L<130m and 17kn after		L [m]	
Fishing	constant	12			
Container ship	linear	$3.49 \cdot 10^{-2}$	$1.42 \cdot 10^{1}$	L [m]	0.62
Oil chemical tanker	two constant value	11kn for L< 80m and 15kn after		L [m]	
Passenger	power	3.69	$5.70 \cdot 10^{-1}$	L [m]	0.24
	linear	$3.97 \cdot 10^{-2}$	$1.19 \cdot 10^{1}$	L [m]	0.65
RoRo cargo	constant	20			
Trawler	constant	14			
Tug	constant	13			
Yacht	constant	15			

For each category, these regressions filled the gaps in the database. In some cases, the speed data distribution did not allow for high-quality regressions; in these cases, a constant speed value equal to the average of the speeds of that category was assigned to that category. Once the database was completed, emission rates of NOx, SOx, and PM were calculated. The reference adopted is the recent EMEP-EEA guideline (updated 2019).

The input data necessary are the total power installed onboard, the type of engine in-stalled onboard (HSD, i.e. High Speed Diesel, MSD, i.e. Medium Speed Diesel, and SSD, i.e. Slow Speed Diesel) and the type of fuel used (BFO, i.e. Bunker Fuel Oil, MDO, i.e. Marine Diesel Oil, and MGO, i.e. Marine Gas Oil). Therefore, SFOC (Specific Fuel Consumption) is given depending on the kind of engine and fuel used: for each ship category, the adopted procedure gives 213 g/kWh for HSD or MSD engines using BFO, 213 g/kWh for the same engines and MDO or MGO, 195 and 185 g/kWh for SSD using, respectively, MDO or MGO. In order to estimate the emission rates during navigation in port, the speed must be known. According to AIS data, three typical speeds for each category of ships were identified. Two correspond to the arrival and departure, and the third corresponds to navigation in the port generally at lower speeds. In Figure 21, all the mean speeds obtained for each category are reported. For example, Category 17, general cargo, has a mean speed during in and out of 6 kn and a mean speed during navigation in port of about 4 kn; in the yacht category, these values are, respectively, 7 kn and about 4 kn.

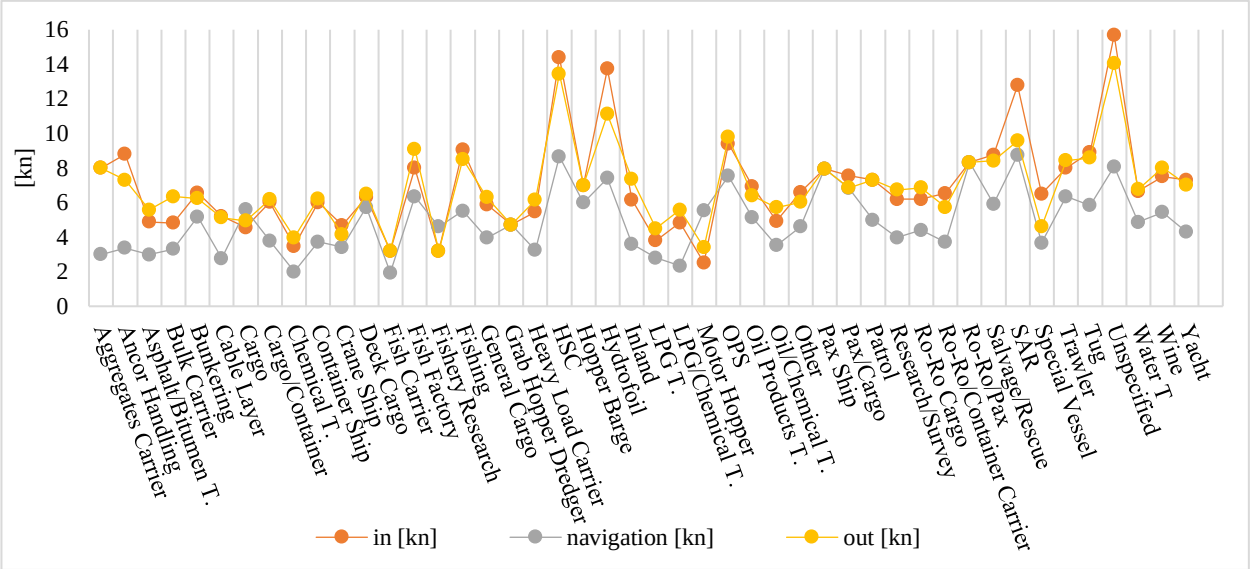

Figure 21. Average speeds of ship categories at arrival (in), during navigation in port and at departure (out)

The average speeds reported in Figure 21 are used to calculate the real power of main engines in each of the three phases (in, out, and navigation at reduced speed in port). For this aim, the cubic law existing between different speeds was used. The procedure adopted allows a more accurate estimation of the actual power when ships are moving in port with respect to that using the typical load factors corresponding to the cruise phase. The total power of auxiliary engines was evaluated on the basis of the total power onboard and using the load factors reported by Trozzi et al. (2019). According to Trozzi et al. (2019), during the navigation phase, a 30% load factor is assumed for the auxiliary engines. During the hoteling phase, it was assumed for all categories that the engine loads are 20% on main engines and 40% on auxiliaries, except for tankers, in which case the factor load of auxiliary engines is 60%.

Finally, the emissions for each ship in the navigation phases and in the mooring phase have been estimated using the emission factors shown in Table 18. Since each category of ships is characterized by a specific combination of fuel and engine types, a specific emission factor is defined for each category of ships and activity phase. Due to the lack of precise data about the duration of the individual maneuver phases and the possible presence of tugs, the emissions occurring during the maneuvers have been incorporated into the pure navigation phases defined.

Table 18. Emission factor as a function of engine type, operational phase and fuels (EMEP/EEA, 2019).

EF NOx	**TIER III**		**HSD**	**HSD**	**MSD**	**MSD**	**SSD**	**SSD**
[g/kWh]	Engine type	Phase	BFO	MGO	BFO	MGO	BFO	MGO
(2010 fleet)	Main	Cruise	11.8	11.2	13	12.3	16.9	15.8
		Manouvering, Hotelling	9.5	8.9	10.4	9.9	13.5	12.7
	Auxiliary	Cruise, Manoeuvring, Hotelling	10.8	10.2	13.7	13		
PM10 and	Main	Cruise	0.8	0.9	0.8	0.3	1.7	0.3
PM2,5		Manouvering, Hotelling	2.4	0.9	2.4	0.9	2.4	0.9
[g/kWh]	Auxiliary	Cruise, Manoeuvring, Hotelling	0.8	0.3	0.8	0.3		

As regards the emissions of SO_2, a content of sulfur in fuel equal to 0.1% in port was assumed according to the deliberation of the port authority. As an example of the result obtained, the following diagrams (Figure 22) show the emissions of NOx, SO_2, and PM in g/s during the navigation and hoteling phases as a function of the total power installed onboard the ships.

a)

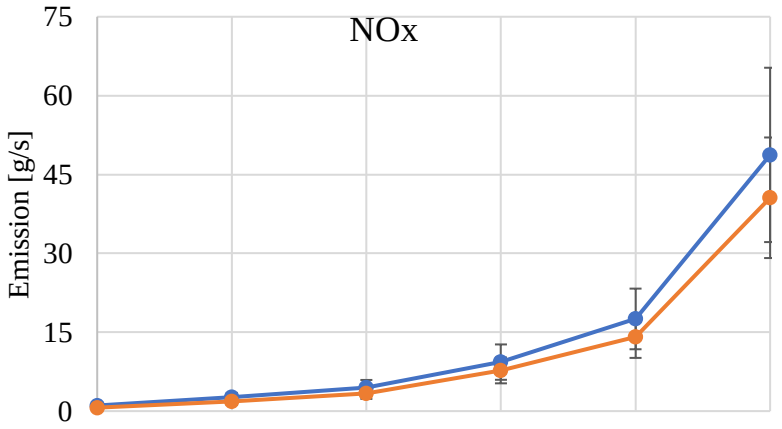

b)

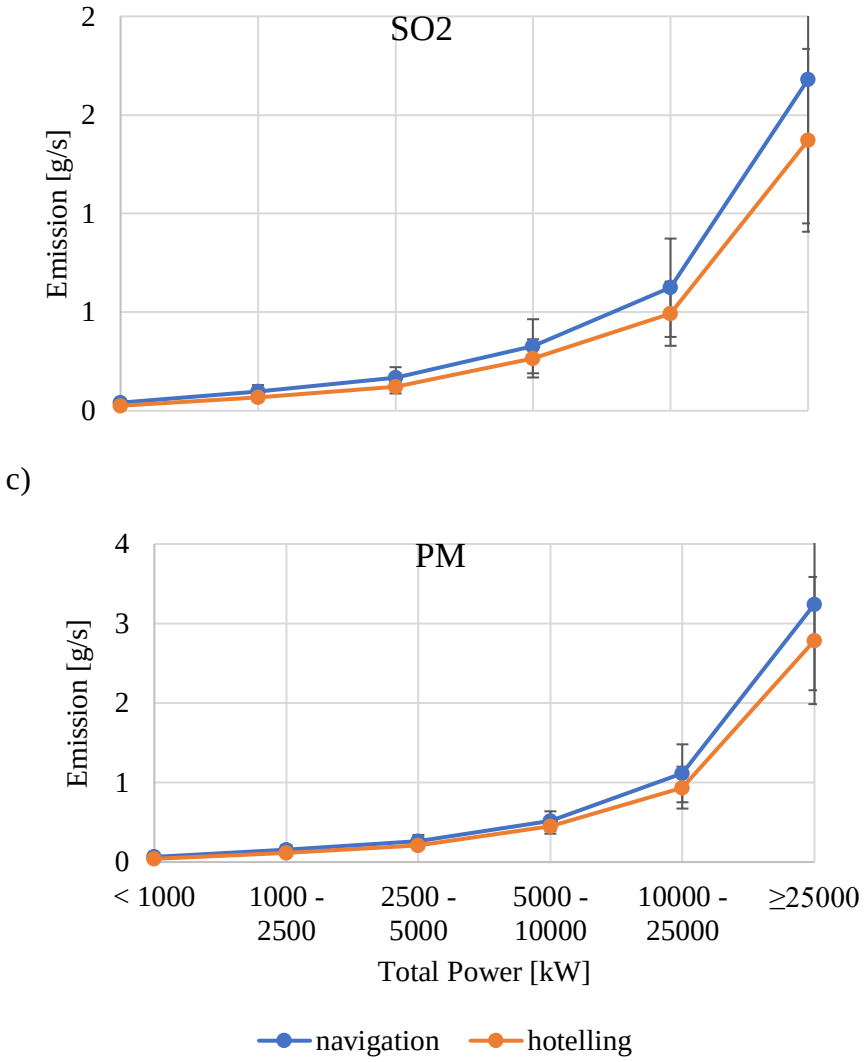

Figure 22. Emission rates estimated for pollutants during navigation in port and hotelling as function of total power installed: a) NOx, b) SO_2 and c) PM.

4.2.3 Definition of routes in port

The first step for the definition of the route in port for each ship requires the identification of the reference pier. By analysing the AIS data of each ship category, similar routes on the same pier were identified. Successively, for each ship category, piers and routes that are very close were merged. In Figure 23, real and merged piers are reported. Circles include the real piers that have been merged. In Figure 24, some of the defined routes are reported.

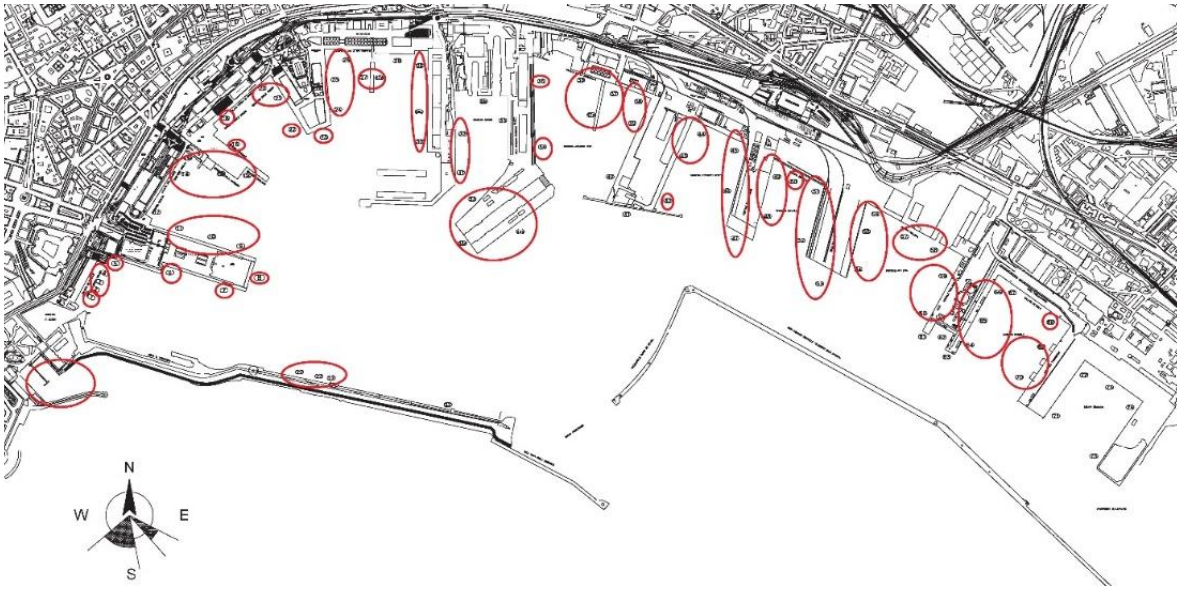

Figure 23. Grouping of piers.

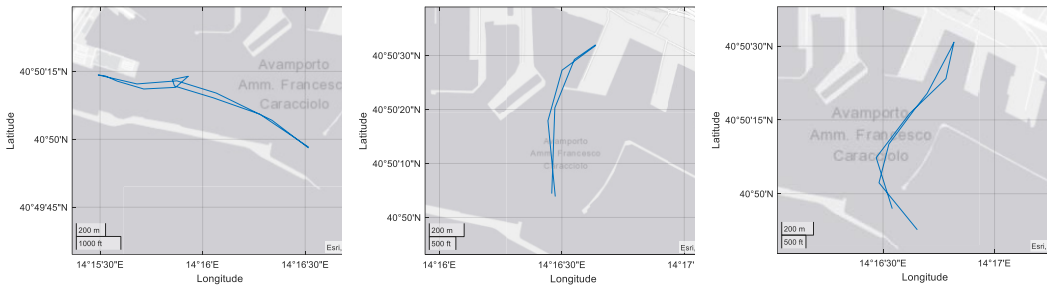

Figure 24. Examples of routes defined

4.2.4 Definition of sources

The height above sea level and the diameter of the funnels are important parameters for studying the dispersion of airborne pollutants. The height of the funnels on the base-line is not easy to find from the information generally available. Therefore, 46 general arrangement plans were collected, including bulk, general cargo, pax-cargo ships, cruises, ferries, ro-ro cargo, fishing, trawlers, oil tankers, product tankers, chemical tankers, supply, tugs, and container vessels. The height of the upper side of the funnel on the baseline and the design depth were measured. The difference between these two heights provides the height of the funnel above sea level, when the ship is in full load conditions. By varying the immersion as a function of the load of the ship, this difference changes.

For a more accurate estimation of the H_{BL}, data for each macro-category were fitted by linear regression equations using L_{BP} as predictive variable.

Table **19** shows the parameters of the regression equations and the determination coefficients (m is the slope, and q is the intercept).

Table 19. Coefficients of regression equation $H_{BL} = m\ L_{BP} + q$ (H_{BL}, L_{BP} and q are in meter).

Category	**m**	**q**	**R^2**
Bulk and General cargo	0.16	2.25	0.77
Passenger (cruise, ferry and Ro-Ro)	0.19	6.50	0.92
Fishing	0.22	9.79	0.88
Tanker	0.19	-6.65	0.84
Container	0.06	24.9	0.47
Supply e tug	0.36	0.05	0.40

To obtain the height of the funnel above sea level, the ship depth, available from the database, was subtracted from the value of HBL obtained. In Figure 25, the values of HBL, as a function of the total power installed onboard, are reported for all ship macro-categories.

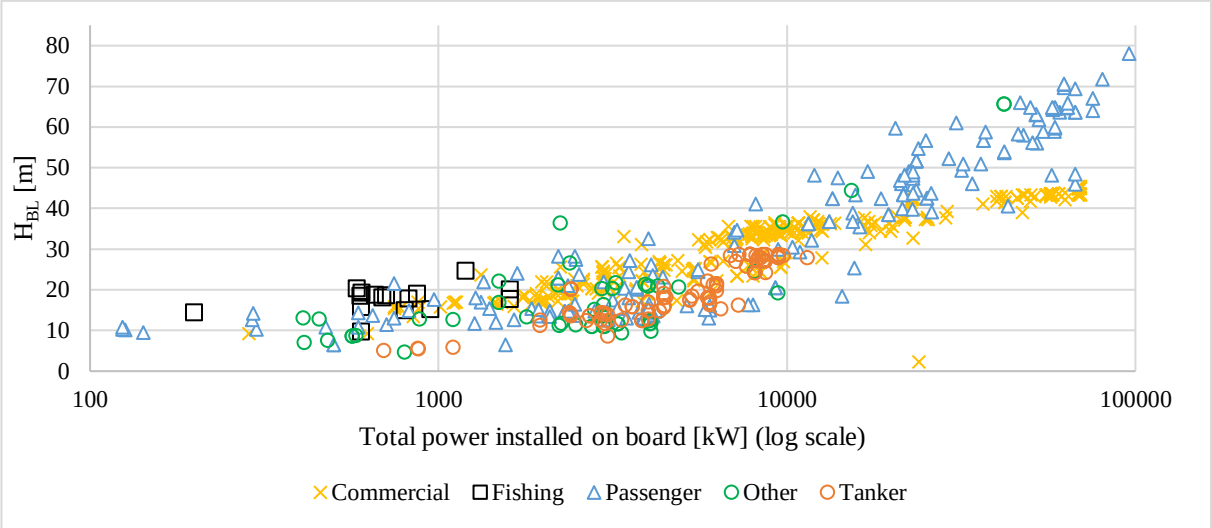

Figure 25. Height over base line (H_{BL}) as a function of the total power installed on board for macro-categories.

For the estimation of the diameters of the funnels, statistics were not relied on because the available database is not sufficiently large and distributed. The calculation process starts from the estimation of a design funnel's diameter based on the maximum continuous rating of engines onboard, assuming an air-fuel ratio equal to 33 kg for each kg of fuel (34 kg of exhaust for each kg of fuel), an exhaust temperature of 400 °C, and an exhaust speed of 12 m/s (Badeke et al., 2020). The exhaust flow rate and speed depend on the load conditions of the engine. By applying the right load factors, the exhaust speed is estimated in correspondence with the navigation in the port and in the hoteling phases. For example, during the hoteling phase, the speed is reduced by 20%.

The heights and the diameters calculated in function of the gross tonnage (GT) were reported in Figure 26. As can be observed both the parameters grow to the increase of the GT. The height is in the range between about 10 m (GT < 1000 t) and 50 m (GT > 75000 t), the diameter is from 1 m to about 4.5 m for GT < 1000 and GT > 75000 respectively.

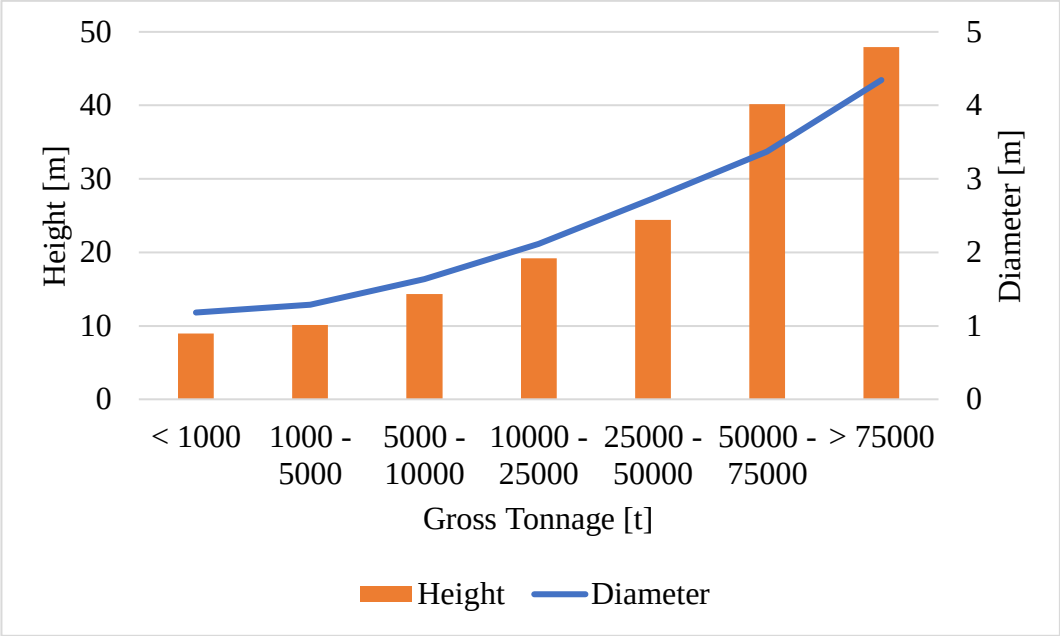

Figure 26. Height and diameter as function of gross tonnage for the fleet visiting the port of Naples in 2018.

4.3. Emission in other ports

Data from 38 ports and 45 annuality were analyzed (Table 20). The ports are organised for geographic area. Data reported are: the year of the study (calendar time); the use of AIS data (yes or not); the methodology adopted ("LF" load factor or "FC" fuel consumption); the references of load factors and emission factors adopted. The traffic data considered are: number of passengers, hours per activity (hotelling, manoeuvring and total as sum of hotelling and manoeuvring) and calls (passenger ships); and tons of good, hours at hotelling and calls (commercial ships). The pollutants considered are NOx, SO_2, and PM10. The methodology adopted consists of: i) review of data reported on ships atmospheric emissions and ships traffic in many ports in the world; ii) their analysis, and homogenization; iii) build-up of a database; iv) correlation with traffic data. In Table 20 are listed the port analysed in the literature review. One of the main difficulties in the elaboration of data on ship emissions in ports is the poor homogeneity. Data on emissions may be reported as global data or divided in the main vessel categories: passenger and commercial. The single global data of emission is of scarce utility for elaboration and comparison with other ports because it depends strongly on the percentage of contribution of passenger and commercial ships. In the same way data on emission of passenger ships can be global or specified for cruise ships or other categories (ferries, hydrofoils or other) also in this case more the data is referred to a specific category higher is its utility. Data on commercial ships are generally rarer than data on passenger ships. Another inhomogeneity is how emissions data are attributed to the different activities in ports. Also, in this case sometimes only a global data is given. More frequently specific activities are indicated as hotelling, manoeuvring or navigation. Hotelling is when the ship is stopped at wharves but emit exhaust gases from engines producing heat and electrical power for all the services necessary for the crew and the passengers or to upload and download of goods, maintenance or others. The terms manoeuvring and navigation in port indicate the activities when the ship is moving inside the port or in its proximity. Some authors make differences between these terms other do not. If both activities are considered, manoeuvring represents the high non-stationary phase during which the ship changes speed or direction to rapidly approach the dock, while navigation is the

movement of the ship inside the port area at quite constant and reduced speed. Another inhomogeneity is the length of the route corresponding to the navigation phase. For some authors it is the distance from the port entrance to the final mooring point and is generally a few miles, for others it is much longer because they consider that ship emissions could impact urban air quality from tens of miles from the coast. However, the hotelling phase represents generally the largest fraction of total emissions in port: NOx 90.1%; PM2.5 78.0% and SOx 88.5% (Papaefthimiou et al., 2016). These percentages can vary depending mainly on time at hotelling and length of manoeuvring phase. Data on traffic reported are also often quite different. For passenger ships data can be: number of passengers, calls, hour at hotelling. For commercial ships: calls, tons of goods or TEU are normally used. Data on special purpose vessels like tugs, military, coast guard ships are rarely given. To analyse this large but inhomogeneous mass of data, passenger ships has been divided in cruise and others while commercial ships are considered as a single category. Special purpose ships are not considered since their emissions are generally not relevant. Data on traffic analysed are: calls, passengers, hours at hotelling, tons per year. Emissions during navigation are evaluated for a length corresponding to navigation in port. If a higher length was considered by the authors it was reduced as necessary.

Table 20. List of ports, calendar time, methodologies, type of the ships, load and emission factors datasources of the reviewed studies organized for geographic area

Area	References	Ports	Calendar Time	AIS	Meth.s	Ships	Sources	
							Load Factor	Emission factor
MS[a]	Tichavska and Tovar (2015a) and Tichavska et al. (2017)	Las Palmas	2011	Yes	FC[b]	All	Jalkanen et al. (2009, 2012)	Agrawal et al. (2008), Agrawal et al. (2010), Petzold et al. (2008), Moldanová et al. (2010), Sarvi et al. (2008a), Sarvi et al. (2008b) and Buhaug et al. (2009)
	Tzannatos (2010a)	Piraeus	June 2008 - May 2009	No	LF[c]	P[d]	Obtained from a survey	ENTEC (2002), ENTEC (2007)
	Maragkogianni et al. (2015)	5 Greek Ports	2013	No	LF	C[e]	Tzannatos (2010a)	ENTEC (2002), ENTEC (2007)
	Papaefthimiou et al. (2016)	18 Greek Ports	2013	No	LF	C	Tzannatos (2010a)	ENTEC (2002), ENTEC (2007)
	De Melo Rodriguez et al. (2017)	Barcelona	2015	No	FC	C		IMO (2009), IMO (2014), ENTEC (2002) and EIAPP certificates from ship owners

	Dragović et al. (2018)	Kotor, Dubrovnik	2012, 2013, 2014	No	LF	C	Tzannatos (2010a), Tzannatos (2010b) ICF (2009)	ICF (2009)
	Saraçoğlu et al. (2013)	Izmir	2007	No	LF	All	NR[f]	ENTEC (2005)
	Kilic and Tzannatos (2014)	Piraeus	2006	No	LF	CO[g]	ENTEC (2005)	ENTEC (2005)
	CAIMANs (2015)	Barcelona, Genoa, Marseille, Venice, Thessaloniki	2013	No	LF	P	EEA (2013)	EEA (2013), Cooper and Gustafsson (2004), Agrawal (2010)
	APICE (2013)	Barcelona,Venice, Thessaloniki	2013	No	LF	All	EEA (2006, 2009)	EEA (2006, 2009), Cooper and Gustafsson (2004)
	APICE (2013)	Genoa, Marseille	2013	No	FC	All		Trozzi and Vaccaro (1998)
	Murena et al. (2018)	Naples	2016	No	LF	C	EEA (2016) integrated with real data	EEA (2016)
AO[h]	Nunes et al. (2017)	Leixoes, Setubal, Sines	2013, 2014	No	LF	All	EEA (2016)	EMEP/EEA (2016), ENTEC (2002), ICF (2009), IVL (2004)
BS[i]	Alver et al. (2018)	Samsun	2015	No	LF	All	Obtained by consulting the port guide captain	ENTEC (2005)

	Deniz and Kilic (2009)	Ambarli	2005	No	FC	All		Trozzi and Vaccaro (1998); Endresen et al. (2003)
	Kiliç and Deniz, (2010)	Izmit Gulf	2005	No	LF	All	NR	ENTEC (2005)
CS[j]	Berechman and Tseng (2012)	Kaohsiung	2010	No	LF	CO	Joseph et al. (2009), Starcrest Consulting Group (2008)	Deniz et al., (2010), Dolphin and Melcer (2008), D'Angiola (2010), ENTEC (2007), Forkenbrock et al. (1999), Kuhns et al. (2004), Lee et al. (2010)
	Yau et al. (2012)	Hong Kong	2007	Yes	LF	All	PL[k], ICF (2006)	ENTEC (2002), Llyod's Register (1995), ICF (2006)
	Ng et al. (2013)	Hong Kong	2007	Yes	LF	All	PL, Starcrest Consulting Group (2008)	ICF (2009), Starcrest Consulting Group (2009)
	Song (2014)	Yangshan	2009	Yes	LF	CO	PL, Starcrest Consulting Group (2010)	ENTEC (2002), CARB (2006), IVL (2004), ICF (2009)
	Chen et al. (2016)	Tianjin	2014	Yes	LF	All	PL, ENTEC 2002, ENTEC 2010, The chamber of shipping of British Columbia 2007	Fan et al. (2016), Cooper and Gustaffson (2004), ICF (2009), USEPA (2009), Goldsworthy and Goldsworthy (2015)

	Chen et al. (2017)	Qingdao	2014	Yes	LF	All	PL, Starcrest Consulting Group (2014)	ENTEC (2002), ICF (2009), IVL (2004), Starcrest Consulting Group (2009)
	Tichavska et al. (2017)	Hong Kong	2011	Yes	FC	All	Jalkanen et al. (2009, 2012)	Agrawal et al. (2008), Agrawal et al. (2010), Petzold et al. (2008), Moldanová et al. (2010), Sarvi et al. (2008a), Sarvi et al. (2008b) and Buhaug et al. (2009)
NS[l]	Saxe and Larsen (2004)	Copenhagen, Elsinore, Koge	2001	No	LF	All	No reference	Oxbol and Wismann (2003a, 2003b)
	Tichavska et al. (2017)	St. Petersburg	2011	Yes	FC	All	Jalkanen et al. (2009, 2012)	Agrawal et al. (2008), Agrawal et al. (2010), Petzold et al. (2008), Moldanová et al. (2010), Sarvi et al. (2008a), Sarvi et al. (2008b) and Buhaug et al. (2009)

[a] MS – Mediterranean Sea
[b] FC – Fuel consumption
[c] LF – Load Factor
[d] P – Passenger Ships
[e] C – Cruise Ships
[f] NR – Not Reported
[g] CO – Commercial Ships
[h] AO – Atlantic Ocean
[i] BS – Black Sea
[j] CS – Chinese Sea
[k] PL – Propeller Law
[l] NS – North Sea

In Figures 27-35 annual emissions (t/year) of NOx, SO_2 and PM10 are reported for the ports studied divided per vessel categories: cruise, "passenger ships other than cruise" and commercial. Absolute values vary in a broad range depending on the specific traffic of each port. As an example for cruise ships NOx and SO_2 emissions range from 102 t/y to 955 t/y and 5 to 900 t/y respectively, corresponding to Las Palmas port (Tichavska et al., 2015a), (Tichavska et al., 2017) and Barcelona port (De Melo Rodriguez et al., 2017); while PM10 emissions range from 2 t/y to 94 t/y corresponding to Copenhagen port (Saxe and Larsen, 2004) and Barcelona port (De Melo Rodriguez et al., 2017). For "passenger ships other than cruise" the minimum and the maximum emissions of NOx are 20 t/y and 1300 t/y calculated at Hong Kong and Marseille, for SO_2 the range is 3 t/y to 405 to/y in the same ports; while for PM10 the range is between 1 t/y and 80 t/y in the same ports. For commercial ships NOx and SO_2 emissions range are calculated in the ports of Koge (Saxe and Larsen, 2004) and Tanjin (Chen et al., 2016) NOx emissions range is from 30 t/y to 22822 t/y and SO2 emissions range is between 11 t/year and 14785t/y, while for PM10 the range is 1 t/y to 1836 t/y in Koge (Saxe and Larsen, 2004) and Qingdao (Chen et al., 2017).

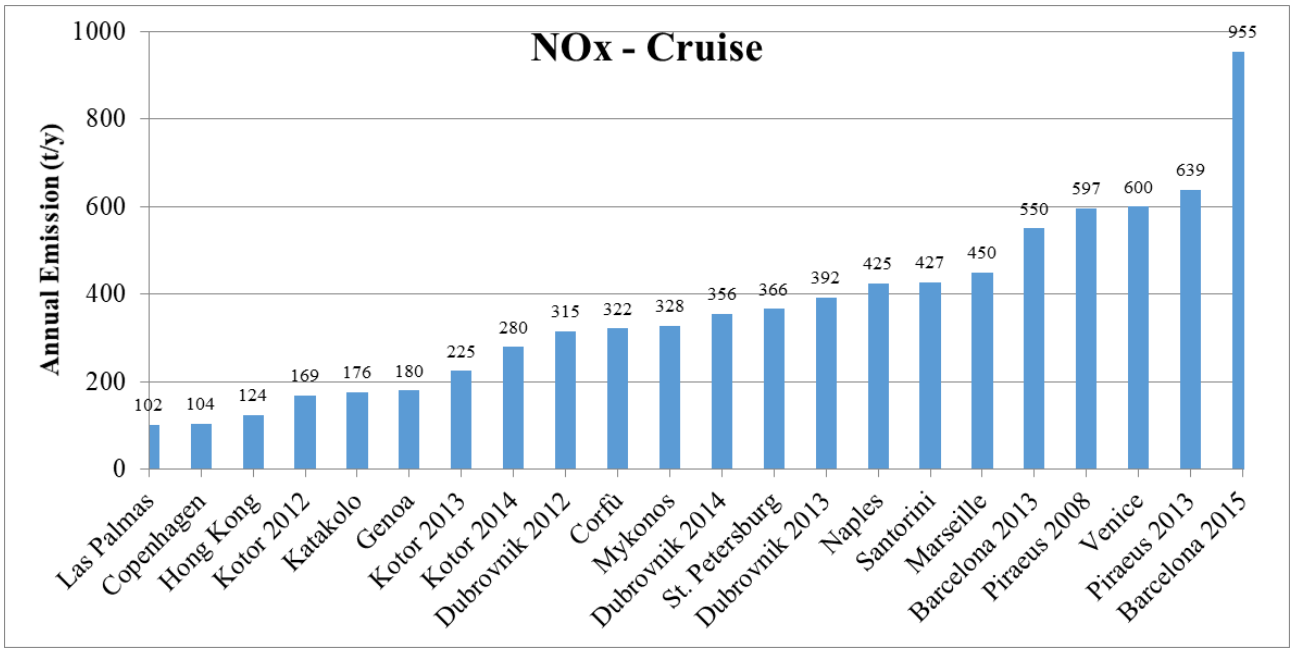

Figure 27. NOx emissions of cruise ships for all ports in the reviewed studies.

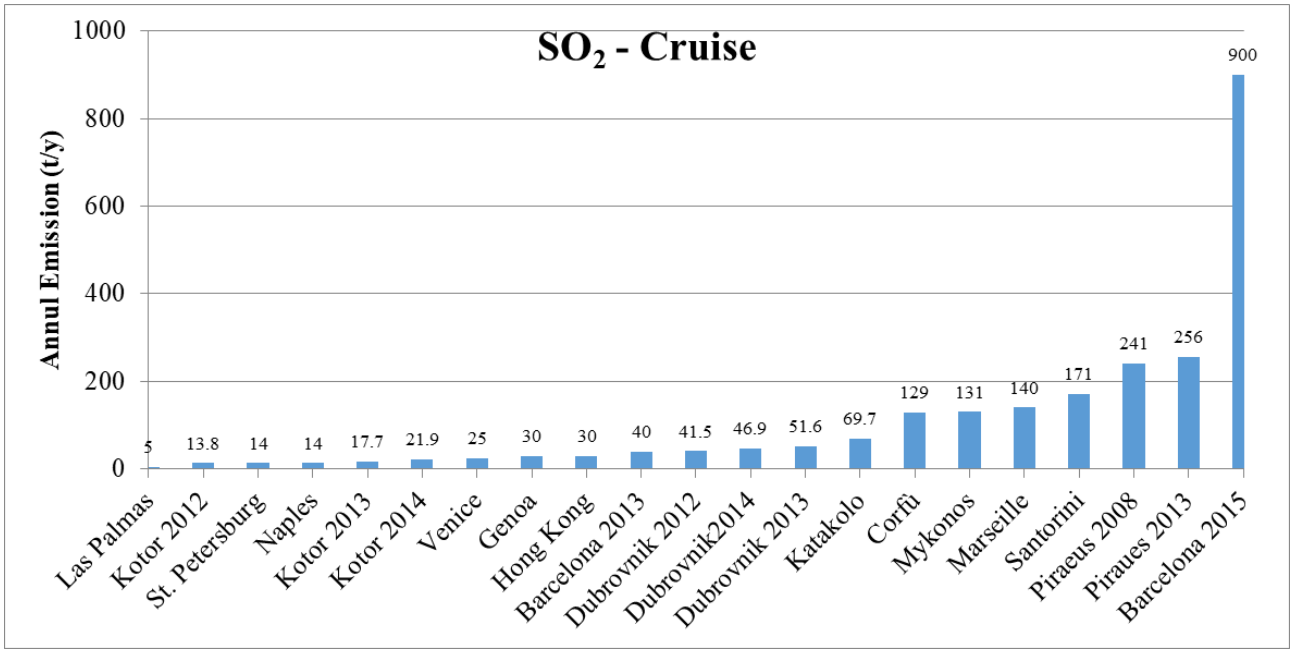

Figure 28. SO_2 emissions of cruise ships for all ports in the reviewed studies.

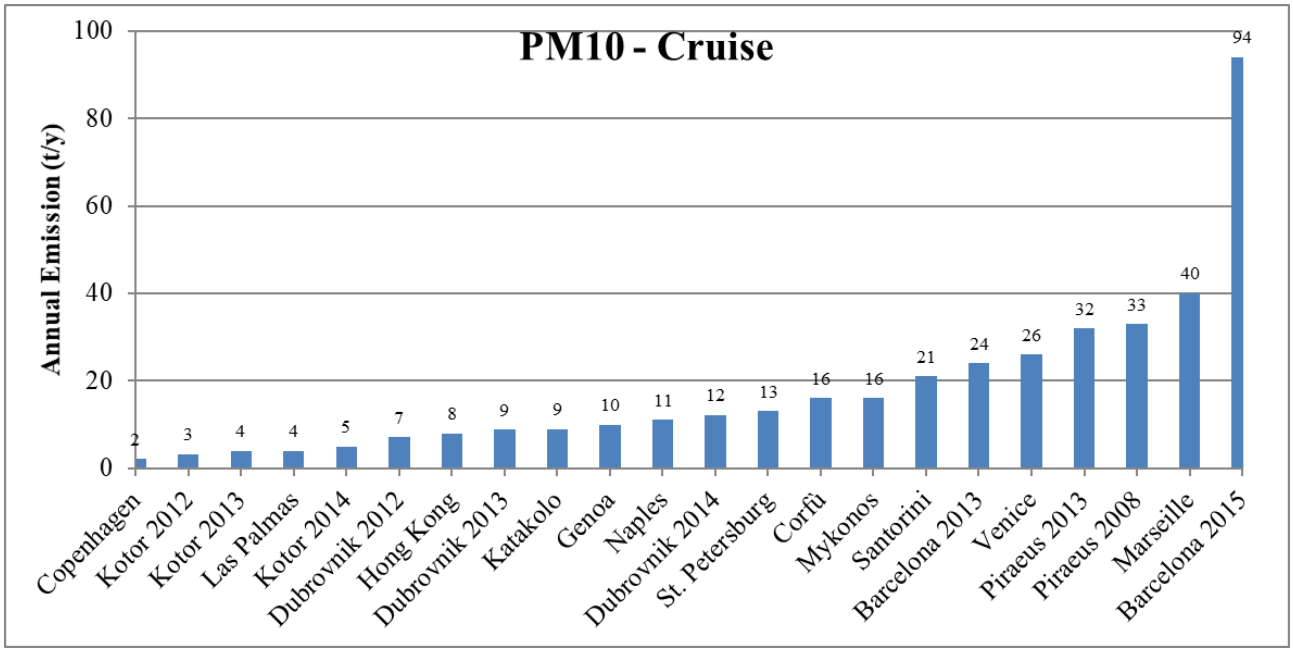

Figure 29. PM10 emissions of cruise ships for all ports in the reviewed studies.

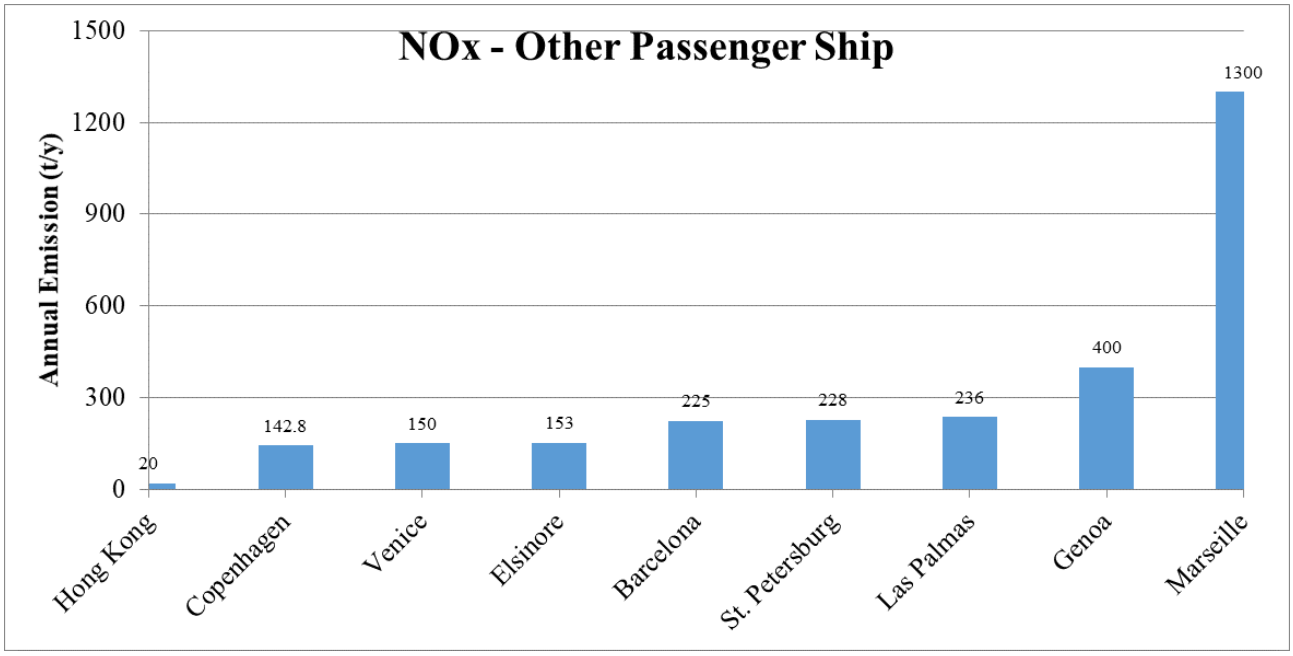

Figure 30. NOx emissions of other passenger ship for all ports in the reviewed studies.

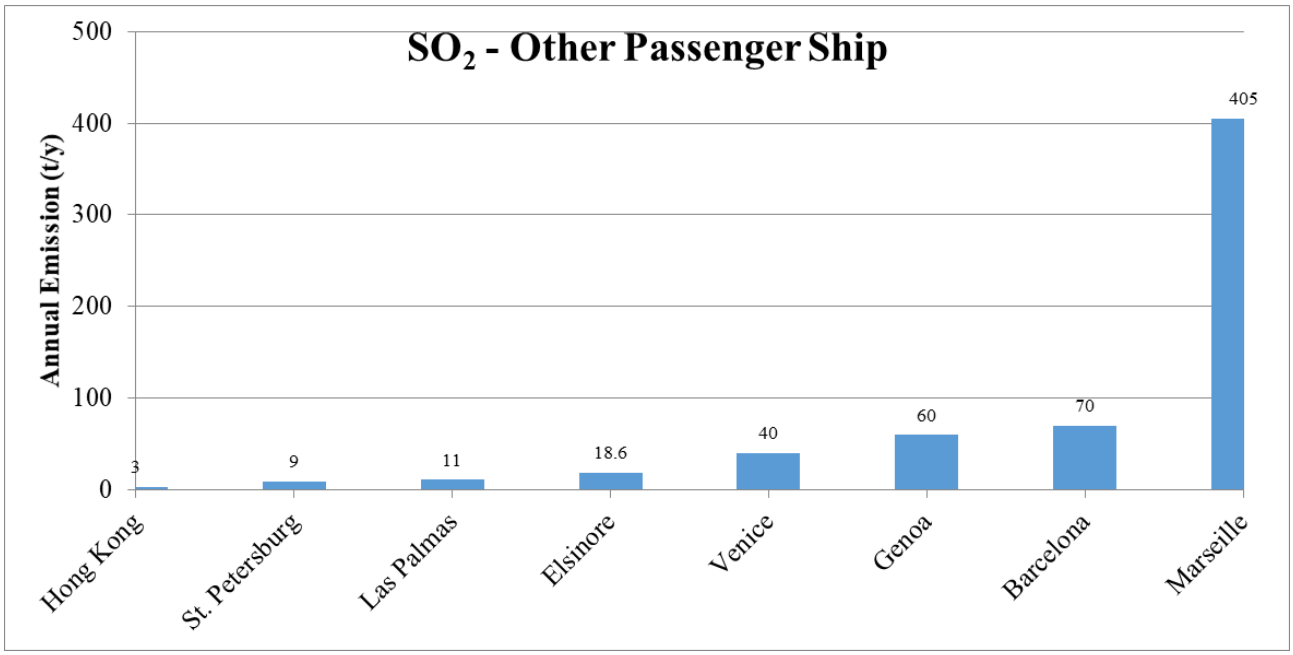

Figure 31. SO_2 emissions of other passenger ship for all ports in the reviewed studies.

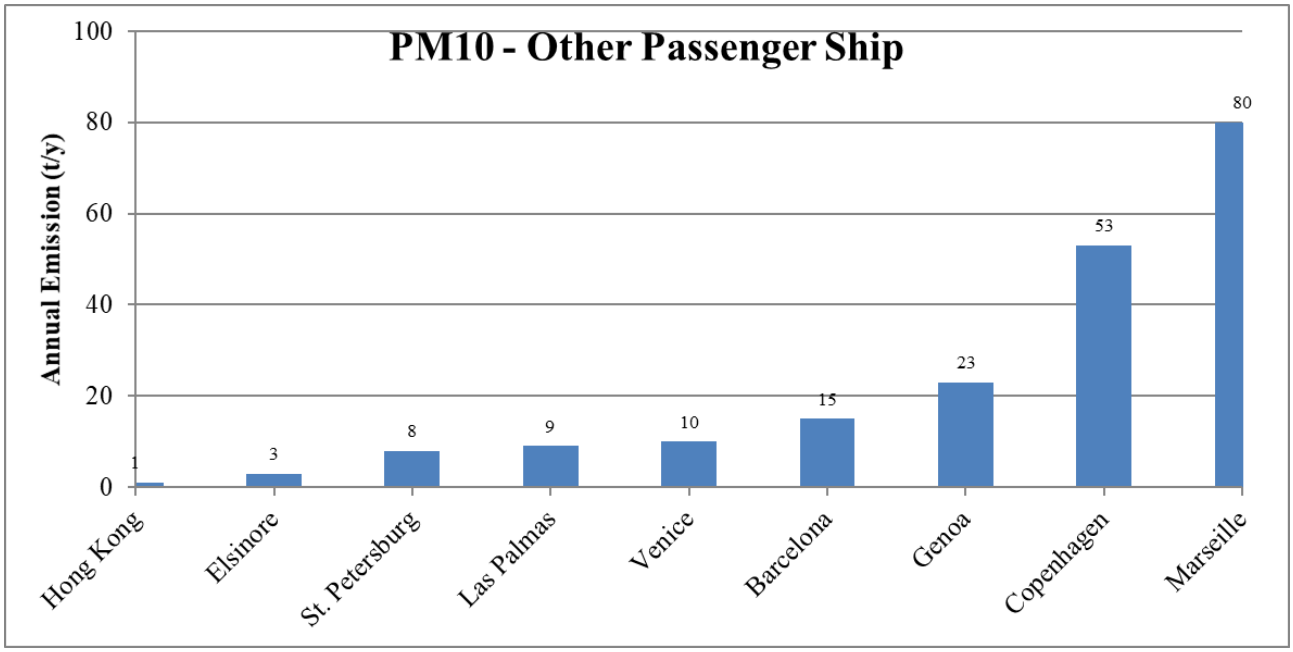

Figure 32. PM10 emissions of other passenger ship for all ports in the reviewed studies.

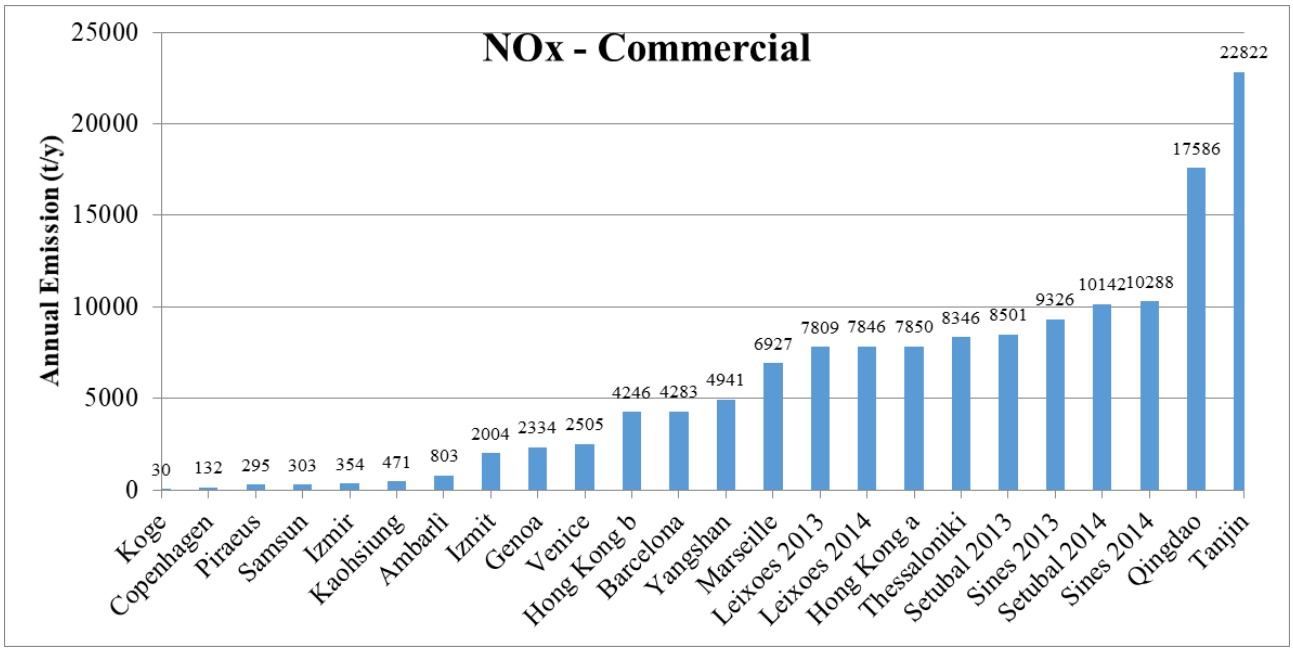

Figure 33. NOx emissions of commercial ship for all ports in the reviewed studies.

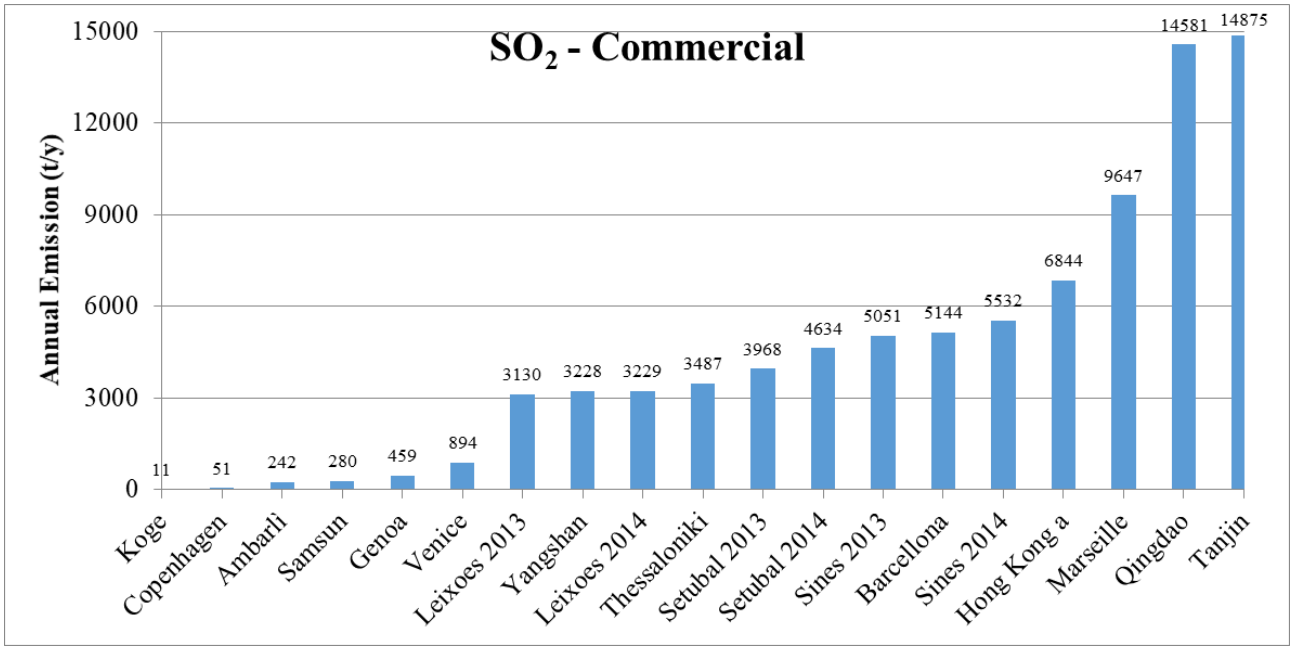

Figure 34. SO_2 emissions of commercial ship for all ports in the reviewed studies.

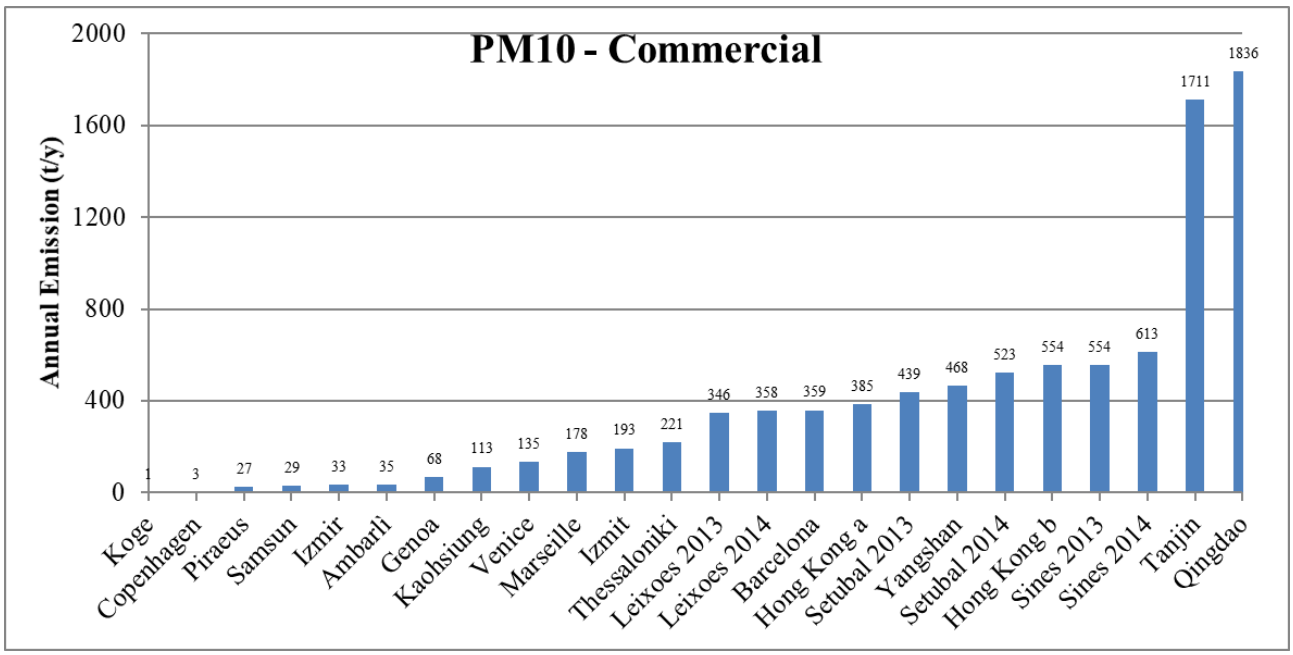

Figure 35. PM10 emissions of commercial ship for all ports in the reviewed studies.

4.4. Correlation of ship emissions in ports with data of ship traffic

Data of ship emissions for each of the three categories (cruise, passenger ships other than cruise and commercial) and for different phases of activity (hotelling, maneuvering and total) are correlated with data of traffic. For the correlation SO_2 emissions were excluded because they strictly depend on the sulfur content in the fuel.

4.4.1 Cruise Ships

Figure 36 shows the correlations between cruise ship emissions against the number of passengers. Data of NOx and PM10 are reported respectively on the left and on the right diagrams. The graphs also show the interval of confidence lines ± 25% and ± 50%. Data comes from 8 different studies concerning 20 ports, all in the Mediterranean area. Five studies (Tzannatos, 2010), (CAIMANs, 2015), (Papaefthimiou et al., 2016), (Dragović et al., 2018), (Murena et al., 2018) calculate the engine energy output, corresponding to each activity phase, from data of MCR (maximum continuous rated) engine power applying a LF (load factor). Sources of data of LFs are in Table 21. De Melo Rodriguez et al., (2017) use real data to estimate fuel consumption in function of the actual power applied in the different phases (reported as square in Figure 36). Generally, data show a limited spread with some points outside ± 25 % and only few outside ± 50%. The spread is higher in the maneuvering phase and lower if total emissions are considered. Focusing on the hotelling phase, the results are that 65 % of points for NOx and 18% for PM10 lie within the ±25% CI, while 88% for NOx and 59% for PM10 of values are outside the ±50% CI. Emissions of PM10 at Greek ports of Piraeus, Mykonos, Corfù and Santorini (circle in Figure 36 up) are above the confidence line +50%. Higher emission rates evaluated depend on higher load factors used (Table 1 in Papaefthimiou et al., 2016) because authors take in account the effect of yearly season on LFs. In the project CAIMANs for the ports of Barcelona, Genoa, Marseille and Venice (rhombus in Figure 36 up) the authors followed the EMEP guidelines using the gross tonnage to evaluate emissions. Using a fuel-based methodology for the Barcelona port De Melo Rodriguez et al. (2017) obtain data (square in Figure 36 up) about on +25% CI line for NOx but out of +50% CI line for PM10.

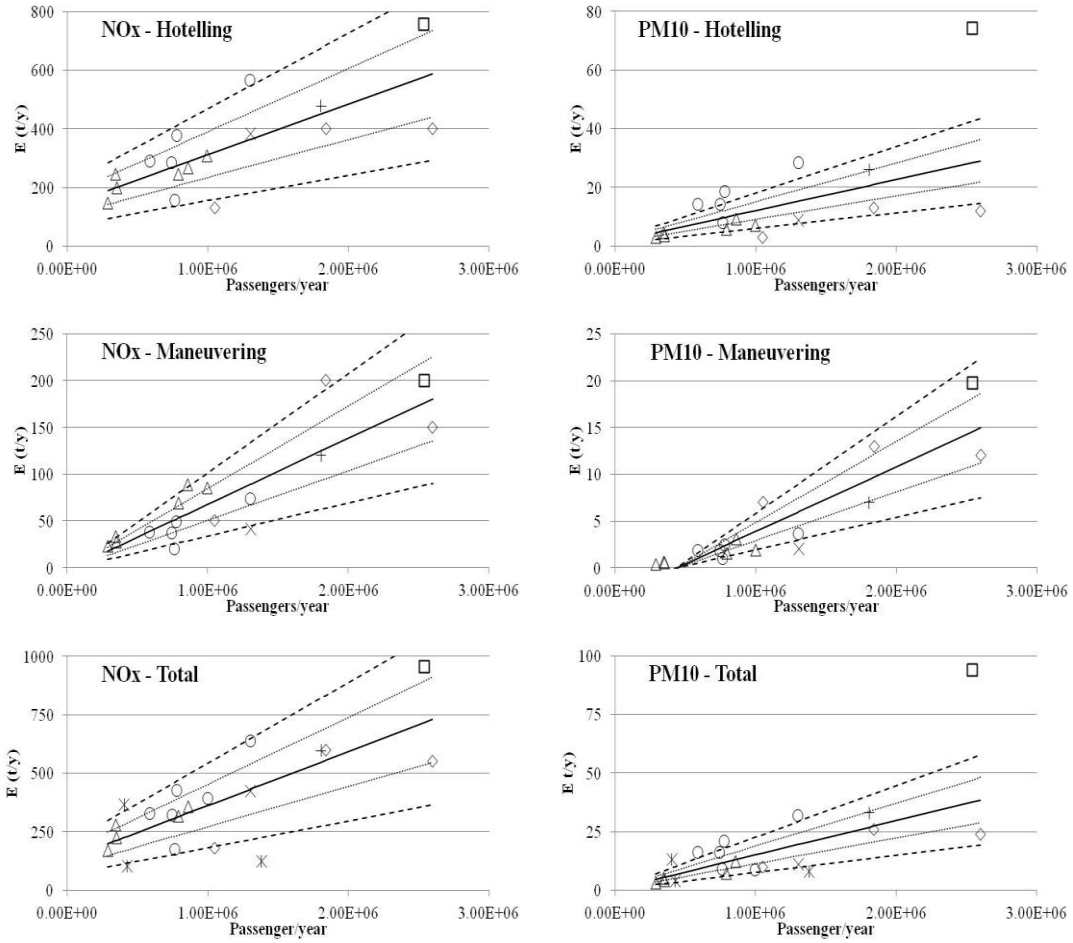

Figure 36. Cruise ship emissions against number of passengers: hotelling (up); manoeuvring (middle); total (bottom).

Manoeuvring phase (Figure 36 middle) shows a higher spread of data. This mainly depends on the differences among the ports in regard to the length of the manoeuvring routes and, therefore, of the corresponding time. However, emissions in this phase are lower than during hotelling, and therefore less relevant. In the diagrams of total emissions (Figure 36 bottom), data from ports of Las Palmas, St Petersburg and Hong Kong are added (Tichavska et al., 2017). In this case the correlations get better. In fact, 55% of data for NOx and 25% for PM10 are within the ±25% CI, and 80% of data (NOx) and 70% (PM10) within the ±50% CI. Concerning total NOx emissions, data of the Genoa port (rhombus) are on the border of -50% CI. This is probably due to the limited number of hours spent in the two phases (hotelling + manoeuvring) by cruise ships in Genoa in one year (CAIMANs, 2015). In fact, if compared with data of Dubrovnik (Dragović et al., 2018) in correspondence to a similar traffic of passengers, cruise ships spent about 3000 hours in Genoa compared to 7300 hours in Dubrovnik

(Dragović et al., 2018). Concerning PM10, the emissions of the Barcelona port, if a fuel based methodology is adopted (De Melo Rodriguez et al., 2017) fall outside the +50% IC (square in Figure 36 bottom), else using a MCR+LF methodology (CAIMANs, 2015) data is inside the -50% of CI interval (rhombus in Figure 36 bottom). Data of greek ports of Mykonos, Santorini and Piraeus are slightly above the +50% CI for the reasons already cited.

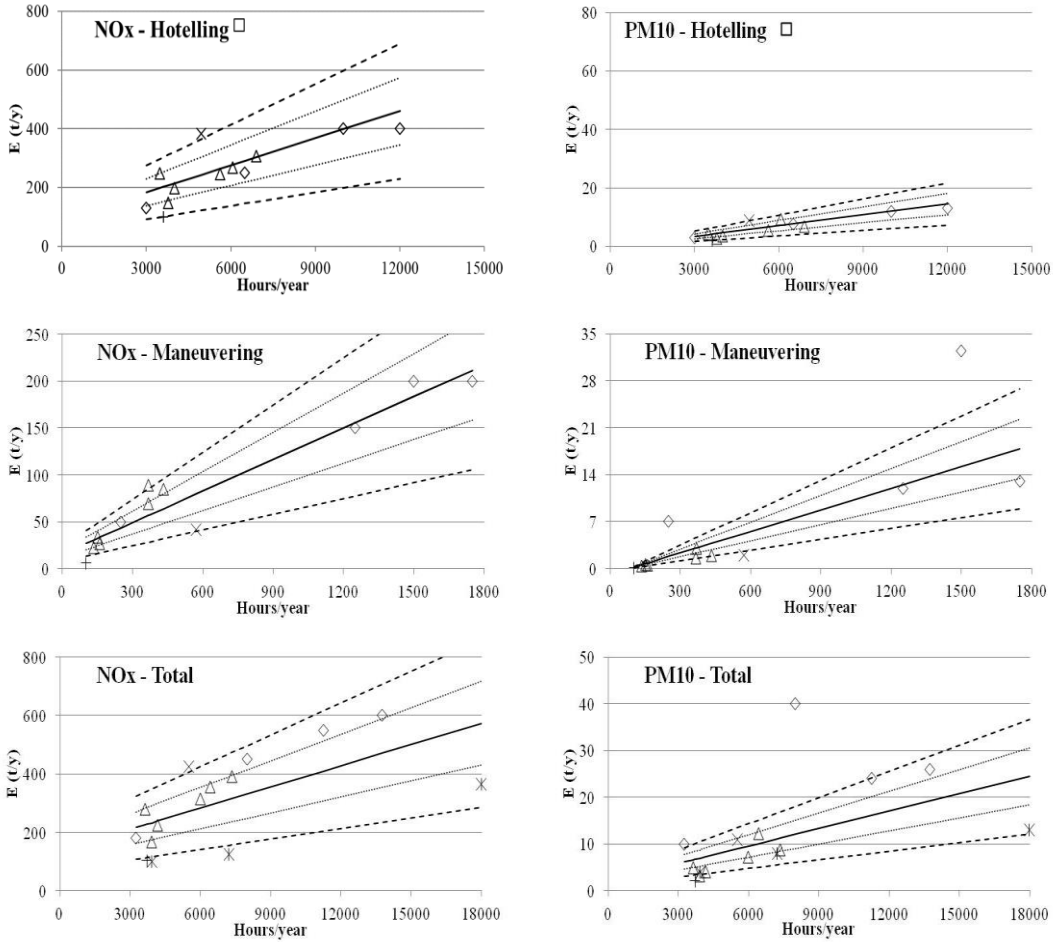

Figure 37. Cruise ship emissions against hours of activity: hotelling (up); manoeuvring (middle); total (bottom).

Figure 37 shows the correlations of cruise ship emissions (t/year) for NOx (left) and PM10 (right) with the time spent in each phase (hours/year). Data come from 6 different studies concerning 15 ports. Analyzing the correlations with hours spent in hotelling, it results that 62% of points for NOx and 54% for PM10 lie within the ±25% CI, while 77% both for NOx and PM10 of values are in the ±50% CI. Data relating to the port of Barcelona (square in Figure 37 up) are considerably higher than in the other ports. In this case the authors (De Melo Rodriguez et al., 2017) used a fuel-based

method, while others studies (Saxe and Larsen, 2004), (Tzannatos, 2010), (CAIMANs, 2015) (Dragović et al., 2018) and (Murena et al., 2018) used a MCR-LF method. Data for the port of Copenhagen for NOx emission (symbol + in Figure 37 up) is below the -25% IC. This is partially due to the lower emission factors used (Saxe and Larsen, 2004) 12 [g/kWh] for NOx, compared to those adopted in other ports: 12.4 [g/kWh] (Dragović et al., 2018) – 13.9 [g/kWh] (Tzannatos, 2010). Emissions at hotelling in the port of Naples (Murena et al, 2018), symbol X in Figure 37 up, are above the +50% CI both for NOx and PM10. In this case EMEP methodology was integrated with real data of engine power determining a higher power applied at hotelling. Correlations of maneuvering emissions against time is good for NOx but relatively low for PM10 (17% of values within ±25% CI). Data of emissions of PM10 during maneuvering for the port of Marseille (rhombus in Figure 37 middle) is much higher compared to the other ports (33 t/y in correspondence of 1500 hours/y). This is a consequence of the assumption (CAIMANs, 2015) of the use of BFO during maneuvering with a emission factor for PM10 equal to 0.8 [g/kWh] more than double the average emission factor used for other ports. The correlations between total emissions (Figure 37 bottom) with total time spent in port (hotelling + maneuvering) are quite high with 40% of data for NOx and 27% for PM10 within ±25% CI and 73% of data (both for NOx and PM10) within the ±50% CI.

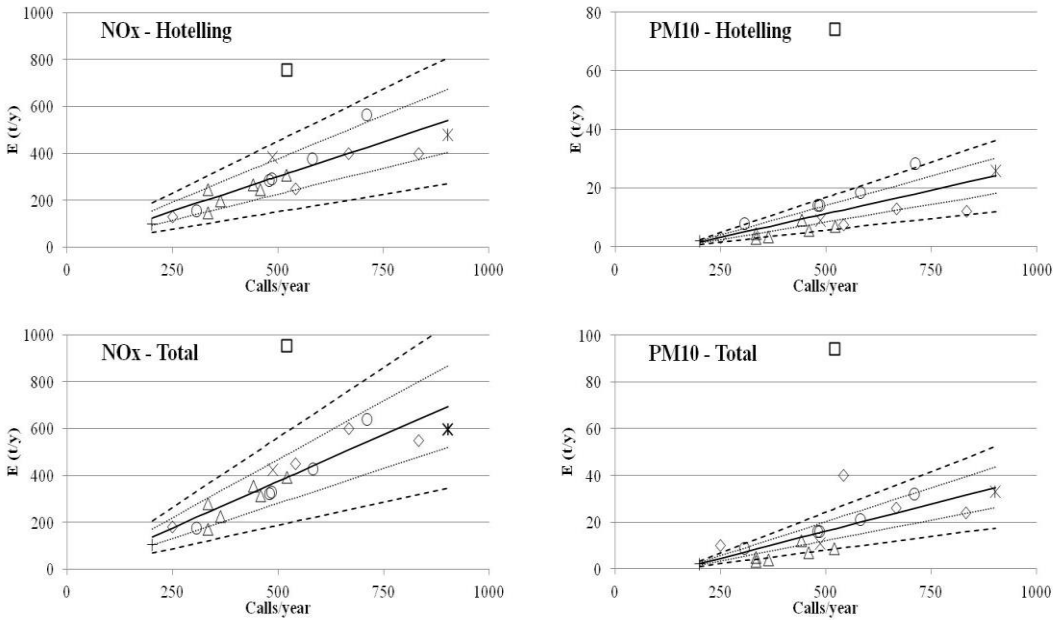

Figure 38. Cruise ship emissions against calls: hotelling (up); total (bottom).

Finally, cruise ships' emissions are correlated with calls number per year (Figure 38). In this case correlations in maneuvering phase are not reported because the spread is very high. Focusing on correlations between emissions at hotelling with number of calls (Figure 38 up), it results that 79% of points for NOx and 32% for PM10 are in the ±25% CI. The correlations get better when total emissions are considered. In fact, 89% of NOx data and 47% of PM10 are within ±25% CI, and 95% of data for NOx and 68% for PM10 are within the ±50% CI. Data of Barcelona (NOx and PM10) and of Marseille (PM10) fall outside the +50% CI (respectively square and rhombus in Figure 38 bottom) for the reasons above reported.

The summary of all regression equations for cruise ships is reported in Table 21 with: R^2, number of points for regression and degree of reliability. It has been assumed: i) "high" reliability of the correlation equation if $R^2 \geq 0.6$ and n° points ≥ 10; ii) "medium" when $R^2 \geq 0.4$ and n° points $5 \leq n < 10$; iii) "low" in all other cases. Table 21 shows how correlations of cruise ship emissions with traffic data are generally quite good and characterized by "high" or "medium" reliability. This is not surprising because "cruise ships" is a quite homogeneous and well-studied ships category with many data available. However, in the case of PM10 it must be observed the presence of a "outlier" when a different methodology based on fuel consumption (De Melo Rodriguez et al., 2017) is adopted. It would be necessary to have more data to realize whether results are really different from those coming from the application of load factor methodologies. The same effect is not observed for NOx emissions.

Table 21. Summary of regression equations for cruise ships.

Phase	Traffic data	Pollutant	Correlation equations	R^2	Number of points	Reliability
Hotelling	Passengers	NOx	$140 + 1.72 \cdot 10^{-4}\ P$	0.57	17	Medium
		PM10	$1.46 + 1.06 \cdot 10^{-5}\ P$	0.40	17	Medium
	Hours	NOx	$91.9 + 3.07 \cdot 10^{-2}\ H$	0.70	13	High
		PM10	$-2.18 + 1.22 \cdot 10^{-3}\ H$	0.86	13	High
	Calls	NOx	$6.20 + 5.90 \cdot 10^{-1}\ C$	0.81	19	High
		PM10	$-4.81 + 3.21 \cdot 10^{-2}\ C$	0.65	19	High

Manoeuvring	Passengers	NOx	$-2.84 + 7.06 \cdot 10^{-5} P$	0.77	17	High
		PM10	$-3.03 + 6.91 \cdot 10^{-6} P$	0.80	17	High
	Hours	NOx	$15.7 + 1.12 \cdot 10^{-1} H$	0.98	12	High
		PM10	$-0.87 + 1.07 \cdot 10^{-2} H$	0.66	12	High
Total	Passengers	NOx	$132 + 2.33 \cdot 10^{-4} P$	0.57	20	Medium
		PM10	$0.51 + 1.46 \cdot 10^{-5} P$	0.52	20	Medium
	Hours	NOx	$138 + 2.42 \cdot 10^{-2} H$	0.42	15	Medium
		PM10	$2.13 + 1.24 \cdot 10^{-3} H$	0.58	15	Medium
	Calls	NOx	$-22.1 + 7.95 \cdot 10^{-1} C$	0.89	19	High
		PM10	$-7.14 + 4.66 \cdot 10^{-2} C$	0.62	19	High

P is number of passengers for year [#/year]; H is time spent in each phase for year [hours/year] and C is number of calls per year [calls/year].

4.4.2. "Other than cruise" passenger ships

Passenger ships different from cruise are lumped in a single category named "other passenger ships". Data on emissions from this category of vessels are scarce.

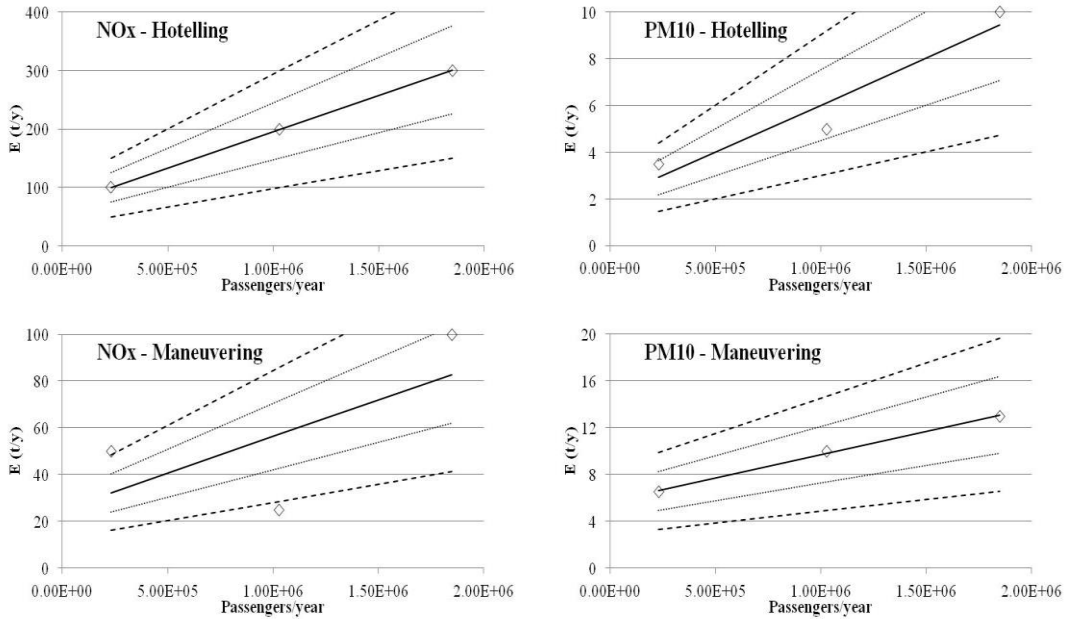

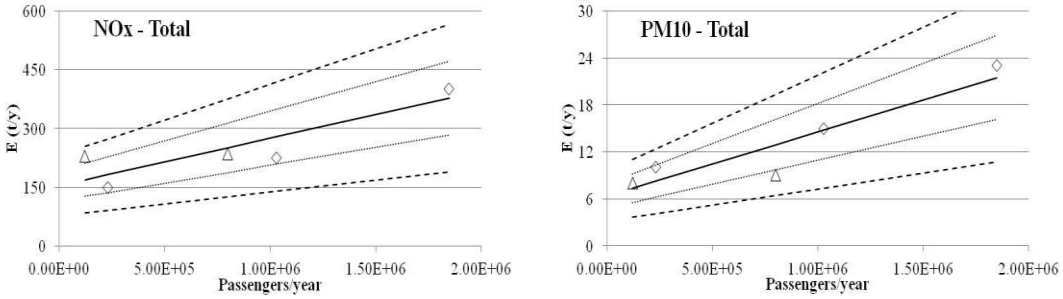

Figure 39. Other passenger ships emissions against number of passengers: hotelling (up); total (bottom).

Figure 39 shows the regressions between emissions and the number of passengers per year. Data are available for each phase from a single reference (CAIMANs, 2015) and only for three ports (Barcelona, Genoa and Venice) using EMEP/EEA methodology. Therefore, the correlations of emissions at hotelling are good both for NOx and PM10. On the contrary, emissions at manoeuvring show a high spread for NOx while a good correlation for PM10 (Figure 39 Middle). This depends mainly on the differences among the ports regarding the length of the manoeuvring routes (longer for Venice) and the sulfur content in the fuel used during navigation in port, higher in Genoa and Barcelona (CAIMANs, 2015). The correlations with total emissions include also the ports of Las Palmas and St. Petersburg (triangle in Figure 39). Data of Hong Kong (Passengers = $2.60 \cdot 10^7$, E= 20 t/y for NOx and 1 t/y for PM10) (Tichavska et al., 2017) are not reported in Figure 39 bottom because the emission is so low to seem unrealistic.

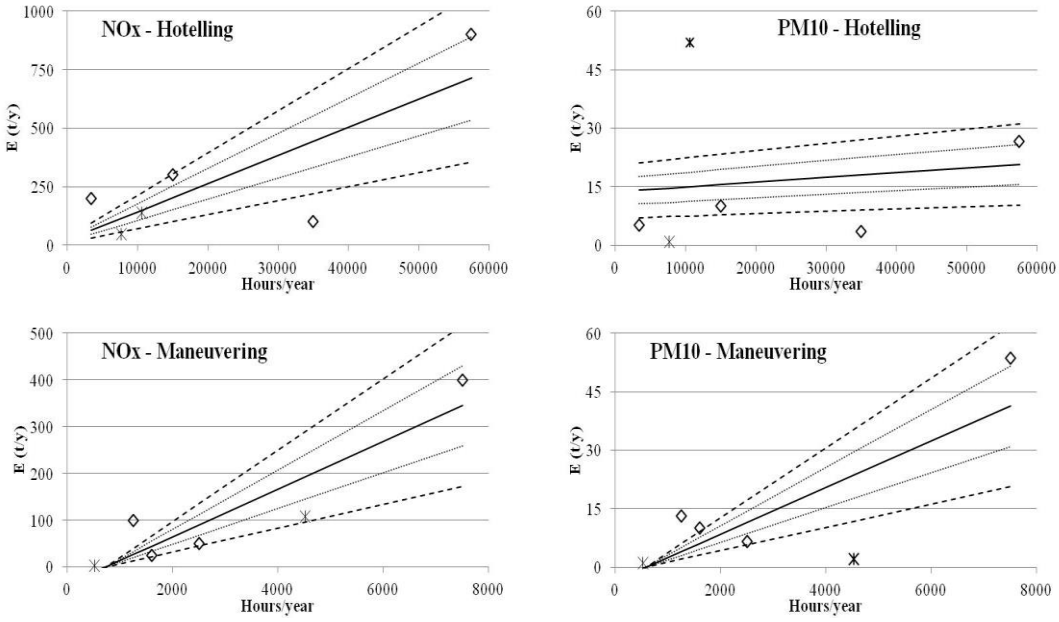

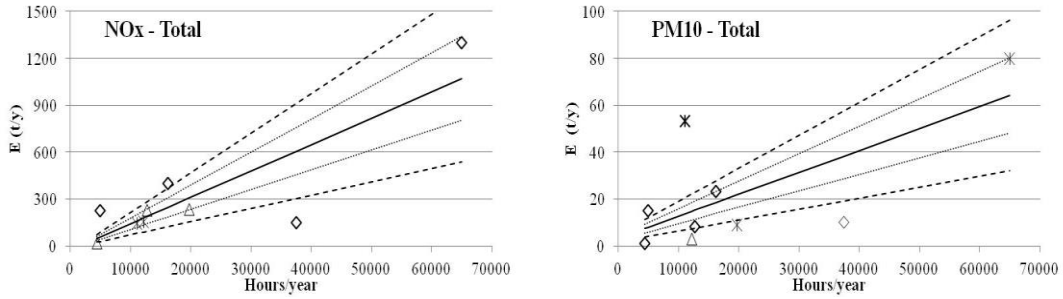

Figure 40. Other passenger ship emissions against hours of activity: hotelling (up); manoeuvring (middle); total (bottom).

Correlations of "other passenger ship" emissions (t/year) for NOx (left) and PM10 (right) with the time spent in each phase (hours/year) (Figure 40) include data from two different studies concerning 6 ports for hotelling and manoeuvring and from nine ports for the total. In some cases, the spread is very high (mainly for PM10 at hotelling and also as total) determining a high uncertainty. A reason of the uncertainty is that generally it is not specified the kind of ships included in the "other passenger ships" category. As an example, Saxe and Larssen (2004), for the ports of Copenhagen and Elsinore, and Tichavska et al. (2017), for the ports of Las Palmas, St. Petersburg and Hong Kong, have considered only ferries. On the contrary in CAIMANs (2015) no information are available about the kind of vessels included in "other passenger ships".

Table 22 shows the summary of all regression equations for "other than cruise" passenger ships. The main finding is that for this ship category the sample size is very limited. For this reason, the reliability of correlation equations is "low" or "medium". In some cases, only three data are reported. This is an insufficient sample size to make a correlation. For this reason, the reliability of the correlation is "low" even though $R^2 > 0.92$.

Table 22. Summary of regression equations for other passenger ships.

Phase	Traffic data	Pollutant	Correlation equations	R^2	Number of points	Reliability
Hotelling	Passengers	NOx	$71.9 + 1.24 \cdot 10^{-4}\ P$	1.0	3	Low
		PM10	$1.99 + 4.03 \cdot 10^{-6}\ P$	0.92	3	Low
	Hours	NOx	$22.0 + 1.20 \cdot 10^{-2}\ H$	0.63	6	Medium
		PM10	$13.7 + 1.22 \cdot 10^{-4}\ H$	0.63	6	Medium
Manoeuvring	Passengers	NOx	$26.0 + 3.12 \cdot 10^{-5}\ P$	0.44	3	Low
		PM10	$5.67 + 4.02 \cdot 10^{-6}\ P$	1.0	3	Low

	Hours	NOx	$-38.1 + 5.10 \cdot 10^{-2}\ H$	0.83	6	Medium
		PM10	$-3.48 + 5.98 \cdot 10^{-3}\ H$	0.62	6	Medium
Total	Passengers	NOx	$155\ + 1.15 \cdot 10^{-4}\ P$	0.83	5	Medium
		PM10	$6.32 + 8.29 \cdot 10^{-6}\ P$	0.85	5	Medium
	Hours	NOx	$-26.8 + 1.69 \cdot 10^{-2}\ H$	0.73	9	Medium
		PM10	$3.35 + 9.34 \cdot 10^{-4} H$	0.59	9	Medium

P is number of passengers for year [#/year]; H is time spent in each phase for year [hours/year].

4.4.3 Commercial ships

The last category examined is commercial ships. Several kinds of vessels belong to this class: dry bulk cargo, liquid bulk cargo, solid bulk cargo, container, general cargo, carrier, cargo Ro-Ro, fridge cargo, other cargo. Due to the high number of different vessels of commercial ships and the absence, in many cases, of specific traffic data for each kind of vessel it has been correlated emissions of the whole of commercial ships with data of traffic in terms of: tons of goods, hours at hotelling and number of calls.

Data of emissions in port are more limited with respect to cruise ships.

Figure 41 shows the correlations between emissions and tons of goods per year, left for NOx and right for PM10. Data comes from 6 different studies concerning 9 ports: Barcelona, Genoa, Marseille, Venice, Thessaloniki and Izmir in the Mediterranean area (Saraçoğlu et al., 2013), Samsun in the Black sea (Alver et al., 2018), and Tanjin and Qingdao in the Chinese Sea (Chen et al, 2016; Chen et al., 2017). All these studies calculate the engine energy output corresponding at each activity phase starting from data of MCR (maximum continuous rated) engine power and LF (load factor), two of these studies (Chen et al., 2016) and (Chen et al., 2017) use data from AIS. The main observation is the absence of data of ports with medium traffic of goods (from 1 to 3 $\cdot 10^8$ tons per year). The correlation with total emissions (Figure 41 bottom) includes also data of the ports of Barcelona, Genoa, Marseille, Venice reported in APICE (2013). Data of ports of Setubal, Leixoes and Sines in the Atlantic Ocean (Nunes et al., 2017a) are not reported in Figure 41 because emissions are very higher than the others.

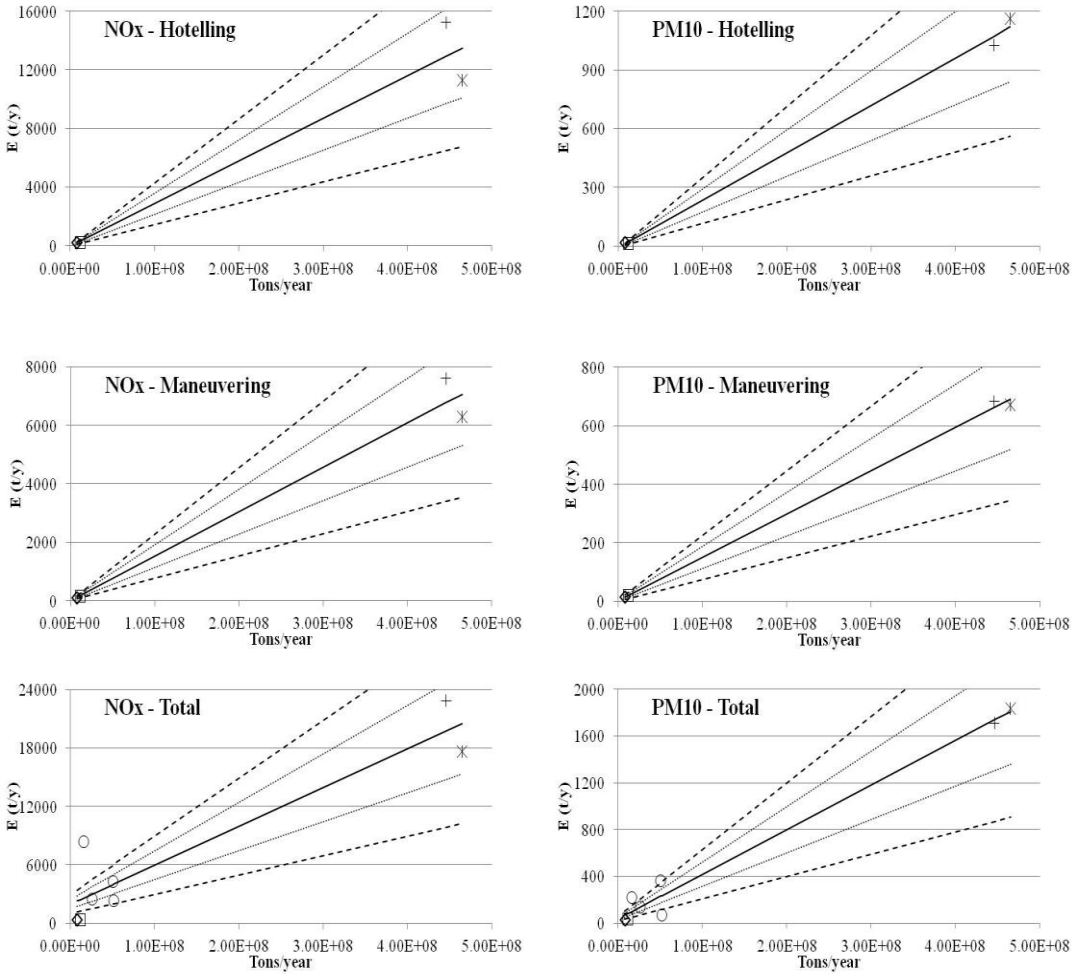

Figure 41. Commercial ship emissions against tonnes of goods: hotelling (up); manoeuvring (middle); total (bottom).

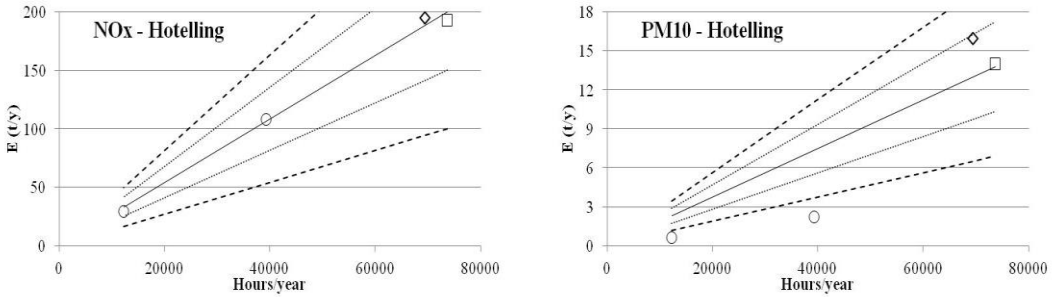

Figure 42. Commercial ships hotelling emissions against hours.

Data of emissions of commercial ships against time spent in each phase are very limited. Only data in function of time at hotelling are available from 4 ports: Copenhagen, Koge, Samsun and Izmir (Figure 42). Emissions of PM10 in the ports of Koge and Copenhagen (Saxe and Larsen, 2004) are below the -50% CI (circles in Figure 42). This is due to the emission factor 0.22 [g/kWh] used by Saxe and Larsen

(2004) lower than that adopted by Saraçoğlu et al. (2013) and Alver et al. (2018) which is in the range 0.9-1.7 [g/kWh] in function of the different vessels type.

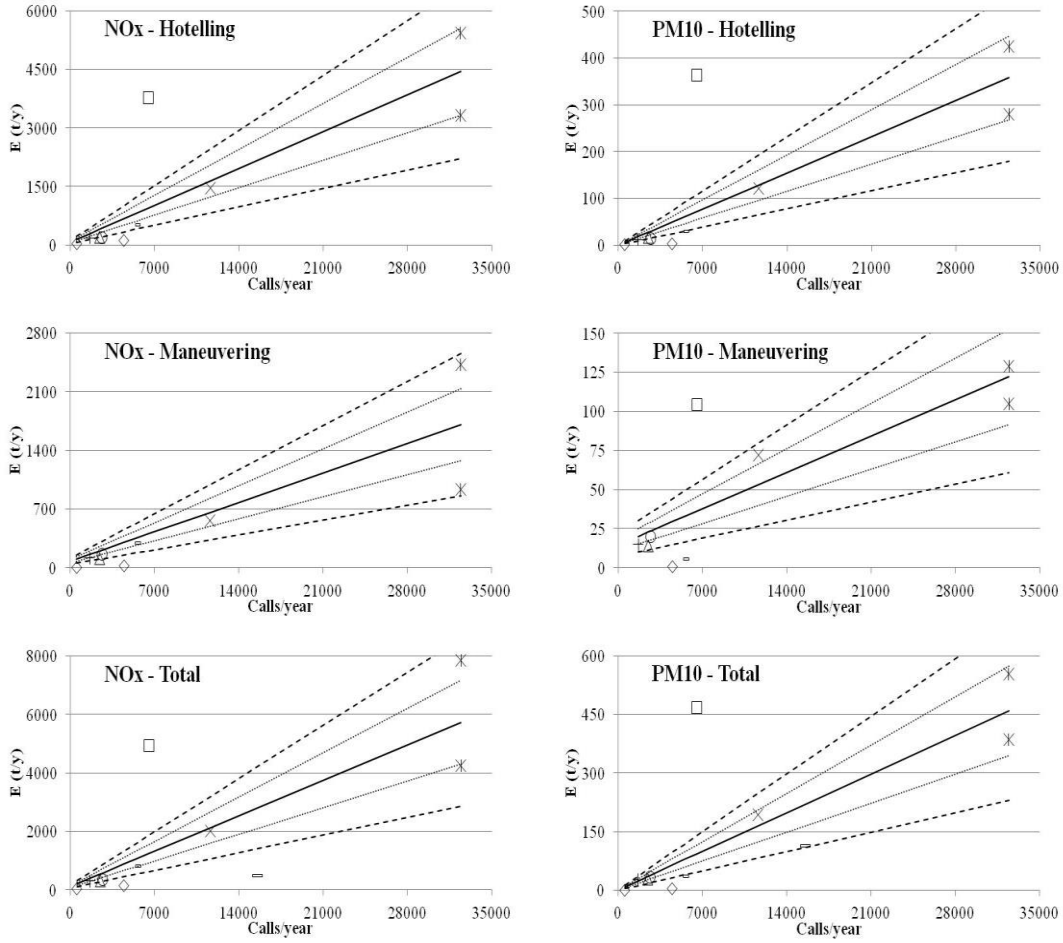

Figure 43. Commercial ship emissions against calls: hotelling (up); manoeuvring (middle); total (bottom).

Figure 43 shows the regression between emissions and number of calls for commercial ships. In this case data comes from 10 different studies concerning 10 ports. Data from Yangshan (Song, 2014) of the emissions in different phases are outside the +50% CI (square in Figure 43), while those from Copenhagen (rhombus) are below the -50% CI. This finding is in contrast with Figure 41 where emissions of NOx vs. hours at hotelling of Copenhagen's port are well correlated with those of other ports. The apparent discrepancy is due to the value of the ratio hours at hotelling per call in Copenhagen (8,8 hours per call) lower with respect to other ports (22- 36 hours per call).

The summary of all regression equations for commercial ships is reported in Table 23. In this case the sample size is intermediate between cruise and "other than cruise" ships. The reliability of correlations is in the most of cases "high" or "medium". This seems a good result considering the large inhomogeneity of the category with the presence of many different types of vessel. Correlations with "tons of goods" refer to only small or big ports with the absence of data from ports of medium dimension. For this reason, in all cases a "low" reliability has been assumed.

Table 23. Summary of regression equations for commercial ships.

Phase	Traffic data	Pollutant	Correlation equations	R^2	Number of points	Reliability
Hotelling	Tons	NOx	$2.91 \cdot 10^{-5}\, T - 49.3$	0.94	4	Low
		PM10	$2.43 \cdot 10^{-6}\, T - 10.2$	1.0	4	Low
	Hours	NOx	$2.71 \cdot 10^{-3}\, H$	0.96	4	Low
		PM10	$1.87 \cdot 10^{-4}\, H$	0.48	4	Low
	Calls	NOx	$1.35 \cdot 10^{-1}\, C + 73.0$	0.72	10	High
		PM10	$1.10 \cdot 10^{-2}\, C + 801$	0.67	10	High
Manoeuvring	Tons	NOx	$1.52 \cdot 10^{-5}\, T - 0.85$	0.97	4	Low
		PM10	$1.48 \cdot 10^{-6}\, T + 2.59$	0.99	4	Low
	Calls	NOx	$5.03 \cdot 10^{-2}\, C + 75.6$	0.65	10	High
		PM10	$3.31 \cdot 10^{-3}\, C + 14.6$	0.66	9	Medium
Total	Tons	NOx	$3.98 \cdot 10^{-5}\, T + 1.96 \cdot 10^{3}$	0.87	8	Medium
		PM10	$3.81 \cdot 10^{-6}\, T + 36.4$	0.98	8	Medium
	Calls	NOx	$1.73 \cdot 10^{-1}\, C + 112$	0.73	11	High
		PM10	$1.41 \cdot 10^{-2}\, C + 1.05$	0.85	11	High

T is tons of good for year [t/year]; H is time spent in each phase for year [hours/year]; C is number of calls per year [calls/year];

5. Assessment of the impact of ship emissions on air quality for the port of Naples

Over the past 20 years, interest in studying the impact of maritime emissions on air quality in cities and ports has been growing. Two approaches are typical: i) experimental measures of concentration of airborne pollutants (Contini et al., 2011; Prati et al., 2015; Merico et al., 2016; 2017; Murena et al., 2018a; Gobbi et al., 2020); ii) use of air quality models (AQMs) (Saxe and Larsen, 2004; Gariazzo et al., 2007; Deniz and Kilic, 2010; Aulinger et al., 2016, Merico et al., 2017, Murena et al., 2018b; Ramacher et al., 2020, Nunes et al., 2020, Tang et al., 2020). Furthermore, in recent years, the common use of an activity-based method using the Automatic Identification System (AIS) has admitted a very accurate way to obtain detailed information of ship specifications and operational data. However, most studies on the impact of shipping emissions on air quality using AIS data were performed with chemical transport models such as CAMx, WRF/Chem, and CMAQ (Aulinger et al., 2016; Marelle et al., 2016; Liu et al., 2017; Chen et al., 2018, Tang et al., 2020; Nunes et al., 2020). The port of Naples was investigated in two recent research papers (Murena et al., 2018 and Mocerino et al., 2020) in order to assess the impact only of emissions from ships passenger traffic on air quality.

The purpose of this chapter is to use a complete emissions inventory for the port of Naples as input in CALPUFF model to assess its impact on air quality on an urban scale and for one year. In performing the CALPUFF simulations the previous parametrization of dispersion coefficients was not considered, because more simulations with wind tunnel or CFD would be necessary in correspondence of different wind conditions. To consider different wind directions it is necessary to construct models of other parts of the urban area, downwind with respect to the port, and it is quite time consuming both for WT than for CFD tests. However, on the basis of previous analysis a certain knowledge of CALPUFF performances in the different configurations is known.

5.1 CALMET/CALPUFF model

The contribution of shipping to air quality in the urban area of Naples was assessed using the modelling chain composed by LANDUSE®, CALMET, CALPUFF, and CALPOST. The orography in the calculation domain was evaluated using the software LANDUSE®.

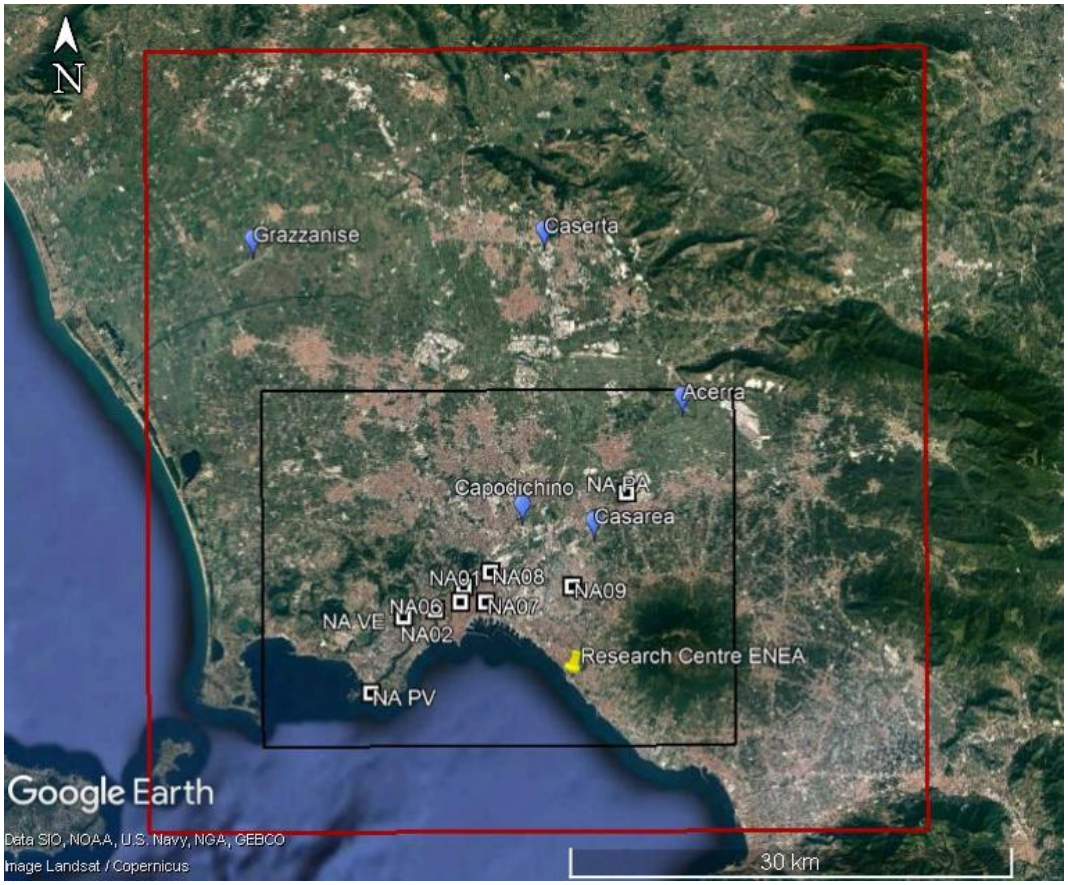

Figure 44. CALMET and CALPUFF domain and position of meteorological and air quality monitoring stations

The orographic file is included with i) surface files containing hourly average values of meteorological parameters measured at ground level at Naples Airport of "Capodichino", Caserta, Acerra, Grazzanise, and Casarea (Blu indicators in Figure 44), ii) the overwater sea file containing air-sea surface temperature, air temperature, wind speed, and wind direction, iii) vertical profiles of wind velocity, direction, and temperature from Airport of "Capodichino" input into CALMET producing the 3D weather file. Meteorological fields for the reference year 2018 were generated by the CALMET model for an approximately 3000 km^2 Cartesian grid subdivided into a 265

× 265 cell grid system with 200 m cell spacing (Figure 44, Black boundary); Ten vertical layers were defined in CALMET at the following heights: 0, 20, 40, 80, 160, 320, 640, 1200, 2000 and 3000 m.

In this study, in order to model the emission of ships in movements, each continuous route of every ship was discretized into a series of virtual geo-referenced sources, and it was assumed that, at these specific points, air pollutants were emitted at the time corresponding to the vessel's navigation. In this way, a point source emission file PTEMARB (i.e. a point source emissions file with arbitrarily varying emissions) of time-dependent emissions was created to simulate real emissions when ships are moving in the port. The PTEMARB.DAT file contains two types of records: i) time-invariant and ii) time-dependent. The time-invariant records contain for each source the stack height, diameter, and UTM coordinates. The time-dependent records contain the temperature of the funnel flue gas outlet (K), the outlet air velocity (m/s), and the pollutant emission rate (g/s) for each hour and for each source.

The CALPUFF domain was nested in the CALMET domain and is about 32 x 24 km^2. The computational domain is 160 × 120 cells, with 200 m cell spacing (Figure 44, red boundary).

Chemical transformation module RIVAD/ARM3 was adopted to simulate chemical reactions of NOx and SOx in the atmosphere (Morris et al., 1988). Ambient ozone monitoring data for 2018 from the ARPAC monitoring station were used to develop the hourly ozone monitoring data file (OZONE.DAT) for modelling. Since field data for NH_3 were not available, default values were assumed. Calculations were performed to evaluate the maximum of the 1-hour average concentrations, the maximum of the 24-hour average concentrations, the annual average concentrations of NO_2, SO_2, primary particulate matter (PPM), and secondary inorganic aerosols (SIA) resulting from emissions of NOx and from emissions of SO_2, and the sum of PPM and SIA below 10 μm (PM10).

5.2. Results

5.2.1 Analysis of air quality data

Air quality data provided by the Regional Environmental Agency (ARPAC - "Agenzia Regionale per la Protezione dell'Ambiente della Campania") were analyzed for a comparison with simulation results. Among all the monitoring stations located inside the study domain, those measuring continuously NO_2 and SO_2 (hourly average) and PM10 (daily average) are considered. They are NA01, NA02, NA06, NA07, NA08, NA09, Napoli Parco Virgiliano (NA-PV), Napoli via Epomeo (NA-VE), and Pomigliano d'Arco (NA-PA). Their location is indicated in Figure 44 (square indicators).

The analysis of the data from the monitoring stations in 2018 is reported in Table 24. The results show that, for SO_2, both the hourly limit (350 $\mu g/m^3$ should not be exceeded more than 24 times a year) and the daily limit (125 $\mu g/m^3$ not be exceeded more than three times per year) are respected. For NO_2, the annual limit was exceeded in four stations, NA06, NA07, NA08, and NA09, while the maximum hourly average concentrations of NO_2 were in accordance with the limit established by the EU for the protection of human health (200 $\mu g/m^3$ cannot be exceeded 18 times a year). The situation of PM10 was more critical: the number of exceedances of the daily limit (50 $\mu g/m^3$ cannot be exceeded more than 35 times a year) was exceeded at NA07 and NA-PA. The NA-PA monitoring site showed the highest number of exceedances (99 times) of the daily limit value and was the only monitoring station that did not comply with the annual limit value of 40 $\mu g/m^3$ during 2018.

Table 24. Annual mean concentration for NO_2, SO_2 and PM10 [$\mu g/m^3$], number of exceedances of daily limit values and efficiency of single sites. In bold the measurements exceeding the limit value

		NA01	**NA02**	**NA06**	**NA07**	**NA08**	**NA09**	**NA-PV**	**NA-VE**	**NA-PA**
NO_2	Annual mean	21.97	38.03	**44.47**	**56.69**	**45.53**	**45.38**	11.15	29.59	22.99
	Number of exceedances [a]	0	0	2	0	0	0	0	0	0
	Efficiency	93%	96%	94%	94%	95%	94%	92%	63%	90%
SO_2	Annual mean				1.12		6.03		0.92	4.73
	Number of exceedances [a,b]				0		0		0	0
	Efficiency				94%		84%		85%	86%
PM10	Annual mean	31.65	21.25	31.12	34.64	25.94	30.22	16.41		**44.63**
	Number of exceedances [b]	17	4	17	**40**	29	31	3		**99**
	Efficiency	93%	100%	99%	99%	94%	96%	84%		93%

[a] number of exceedances of 1-hour limit value; [b] number of exceedances of daily limit value

5.2.2 Shipping emissions

Following the methodology reported in Section 4, the total ship emissions of the Naples port estimated in 2018 are 5418 t/year for NOx, 193 t/year for SO_2, and 602 t/year for PM10.

The emissions evaluated in this study were compared with estimations based on the regression equations based on the tons of good for commercial ships and for the number of passengers in passenger ships reported in Chapter 4 based on data from several ports (Figure 45). The 2018 data on tons of goods handled and the number of passengers for Naples port were downloaded at https://adsptirrenocentrale.it/.

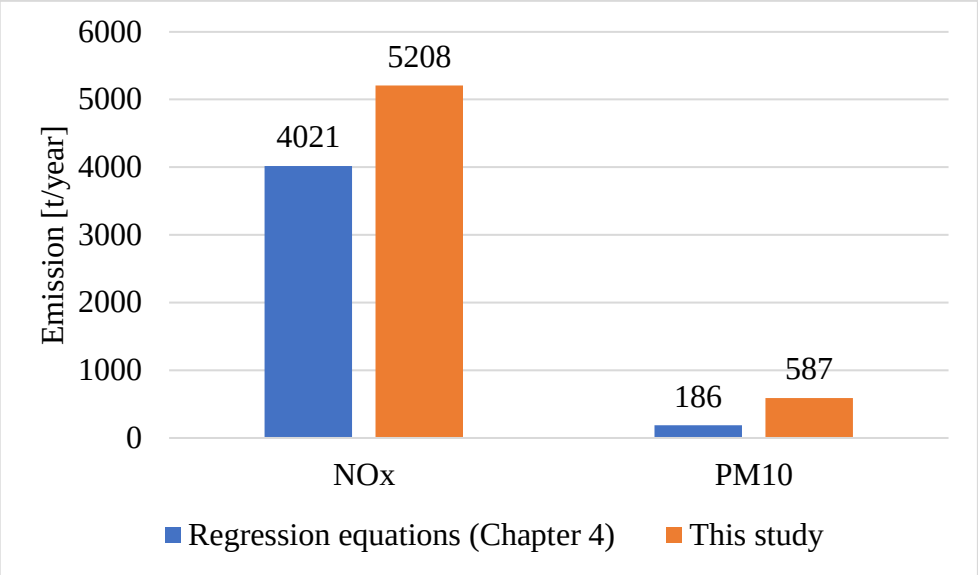

Figure 45. Comparison of NOx and PM10 emission estimated with the regression equation (Chapter 4) and the method adopted in this study

As can be seen, NOx annual emissions estimated are in sufficiently good agreement with those from the regression study. On the contrary, our estimation of PM10 is significantly higher with respect to that obtained by Chapter 4. In fact, the ratio of annual emissions in these regression equations is 1.3 for NOx and 3.2 for PM10. However, in both cases, the assessment of the impact of ship emissions is conservative.

In order to evaluate the importance of shipping emission respect other anthropogenic sources, the in-port and cruising estimated emissions of NOx, SO_2 and PM for 2018 were compared with the total national emissions reported on the "Disaggregazione dell'inventario nazionale 2015 performed by Istituto superiore per la protezione e la ricerca ambientale (ISPRA)". This report is the official inventory accounting of all anthropogenic (human-induced) emissions of greenhouse gases and other gases species such as NOx, SO_2 and PM in Italy and in particular in Naples area. In this report, emissions were estimated taking into account eleven large sectors (Combustion in the production and transformation of energy, non-industrial combustion plants, industrial combustion plants, industrial processes without combustion, extraction and distribution of fossil fuels and geothermal energy, use of solvents and other products, road transport, other mobile sources and machinery, waste treatment and disposal, agriculture and other sources and sinks).

Focused on the emission of transport sector, Figure 46 shows the comparison of total and in-port ship air pollutant emissions (NOx, SO_2 and PM) to the total national traffic emissions during 2015. As can be seen in Figure 46 for the NOx and PM10 the major sources is the road traffic (13744 t/year) followed by the marine sector (9608 t/year according to ISPRA and 5418 t/y according to the estimation in this study), for the SO_2, the major sources, as already known, is the maritime sector. The aviation sector is the least emission source among these, (1463 t/year for NOx, 106 t/year for SO_2 and 17 t/year for PM10).

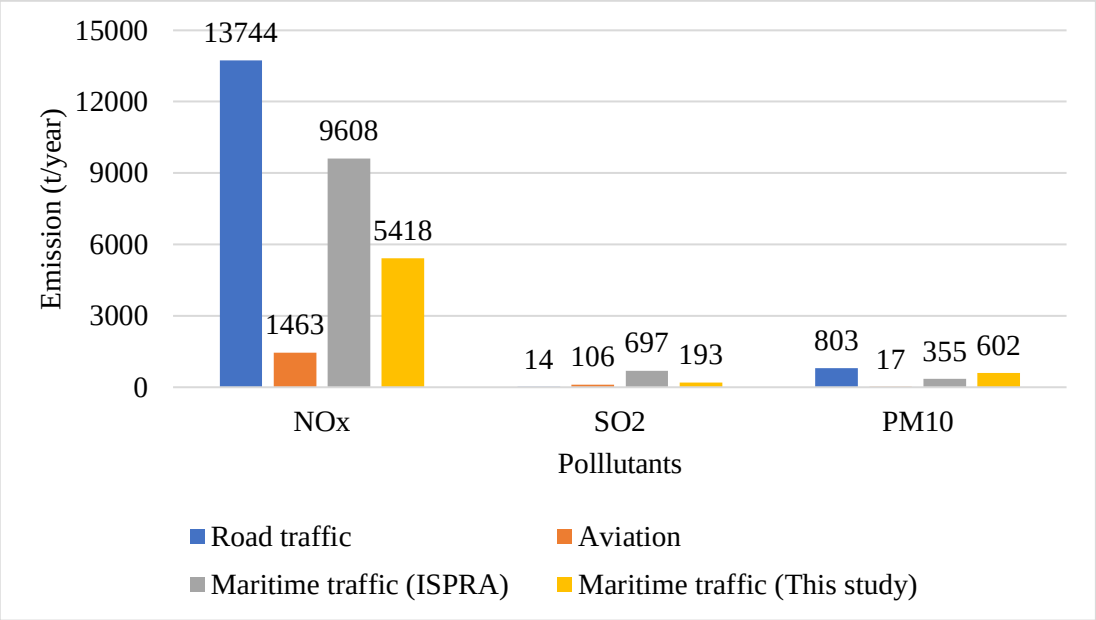

Figure 46. Shipping emissions contribution to the national emissions in 2015

Emissions during the hoteling phase represent about 95% of the total emissions, while about 5% is emitted during navigation in port. This result is in agreement with (Murena et al., 2018). The small contribution of emissions during navigation with respect to other ports (Papaefthimiou et al. 2016) depends on the small length of ship routes in the port of Naples.

The distribution of annual emissions for different ship types is shown in Figure 47. For NOx and SO_2, the passenger ships produce the greatest percentage of emissions (52-56%), followed by commercial ships (30-34%), tankers (9-10%), other ships (4-5%), and fishing ships (<1%). For PM10, the largest amount of emission is from commercial ships (52%), followed by passenger ships (33%), tankers (12%), and other ships (5%).

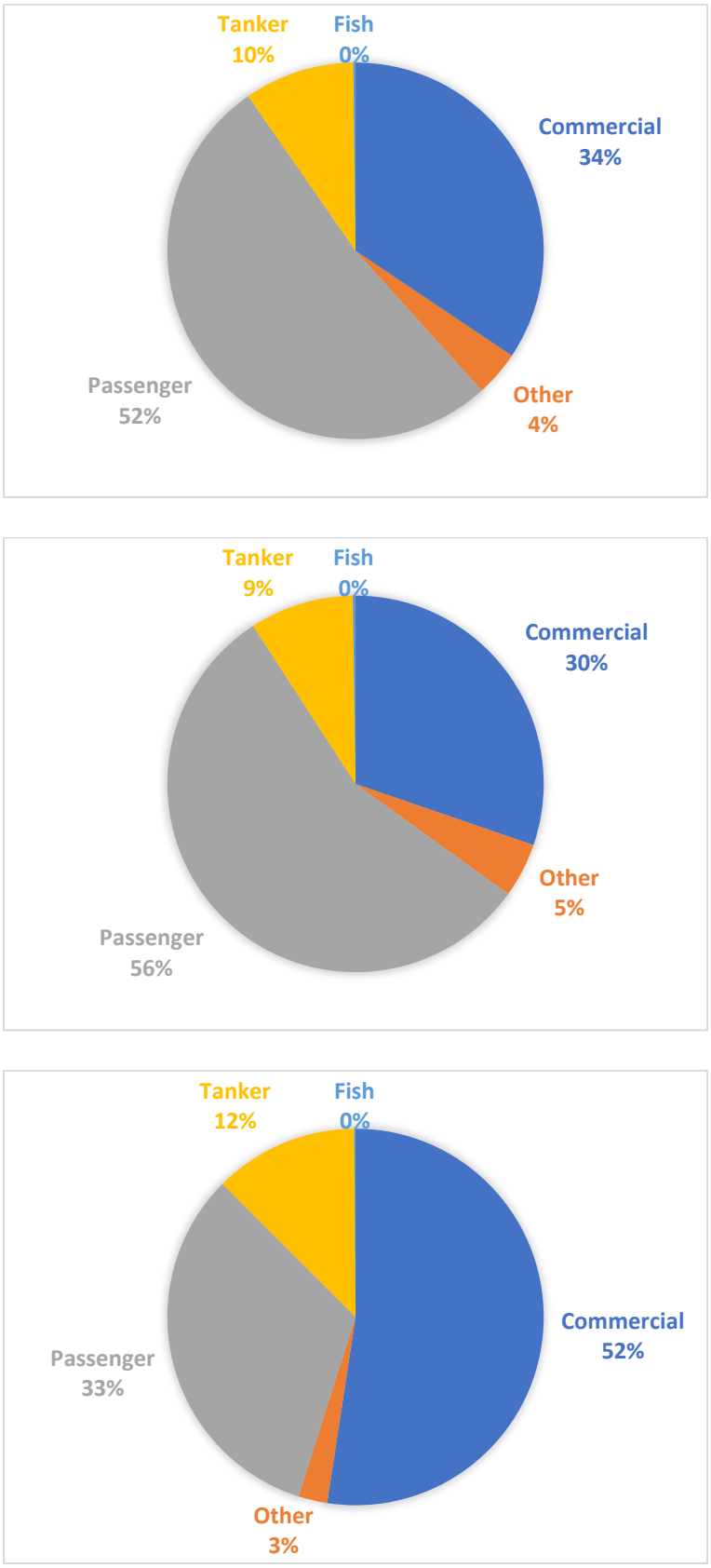

Figure 47. Ship types contribution to total emissions in the port of Naples during year 2018 up) NOx; center) SO_2; bottom) PM.

5.2.3 Meteorological data

From the results of CALMET meteorological simulation, data of wind speed, wind direction and temperature at ENEA Centre of Research (Portici) (Figure 44) for 2018 were extracted and were compared with the observations measured in the same point.

In Figure 48 is reported the comparison of the two wind rose, as can be seen the results are in good agreement.

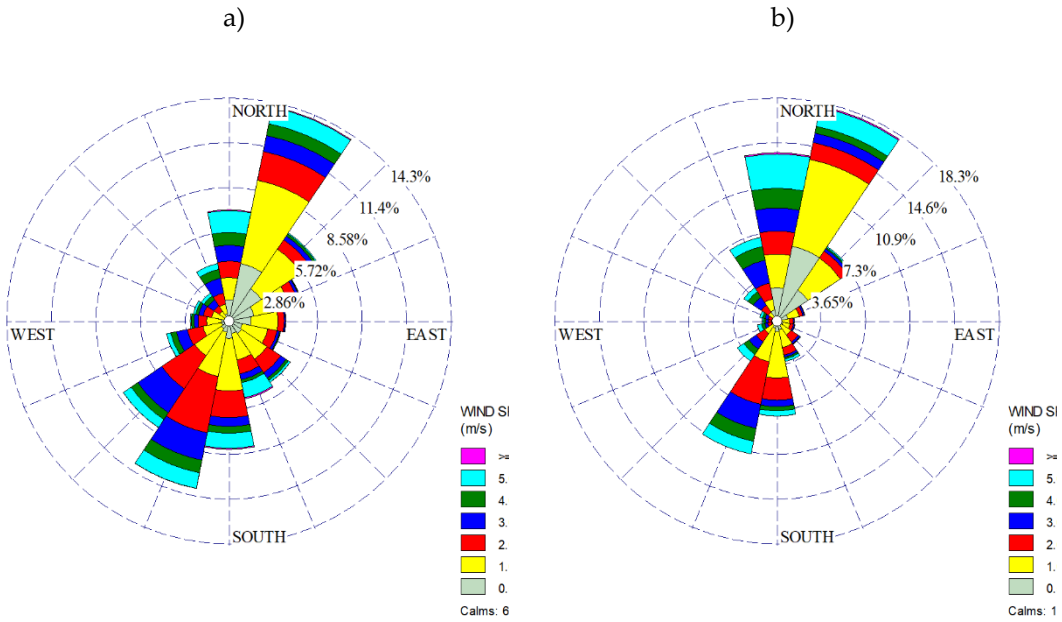

Figure 48. Comparison wind rose graphs: a) real data; b) result of CALMET simulation

Table 25. Correlation between real data and CALMET simulation result at ground level: statistical parameters

Parameter	BIAS	NMSE	CORR	FAC2	FB
Temperature	0.11	0.00	0.971	1.000	0.000
Wind speed	0.09	0.72	0.457	0.618	0.040
Wind Direction	2.62	0.79	0.165	0.505	0.017

To quantify the correspondence between the results of CALMET simulation and real data, the values of statistical parameters BIAS, NMSE, CORR, FAC2 and FB are reported in Table 25. FB quantifies the systematic bias while NMSE measures systematic bias and random scatter, providing a balance in evaluating the quality of numerical results. The FAC2 is highly robust as the effect that outliers have on it is

limited. The agreement is good. In fact, the performance measures (NMSE = 0; FAC2 = 1; FB = 0), reported in Chang and Hanna (2004), are all satisfied.

The wind rose of year 2018 (Figure 49) shows that winds blown predominantly from WNW (16.4 %) followed by South (13.1%) and East (10%). The range of most frequent velocities are 1-2 m/s (27%), 0.5-1 m/s (19.6%) and 2-3 m/s (17.1%).

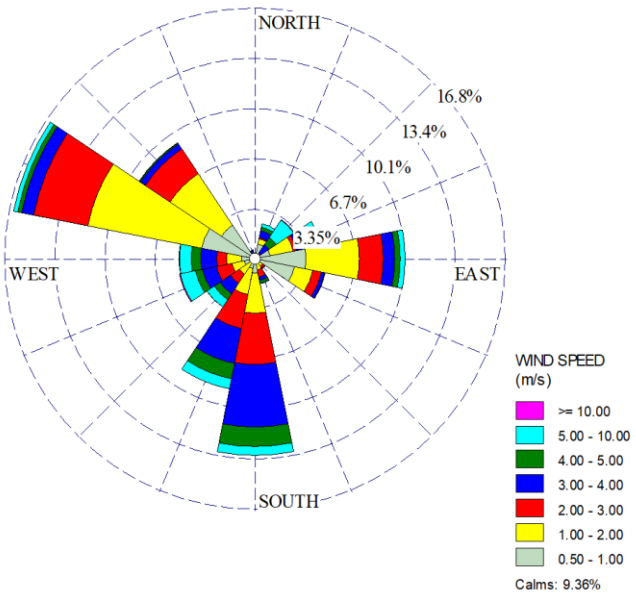

Figure 49. Wind rose of data of 2018 extracted at Airport of Naples "Capodichino"

5.2.4 Gaseous and particulate matter concentration

The contour maps of annual average concentration for NO_2, SO_2, primary PM10 (PPM10), secondary inorganic aerosols (SIA), and total PM (as a sum of PPM10 and SIA) are reported in Figure 50 and Figure 51. The area of maximum impact of all pollutants considered is inside the port area and near the industrial area east of the center of Naples. However, a portion of the urban area is also impacted. The impact of ship emissions decreases steeply at larger distances from the harbour.

NOx is mainly emitted as nitrogen oxide (NO); in this study, the NO_2 was considered to be 5% NOx as in the STEAM model (Jalkaneen et al, 2009). In the atmosphere, NO is quickly converted to NO_2 in reaction with ozone; thus, further from the source, atmospheric NOx is dominated by NO_2. A map of modeled annual mean atmospheric

concentrations of NO_2 over the Naples area is shown in Figure 50a. The annual concentration of NO_2 spatially averaged on the entire model domain is 3.3 μg/m^3 (5.7 μg/m^3 when considers the area in Figure 50a). Passenger ships contribute with 52%, followed by commercial ships (27%), tankers and other ships (12% and 9%, respectively), and fishing ships (<1%). The highest NO_2 contributions were found in the port area (Figure 50b).

The modeled SO_2 concentrations in Naples are relatively low (Figure 50b). The annual mean concentration of SO_2 spatially averaged on the entire model domain is about 0.1 μg/m^3 (0.16 μg/m^3 in the area considered in Figure 50b). The relative contribution of each ship category is similar to that of NO_2.

The concentration levels obtained in this study are much higher than those reported by Murena et al. (2018a) whose estimated maximum values of the annual concentrations of NO_2 and SO_2 were 4 and about 0.15 μg/m^3, respectively. In this study, the maximum concentrations of annual average of NO_2 and SO_2 were about 140 and 5 μg/m^3, respectively. The reason for this apparent discrepancy is due to the different ships considered in the two studies. In (Murena et al. 2018a) only cruise ship emissions during 2016 were considered; in this study, emissions from all ship categories visiting the port of Naples in 2018 are considered. However, it must be highlighted that the estimation of cruise ship emissions is also different. In fact, cruise ship emissions in Murena et al. (2018a) were 419 and 14 t/year for NOx and SO_2, respectively, whereas these values were estimated at 647 (NOx) and 25 t/year (SO_2) in this study. Despite a higher number of calls in 2016, the emissions of cruise ships with the new methodology considered in this study are about 1.5 times higher than the previous estimation. This difference can be attributed to the more accuracy-oriented procedure adopted in this study.

The results of SO_2 concentration in this study are comparable to results obtained by Merico et al. (2019). Those authors used the ADMS model to calculate a maximum annual average concentration of 5 μg/m^3.

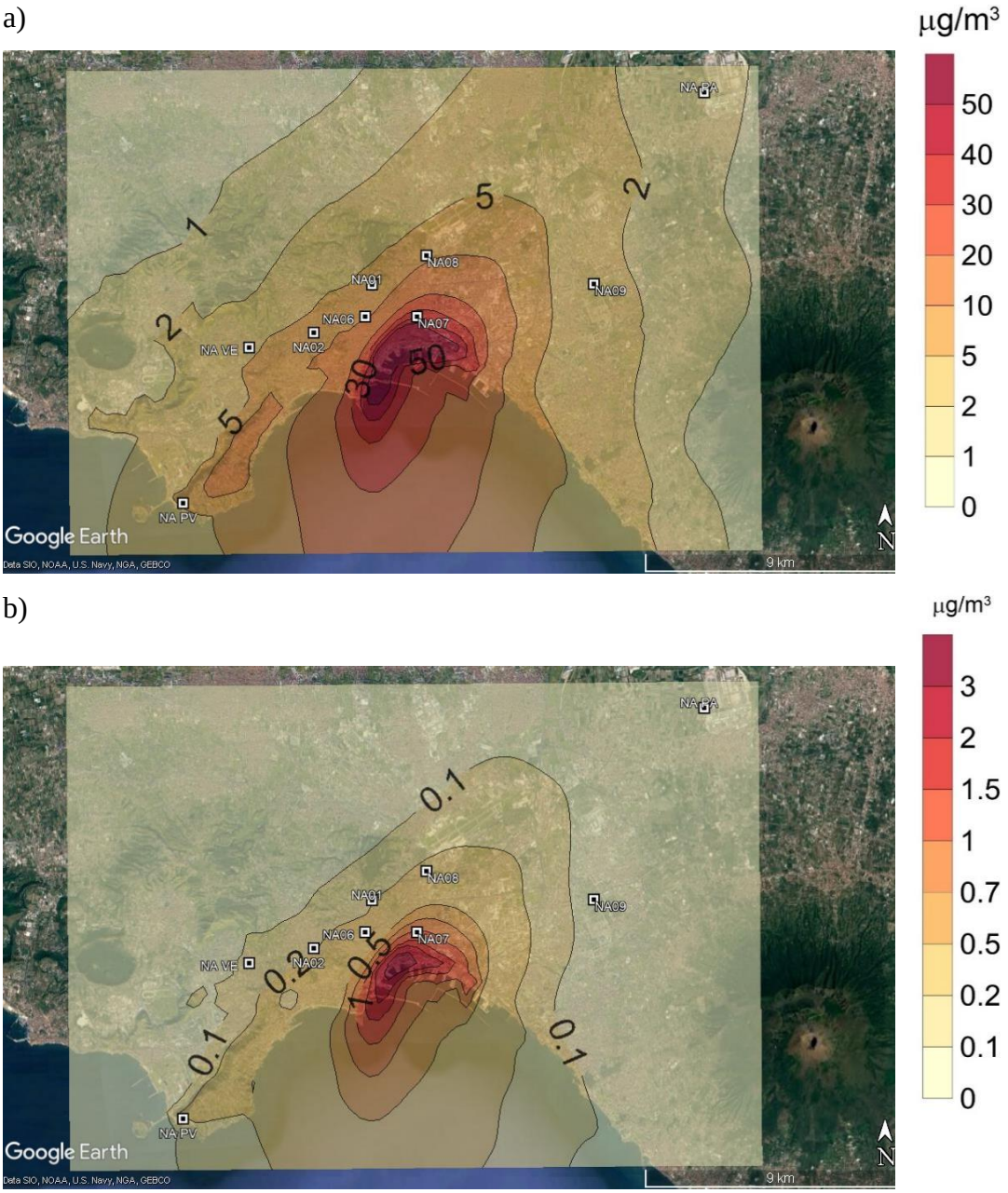

Figure 50. Simulations: maps of value of year average [µg/m^3]. a) NO_2 and b) SO_2

PM includes primary, directly emitted particles and secondary PM formed by chemical processes of emissions in the atmosphere. The secondary aerosol formation in CALPUFF is parameterized by RIVAD/ARM3 chemical schemes; it calculates the secondary particle formation, such as the formation of sulfate and nitrate following SO_2 and NO_2 oxidation. The maximum concentrations of primary PM (Figure 51a) are located inside the port area, and the maximum value is about 12 ug/m^3. Modeled secondary PM concentrations from shipping are given in Figure 51b. The secondary

PM, mainly formed far from the sources, tends to disperse and accumulate in the eastern part of Naples due to the prevailing wind directions. The concentrations of primary PM are comparable to concentrations calculated by Kuzu et al. (2020). In fact, the ground level concentration is 13.1 μg/m^3. Merico et al. (2019) calculated a maximum total PM10 concentration of 5 μg/m^3, which is lower than the PM10 calculated in this study by about 14 μg/m^3.

a)

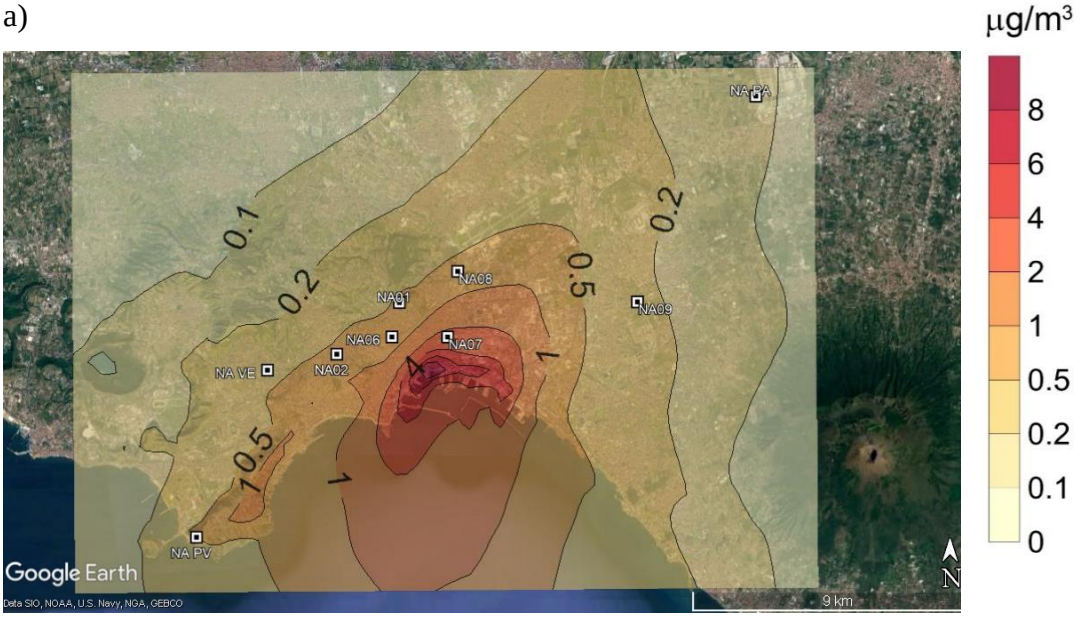

b)

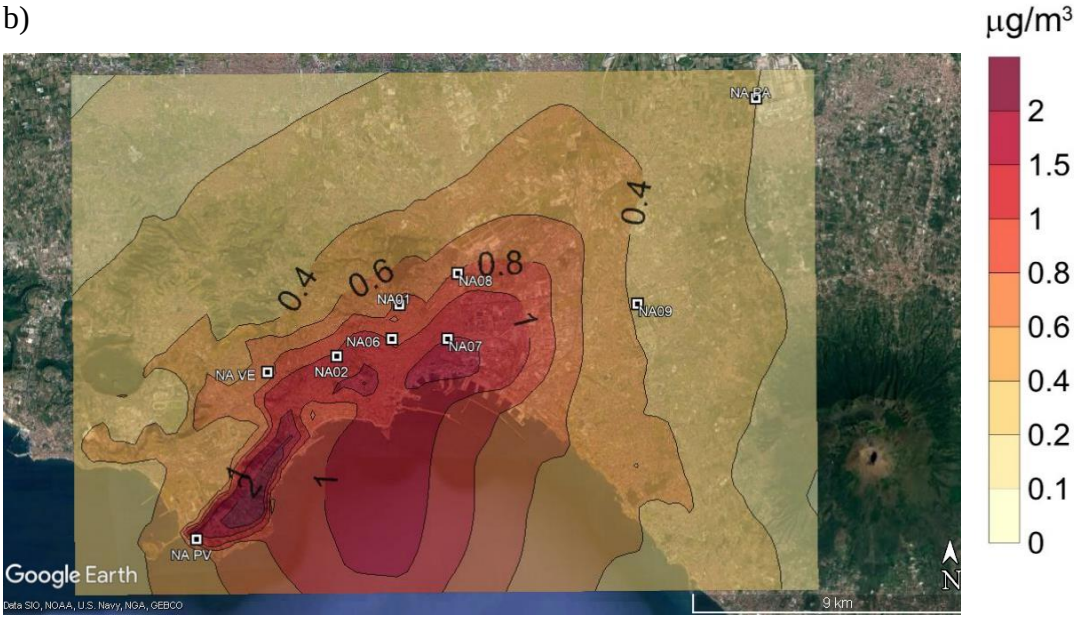

c)

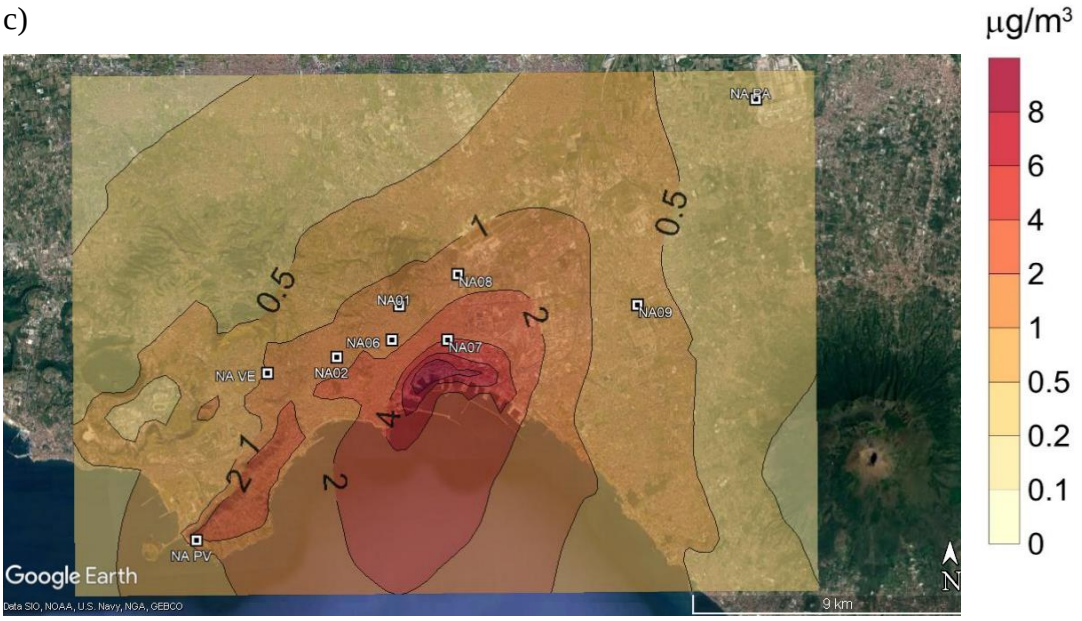

Figure 51. Simulations: maps of value of year average [µg/m^3]. a) primay PM10, b) secondary PM10 and c) total PM10

5.2.5 Impact on air quality

The relative impact of ship emissions (i.e. the ratio of concentration due to the ships obtained from simulations with measured concentration) was estimated in the location in which the monitoring stations were installed. Ground concentrations calculated by simulation models were compared with those obtained from air quality monitoring data, and the relative contribution was calculated by $C\% = {C_{Sim}}/{C_{Obs}}$, where C% is the percentage of ground concentration due to ship emissions; C_{Sim} is concentration simulated with CALPUFF and C_{Obs} is concentration obtained by air monitoring stations.

To obtain an indication of the contribution of ship emissions to long-term and short-term exposures to NO_2 and SO_2, annual averages and 98th percentiles of hourly averages obtained from the simulation results were compared with the air quality data measured at 9 NO2 and 4 SO_2 receptor points (Table 26).

Table 26. Contribution of ship emissions to hourly concentration levels measured at monitoring stations: annual mean and 98th percentiles of 1-hour averages of NO_2 and SO_2.

Monitoring station	**Percentage contribution of ship emissions**			
	NO_2		SO_2	
	Annual mean	98th percentile	Annual mean	98th percentile
NA01	27%	82%		
NA02	13%	54%		
NA06	20%	93%		
NA07	64%	>100%	92%	>100%
NA08	18%	58%		
NA09	6%	26%	1%	5%
NA-PV	33%	86%	11%	38%
NA-VE	10%	42%		
NA-PA	5%	23%	1%	3%

Table 26 shows how the contributions of ship emissions are greater for the receptors near the port area (NA07 and NA06, see Figure 44) and lower for receptors located far from the port area, as also confirmed by the ground concentration maps (Figure 50).

In fact, with respect to yearly averages, for NA07, which is closest to the port area, the modeled impact of shipping on NO_2 concentrations is responsible for 64% of the measured concentration, while at other stations in the city, the impact ranges from 6% to 33%. Far away to the Naples urban area at NA-PA, the contribution to the annual mean is 5%.

For SO_2, the annual mean concentration at NA07 is 92%. The very high contribution concentration is mainly due to the fact that the SO_2 is a pollutant emitted principally by the ships.

The contributions for the peak events (98th percentile) are greater than those for the annual mean. This effect was also observed by Murena et al. (2018). In some cases, the contribution is very high (>80%), and for NA07 it is greater than 100%. The latter is an unrealistic result and is an indication that the model overestimates the impact of ship emissions.

The overestimate of concentrations is probably due to a certain degree of overestimation in the calculation of emissions. In fact, as previously reported, the emission values calculated in this study are greater than the values estimated through the regressions by Chapter 4 (Figure 45). It is also possible that the model underestimates the dispersive properties of the atmosphere in some conditions

Simulation results for PPM10, SIA, and total PM10 were compared to air quality data from the ARPAC from eight measurement sites (Table 27). Regarding the annual mean concentrations, the highest contribution is shown in NA07 (7% for PPM10, 4% SIA, and 11% total PM10). As regards the other stations, the contributions in ranges of 1-2%, 2-7%, and 2-5% for PPM10, SIA, and total PM10, respectively were calculated. The contribution of ship emissions at the NA-PA station is relatively negligible, with a contribution of 1%.

Table 27. Contribution of ship emissions to concentration levels measured at monitoring stations: annual mean and 98th percentile for primary PM10, secondary PM10 and total PM10.

Monitoring station	**Percentage contribution of ship emissions**					
	PPM10		SIA		Total PM10	
	Annual mean	98th percentile	Annual mean	98th percentile	Annual mean	98th percentile
NA01	1%	3%	2%	5%	3%	8%
NA02	2%	4%	3%	7%	5%	10%
NA06	2%	4%	3%	6%	5%	11%
NA07	7%	11%	4%	10%	11%	18%
NA08	2%	3%	3%	5%	5%	7%
NA09	1%	1%	1%	2%	2%	3%
NA-PV	2%	4%	3%	6%	5%	9%
NA-PA	0%	0%	0%	1%	1%	1%

5.2.6 Seasonality variations

Regarding the effect of seasons on the impact of ship emissions, significant differences were found for all pollutants between winter (December, January, and February) and summer (June, July, and August) with the higher contributions of shipping emissions to the concentration levels registered during the summer period (warm season).

The average NO_2 concentration calculated over the entire domain in summer is 3.12 $\mu g/m^3$ (5.51 $\mu g/m^3$ if it considered the urban area near the port area), while in winter the average concentration is 2.83 $\mu g/m^3$ (4.83 $\mu g/m^3$). For SO_2, on the other hand, an average concentration of 0.09 $\mu g/m^3$ (0.16 $\mu g/m^3$) was calculated for the warm season and 0.08 $\mu g/m^3$ (0.13 $\mu g/m^3$) for the cold season. This is correlated to the fact that ship emissions of NOx and SO_2 are higher in the summer season with respect to the winter.

The seasonal difference for primary PM is less evident. In fact, the average concentration over the entire domain is 0.27 $\mu g/m^3$ in summer and 0.24 $\mu g/m^3$ in winter (0.47 $\mu g/m^3$ vs. 0.41 $\mu g/m^3$ if it considered the port area), and the difference calculated for the SIA—0.36 $\mu g/m^3$ (0.55 $\mu g/m^3$) and 0.18 $\mu g/m^3$ (0.28 $\mu g/m^3$)—for summer and winter, respectively, is much higher.

Table 28 shows the average contributions for all the receptors considered, for all pollutants, for the winter and the summer. On average, the contribution of NO_2 pollution in winter is 13%, while in summer there is a contribution of 27%. When NA-PA monitoring site was excluded because it is far away from the port area, the contribution increases from 14% in winter to 29% in summer. For NA07, there is a 29% contribution of NO_2 in winter and an 85% contribution in summer. For SO_2, there is an average contribution of 24% in winter and 36% in summer, without considering the NA-PA site. It is important to note that, for NA07, the contribution of SO_2 increases from 60% in winter to 100% in summer. This is also true for primary PM10, SIA, and total PM10, with a contribution of 2% in winter and 3% in summer for primary PM10, 2% in winter and 4% in summer for SIA, and 3% in winter and 7% in summer for total PM10. This pattern seems to be related to the increase in ship traffic during summer due to the improved meteorological conditions that allow for improved navigation, which increases traffic and subsequently emissions and atmospheric pollution. The

calculated average increases in emissions in summer compared to winter were 17%, 18%, and 16%, respectively, for NOx, SO_2, and PM10.

Table 28. Contribution of ship emissions to concentration levels measured at monitoring stations for winter and summer season for NO_2, SO_2, primary PM10, secondary PM10 and total PM10.

Monitoring stations	**Seasonal percentage contribution of ship emissions**									
	Winter					Summer				
	NO_2	SO_2	PPM10	SIA	Total PM10	NO_2	SO_2	PPM10	SIA	Total PM10
NA01	14%		1%	1%	2%	34%		1%	2%	4%
NA02	11%		2%	3%	4%	15%		2%	4%	6%
NA06	11%		2%	2%	3%	23%		2%	3%	5%
NA07	29%	60%	3%	1%	4%	85%	100%	10%	6%	16%
NA08	7%		1%	1%	2%	27%		4%	6%	10%
NA09	4%	1%	1%	1%	1%	7%	3%	1%	2%	3%
NA PV	29%	11%	3%	3%	6%	29%	6%	1%	3%	5%
NA VE	9%					12%				
NA PA	4%	1%	0%	0%	0%	4%	0%	0%	0%	1%

6. Conclusion and perspectives

The final objective of this thesis is to assess the impact of the in-port ship emissions on the air quality of the urban area of Naples, with 2018 calendar year as period of study.

According to the results, total estimated emissions for NOx, SO_2, and PM10 were 5418, 193, and 602 t/year, respectively. Emissions during the hoteling phase represent about 95% of the total emissions, while about 5% is emitted during the navigation in port. In other ports emissions at hoteling represent about 90% of total emissions. The higher value estimated in this thesis can be due to the short length of in-port routes in the case of Naples. For NOx and SO_2, the passenger ships produce the greatest percentage of emissions (52-56%), followed by commercial ships (30-34%), tankers (9-10%), other ships (4-5%), and fishing ships (<1%). Slightly different for PM10, the largest amount of emission is from commercial ships (52%), followed by passenger ships (33%), tankers (12%), and other ships (5%).

The contribution of shipping emissions to air quality has been assessed comparing the results of the CALPUFF simulations with the air quality data measured by the regional network of fixed monitoring stations. The area of maximum impact of all pollutants considered is inside the port area and near the industrial area east of the center of Naples. However, a portion of the urban area is also impacted. The impact of ship emissions decreases steeply at larger distances from the harbour. The contributions calculated to annual mean concentration are in the range of 5-64% for NO_2, 1-92% for SO_2, and 1-11% for total PM10 (as the sum of primary PM10 and SIA), in dependence of the distance of the emission sources. The highest contribution of three pollutants (64% for NO_2, 92% for SO_2 and 11% for total PM10) is observed at NA07 station, which is about 2 km far from the port area. While at other stations in the city located between 2 to 15 km from the port area, the impact of NO_2 ranges from 6% to 33%, 1-11% for SO_2 and 3-5% for total PM10. At distance of 15 km far away to the Naples urban area at station NA-PA, the contribution to the annual mean are 5%, 1% and 1% for NO_2, SO_2 and PM10 respectively. The calculated contributions to peak short-term averaged concentrations obtained by comparing results of the 98th percentile of 1-hour or 24-hour averages are greater than those of the yearly average values. This confirms

results of previous studies and indicates a possibly more significant contribution of ship emissions to peak-values events. However, these results could be overestimated. In fact, the contribution calculated for the 98th percentiles of 1-hour averages of NO_2 and SO_2 is higher than 100% at station NA07. The overestimation of the impact may be due to both an overestimation in the calculation of emissions or to an underestimation of the dispersive properties of the atmosphere in some conditions. Therefore, also the percentage of contribution of annual average assessed could be overestimated.

Finally, the contributions to pollutants concentrations in winter (December, January and February) and summer (June, July and August) were analyzed. The results show that the ship emission contribution is higher in summer that during winter. In fact, on average, the contribution to NO_2 at selected fixed receptors at air quality stations in winter was 13%, while in summer it was 27%. For SO_2, the average contribution was 24% in winter and 36% in summer; for total PM10, it was 3% in winter and 7% in summer. This is due to the higher ship traffic during summer. In fact, an emission increment of 17%, 18%, and 16%, respectively, for NOx, SO_2, and PM10 from summer to winter was calculated.

Other important result of this thesis is the contribution to the current state of the art of scientific research in terms of: i) estimation of ship emissions during the various phases of activity in the port; ii) reliability of CALPUFF model to simulate the dispersion of atmospheric pollutants in an area characterized by the presence of buildings.

About the first point, a detailed emission inventory for ships in the Naples port in 2018 based on satellite AIS data was created developing a bottom-up procedure that starts from the activity of individual ships in the port and leads to the creation of a complete inventory of emissions. The AIS data used include more than one million records associated with 922 objects. AIS messages provide static information (MMSI number, type, and length) and dynamic information (the ship's position, i.e. latitude and longitude, course over ground (COG), speed over ground (SOG), and UTC. As first step an overall 141 elements were deleted (84,965 records, equal to 7.95% of the total records) because they correspond to stationary objects or to ships lacking adequate information and are not relevant for the purpose of the analysis.

An annual calendar with 70917 records was generated using a MATLAB code. The detailed articulation of the AIS data allowed the subsequent accurate estimation of emissions. For an accurate estimation of the emission rates, a database of 777 different ships visiting the port of Naples in 2018 was created.

Not all records contain all the mandatory information for calculating the emission rates (10.55% of the missing data for the installed power on board and 5.72% for the maximum speed). To fill in the missing data, regressions based on real data were adopted for each category. The EMEP/EEA reference guidelines updated to 2019 have been adopted for the calculation of the NOx, SO_2 and PM emission rates. The NOx, SO2, PM calculated for the navigation and hotelling phases as a function of the total power show that the emissions increase as the total power increases for all three pollutants. Emissions during navigation phase are always greater than their respective emissions during the hotelling phase, because during the navigation phase, propulsion beyond the auxiliary services during navigation should be guaranteed.

In order to determine the height above sea level, 46 general arrangement plans were collected. The height of the upper side of the funnel on the baseline and the design depth were measured. An empirical process for the estimation of the diameters of the funnels was developed. The heights of the funnels calculated are in the range of 10 – 50 m and the diameters are between 1 – 4.5 m.

The AIS data was also used for the definition of the port route for each ship. From a total of 75 piers present in the port of Naples, for each category of ship, similar routes have been identified on the same pier, defining a total of 37 piers and routes.

The second point of this thesis concerned the validation and optimization of the CALPUFF dispersion model by means of a physical model (Wind tunnel) and a computational model (CFD). The first step of this validation process was a comparison between the results of the wind tunnel and those of the CFD. The two models showed a very good agreement. In particular, the agreement was better considering UR = 1 rather than UR = 4 as demonstrated by the statistical indices: NMSE = 0.17 (UR = 1) against 0.29 (UR = 4) and CORR coefficient = 0.931 (UR = 1) against 0.920 (UR = 4). The second step was to analyze three different CALPUFF configurations in order to verify the reliability of the building's downwash module and the parameterization

of the plume diffusion. The cases examined are: Case 1, the dispersion coefficients are estimated as a function of the standard deviations of the wind speed and the parameters of the horizontal and vertical Lagrangian time scales, Case 2, adopting the downwash module of the building, Case 3, the building downwash option was activated and the dispersion coefficients were directly estimated using the wind tunnel measurements of the speed standard deviation as input data. The performance of the CALPUFF model in the three cases was evaluated. The performance was developed with two comparisons. In the first one the calculation domain is divided into three different subdomains: port area, open area and street canyons. In this case CALPUFF Case 3 provides the best fit of the wind tunnel results. In the second comparison, to better analyse the behaviour of the CALPUFF model as a function of the height of the receptor, the results obtained from wind tunnel experiments and CALPUFF are divided into two groups: measurement points below the average roof-top level ($z < 30$ m); and measurement points above the roof-top level ($z > 30$ m). When $z < 30$ m, the differences between the three different configurations of CALPUFF are not relevant. Instead, for $H > 30$ m the Case 3 formulation of CALPUFF shows the best performance. The best agreement between CALPUFF, wind tunnel measurements and CFD data is obtained when adopting the building downwash module and using direct velocity wind tunnel measurements as input data for the dispersion coefficients. Even adopting this model set-up, CALPUFF shows a systematic tendency to underestimate the time-averaged concentration at ground level. At a low value of the velocity ratio (funnel gas velocity/wind speed) UR=1, the percentage of underestimation is about 54%. When UR=4, the percentage of underestimation decreases to 17%. The results show for an accurate assessment of the impact on the urban area of atmospheric pollutants emitted by ship funnels when ships are moored, the use of a Gaussian model such as CALPUFF can be conveniently coupled with wind tunnel or CFD simulations. This approach improves the performance of the operational Gaussian model and reduces the uncertainty in the numerical predictions. Moreover, the importance to know the exit velocity of the fumes, a parameter which is usually poorly documented has been shown.

As future perspectives, due to the lack of the wind velocity and wind direction measurements in the port of Naples, it would be very useful to install a meteorological

station in the port area, releasing data in continuous. Information about wind velocity and wind direction in the port area could be used to evaluate the statistical velocities associated to the lower frequency fluctuations. This information can be used to extend the wind tunnel parameterization to the real case. Furthermore, it would also possible the validation of a dispersion model through specific monitoring campaigns

References

Alver, F., Saraç, B.A., S¸ahin, Ü.A., 2018. Estimating of shipping emissions in the Samsun port from 2010 to 2015. Atmos. Pollut. Res. 9 (5), 822–828.

Andersson, C.; Bergström, R.; Johansson, C. Population exposure and mortality due to regional background PM in Europe— Long-term simulations of source region and shipping contributions. Atmos. Environ. 2009, 43, 3614–3620.

APICE, 2013. Common Mediterranean Strategy and Local Practical Actions for the Mitigation of Port, Industries and Cities Emissions. http://www.apice-project. eu/img_web/pagine/files/Publication/Final%20Publication.pdf.

Aulinger, A., Matthias, V., Zeretzke, M., Bieser, J., Quante, M., & Backes, A. (2016). The impact of shipping emissions on air pollution in the greater North Sea region–Part 1: Current emissions and concentrations. Atmospheric Chemistry & Physics, 16(2).

Badeke, R., Matthias, V., & Grawe, D. (2020). Parameterizing the vertical downward dispersion of ship exhaust gas in the near-field. Atmospheric Chemistry and Physics Discussions, 1-27. (https://doi.org/10.5194/acp-2020-753)

Barregård, L.; Molnár, P.; Jonson, J.-E.; Stockfelt, L. Impact on population health of Baltic shipping Emissions. Int. J. Environ. Res. Public Health 2019, 16, 1954.

Berechman, J., Tseng, P.H., 2012. Estimating the environmental costs of port related emissions: the case of Kaohsiung. Transp. Res. D Transp. Environ. 17 (1), 35–38.

Bloemsma L.D., Wijga A.H., Klompmaker J.O., Janssen N.A., Smit H.A., Koppelman G.H., Brunekreef B., Lebret E., Hoek G., Gehring U., (2019), The associations of air pollution, traffic noise and green space with overweight throughout childhood: The PIAMA birth cohort study, Environmental Research, 169, 348-356.

Boselli, A., de Marco, C., Mocerino, L., Murena, F., Quaranta, F., Rizzuto, E., Sannino, A., Spinelli, N., Xuan, W., 2019. Evaluating LIDAR sensors for the survey of emissions from ships at harbor. In: The 14th International Symposium on Practical Design of Ships and Other Floating Structures 22-26 September, Yokohama, Japan.

Brandt, J.; Silver, J.D.; Christensen, J.H.; Andersen, M.S.; Bønløkke, J.H.; Sigsgaard, T.; Geels, C.; Gross, A.; Hansen, A.B.; Hansen, K.M.; et al. Contribution from the ten major emission sectors in Europe and Denmark to the health-cost externalities of air pollution using the EVA model system—An integrated modelling approach. Atmos. Chem. Phys. 2013, 13, 7725–7746.

Broome, R.A., Cope, M.E., Goldsworthy, B., Goldsworthy, L., Emmerson, K., Jegasothy, E., Morgan, G.G., 2016. The mortality effect of ship-related fine particulate matter in the Sidney greater metropolitan region of NSW, Australia. Environ. Int. 87, 85e93. https://doi.org/10.1016/j.envint.2015.11.012.

Buhaug, Ø., Corbett, J. J., Endresen, Ø., Eyring, V., Faber, J., Hanayama, S., ... & Mjelde, A. (2009). Second imo ghg study 2009. International Maritime Organization (IMO) London, UK, 20.

CAIMANs, 2015. Cruise and Passenger Ship Air Quality Impact Mitigation Actions. June. http://www.medmaritimeprojects.eu/section/caimans.

Chang, J. C., Hanna, S. R. (2004). Air quality model performance evaluation. Meteorology and Atmospheric Physics, 87(1-3), 167-196. https://doi.org/10.1007/s00703-003-0070-7

Chen, D., Wang, X., Nelson, P., Li, Y., Zhao, N., Zhao, Y., Lang, J., Zhou, Y., Guo, X., 2017. Ship emission inventory and its impact on the PM 2.5 air pollution in Qingdao Port, North China. Atmos. Environ. 166, 351–361.

Chen, D., Zhao, N., Lang, J., Zhou, Y., Wang, X., Li, Y., ... & Guo, X. (2018). Contribution of ship emissions to the concentration of PM2. 5: A comprehensive study using AIS data and WRF/Chem model in Bohai Rim Region, China. Science of the Total Environment, 610, 1476-1486.

Chen, D., Zhao, Y.H., Nelson, P., Li, Y., Wang, X.T., Zhou, Y., Lang, J.L., Guo, X.R., 2016. Estimating ship emissions based on AIS data for port of Tianjin, China. Atmos. Environ. 145, 10–18.

Coello, J., Williams, I., Hudson, D.A., Kemp, S., 2015. An AIS-based approach to calculate atmospheric emissions from the UK fishing fleet. Atmos. Environ. 114, 1e7. https:// doi.org/10.1016/j.atmosenv.2015.05.011.

Cohen, A. J., Brauer, M., Burnett, R., Anderson, H. R., Frostad, J., Estep, K., ... & Forouzanfar, M. H. (2017). Estimates and 25-year trends of the global burden of disease attributable to ambient air pollution: an analysis of data from the Global Burden of Diseases Study 2015. The Lancet, 389(10082), 1907-1918.

Contini, D., & Merico, E. (2021). Recent Advances in Studying Air Quality and Health Effects of Shipping Emissions. Atmosphere, 12(1), 92.

Contini, D., Gambaro, A., Belosi, F., De Pieri, S., Cairns, W. R. L., Donateo, A., ... & Citron, M. (2011). The direct influence of ship traffic on atmospheric PM2. 5, PM10 and PAH in Venice. Journal of Environmental Management, 92(9), 2119-2129.

Cooper, D., Gustafsson, T., 2004. Methodology for calculating emissions from ships: 1. Update of Emission Factors Available at: https://www.diva-portal.org/smash/get/ diva2:1117198/FULLTEXT01.pdf.

Corbett, J.J., Fischbeck, P.S., 1997. Emissions from ships. Science 278 (5339), 823–824.

Corbett, J.J., Fischbeck, P.S., Pandis, S.N., 1999. Global nitrogen and sulfur inventories for oceangoing ships. J. Geophys. Res. 104 (D3), 3457–3470. https://doi.org/ 10.1029/1998jd100040.

Corbett, J.J., Koehler, H.W., 2003. Updated emissions from ocean shipping. J. Geophys. Res. 108 https://doi.org/10.1029/2003JD003751.

Corbett, J.J., Koehler, H.W., 2004. Considering alternative input parameters in an activity-based ship fuel consumption and emissions model: reply to comment by Øyvind Endresen et al. on "Updated emissions from ocean shipping". J. Geophys. Res. D Atmos. 109, 1e8. https://doi.org/10.1029/2004JD005030.

Corbett, J.J., Winebrake, J.J., Green, E.H., Kasibhatla, P., Eyring, V., Lauer, A., 2007. Mortality from ship emissions: a global assessment. Environ. Sci. Technol. 41 (24), 8512–8518. https://doi.org/10.1021/es071686z.

De Melo Rodríguez, G., Martin-Alcalde, E., Murcia-Gonzalez, J.C., Saurí, S., 2017. Evaluating air emission inventories and indicators from cruise vessels at ports WMU. J. Marit. Aff. https://doi.org/10.1007/s13437-016-0122-8.2017.

Deniz, C., & Kilic, A. (2010). Estimation and assessment of shipping emissions in the region of Ambarlı Port, Turkey. Environmental progress & sustainable energy, 29(1), 107-115.

Dobaradaran S., Geravandi S., Goudarzi G., Idani E., Salmanzadeh S., Soltani F., Yari A.R., Mohammadi M.J., (2016), Determination of cardiovascular and respiratory diseases caused by PM10 exposure in Bushehr, 2013, Journal of Mazandaran University of Medical Sciences, 26, 42-52.

Dobrucalı, E., & Ergin, S. (2012). A study of exhaust smoke dispersion for a generic frigate. Gemi ve Deniz Teknolojisi Dergisi, 192, 16-22.

Dragovic, B., Tzannatos, E., Tselentis, V., Mestrovic, R., Skuric, M., 2018. Ship emissions and their externalities in cruise ports. Transp. Res. D Transp. Environ. 61, 289–300. https://doi.org/10.1016/j.trd.2015.11.007.

EMEP/EEA, 2016. International Maritime Navigation, International Inland Navigation, National Navigation (Shipping), National Fishing, Military (Shipping), and Recreational Boats.

EMEP/EEA, 2019. International Maritime Navigation, International Inland Navigation, National Navigation (Shipping), National Fishing, Military (Shipping), and Recreational Boats.

Endresen, Ø., Sørgård, E., Behrens, H.L., Brett, P.O., Isaksen, I.S.A., 2007. A historical reconstruction of ships fuel consumption and emissions. J. Geophys. Res. 112, D12301. https://doi.org/10.1029/2006JD007630.

Endresen, Ø., Sørgård, E., Sundet, J.K., Dalsøren, S.B., Isaksen, I.S.A., Berglen, T.F., Gravir, G., 2003. Emission from international sea transportation and environmental impact. J. Geophys. Res. Atmos. 108 https://doi.org/10.1029/2002JD002898 n/ aen/a.

Entec, 2002. Quantification of Emissions from Ships Associated with Ship Move-Ments between Ports in the European Community. A Report for the, EuropeanCommission, Northwich, UK. Final Report.

Entec, 2005. Service Contract on Ship Emissions; Assignment, Abatement and MArket- Based Instruments, a Report for the European Commission.

EPA, Environmental Protection Agency, 2000. Analysis of Commercial Marine Vessels Emissions and Fuel Consumption Data. Office of Transportation and Air Quality U.S., 420-R-00–002.

Ergin, S., & Dobrucalı, E. (2014). Numerical modeling of exhaust smoke dispersion for a generic frigate and comparisons with experiments. Journal of Marine Science and Application, 13(2), 206-211.

Eyring, V., Isaksen, I., Berntsen, T., Collins, W., Corbett, J., Endresen, O., Grainger, R., Moldanova, J., Schlager, H., Stevenson, D., 2009. Transport impacts on atmosphere and climate: shipping. Atmos. Environ. 44, 4735e4771. https://doi.org/10.1016/j. atmosenv.2009.04.059.

Eyring, V., Koehler, H.W., van Aardenne, J., Lauer, A., 2005. Emission from internationalshipping: 1. The last 50 years. J. Geophys. Res. 110 (D17305).

Fackrell JE (1980). A flame ionisation detector for measuring fluctuating concentration. J Phys E Sci Instrum 13:888–893

Gariazzo, C., Papaleo, V., Pelliccioni, A., Calori, G., Radice, P., & Tinarelli, G. (2007). Application of a Lagrangian particle model to assess the impact of harbour, industrial and urban activities on air quality in the Taranto area, Italy. Atmospheric Environment, 41(30), 6432-6444.

GBD 2016 Risk Factors Collaborators, 2017, 'Global, regional, and national comparative risk assessment of 84 behavioural, environmental and occupational, and metabolic risks or clusters of risks, 1990-2016: a systematic analysis for the Global Burden of Disease Study 2016', Lancet 390(10100), pp. 1345-1422 (https://doi.org/10.1016/S0140-6736(17)32366-8).

Gobbi, G. P., Di Liberto, L., & Barnaba, F. (2020). Impact of port emissions on EU-regulated and non-regulated air quality indicators: The case of Civitavecchia (Italy). Science of The Total Environment, 719, 134984.

Hadei M., Shahsavani A., Krzyzanowski M., Querol X., Stafoggia M., Nazari S.S.H., Jafari A.J., Yarahmadi M., Kermani M., Khosravi A., (2020), Burden of mortality attributed to PM2.5 exposure in cities of Iran; contribution of short-term pollution peaks, Atmospheric Environment, 224, 117365.

Hanna, S. R. (1968). A method of estimating vertical eddy transport in the planetary boundary layer using characteristics of the vertical velocity spectrum. Journal of the Atmospheric Sciences, 25(6), 1026-1033.

Hanna, S. R. (1981) Lagrangian and eulerian time-scale relations in the daytime boundary layer. Journal of Applied Meteorology, 20 (3), 242–249.

Hanna, S. R. (1984). Applications in air pollution modeling. In Atmospheric turbulence and air pollution modelling (pp. 275-310). Springer, Dordrecht.

Hanna, S., Chang, J. (2012). Acceptance criteria for urban dispersion model evaluation. Meteorology and Atmospheric Physics, 116(3-4), 133-146.

Hoek, G., Krishnan, R. M., Beelen, R., Peters, A., Ostro, B., Brunekreef, B., & Kaufman, J. D. (2013). Long-term air pollution exposure and cardio-respiratory mortality: a review. Environmental health, 12(1), 1-16.

ICF, 2005. Best Practices in Preparing Port Emission Inventories: Draft for Review, Prepared for Office of Policy, Economics and Innovation.

IMO, 1997. International Convention for the Prevention of Pollution from Ships MARPOL 73/78: the Regulations for the Prevention of Air Pollution from Ships (Annex VI). IMO, London.

IMO, 2016a. Marine Environment Protection Committee (MEPC), 70th Session, 24-28 October 2016. IMO, London.

IMO, 2016b. Methanol as Marine Fuel: Environmental Benefits, Technology Readiness, and Economic Feasibility. IMO, London.

IMO, 2016c. Studies on the Feasibility and Use of LNG as a Fuel for Shipping. IMO, London

IMO, MARINE ENVIRONMENT PROTECTION COMMITTEE, 2010. Designation of an Emission Control Area for Nitrogen, Oxides Sulfur Oxides and Particulate Matter. Interpretations of and Amendments to MARPOL and Related Instruments 61st Session.

Irwin HPAH (1981) The design of spires for wind simulation J Wind Eng Ind Aerod 7(3):361-366.

ISPRA, 2018. Italian Emission Inventory 1990-2016. Informative Inventory Report 2018 Rapporti 284/2018, ISBN 978-88-448-0891-4.

J. Ciencewicki I. Jaspers (2008). Air Pollution and Respiratory Viral Infection. International Forum for Respiratory Research

Jalkanen, J.-P., Brink, a., Kalli, J., Pettersson, H., Kukkonen, J., Stipa, T., 2009. A modelling system for the exhaust emissions of marine traffic and its application in the Baltic Sea area. Atmos. Chem. Phys. Discuss. 9 https://doi.org/10.5194/acpd-9-15339-2009, 15339e15373.

Jalkanen, J.P., Johansson, L., Kukkonen, J., 2014. A comprehensive inventory of the ship traffic exhaust emissions in the Baltic Sea from 2006 to 2009. Ambio 43, 311e324. https://doi.org/10.1007/s13280-013-0389-3.

Jalkanen, J.P., Johansson, L., Kukkonen, J., Brink, A., Kalli, J., Stipa, T., 2012. Extension of an assessment model of ship traffic exhaust emissions for particulate matter and carbon monoxide. Atmos. Chem. Phys. 12, 2641e2659.

Jiménez J (2004) Turbulent flows over rough walls. Annu Rev Fluid Mech 36:173–196.

Jonson, J.; Jalkanen, J.; Johansson, L.; Gauss, M.; Denier van der Gon, H. Model calculations of the effects of present and future emissions of air pollutants from shipping in the Baltic Sea and the North Sea. Atmos. Chem. Phys. 2015, 15, 783–798.

Jonson, J.E.; Gauss, M.; Jalkanen, J.-P.; Johansson, L. Effects of strengthening the Baltic Sea ECA regulations. Atmos. Chem. Phys. 2019, 19, 13469–13487.

Jorgensen FE (2002) How to measure turbulence with hot-wire anemometers - a practical guide. Technical report, Dantec Dynamics.

Kelishadi, R., & Poursafa, P. (2010). Air pollution and non-respiratory health hazards for children. Archives of Medical Science: AMS, 6(4), 483.

Kentair, 2013. Samsun Hava Kalitesi Degerlendirme Raporu: Kentlerde Hava Kalitesi Degerlendirme Sisteminin Geistirilmesi Projesi, G2G11/TR/6/2. https://www.csb. gov.tr/db/cygm/editordosya/SAMSUN.pdf.

Khaefi M., Geravandi S., Hassani G., Yari A.R., Soltani F., Dobaradaran S., Moogahi S., Mohammadi M.J.,Mahboubi M., Alavi N., (2017), Association of particulate matter impact on prevalence of chronic obstructive pulmonary disease in Ahvaz, southwest Iran during 2009-2013, Aerosol and Air Quality Research, 17, 230-237.

Kilic, A., Deniz, C., 2010. Inventory of shipping emissions in Izmit Gulf, Turkey. Environ. Prog. Sustain. Energy 29. https://doi.org/10.1002/ep, 221e232.

Kilic, A., Tzannatos, E., 2014. Ship emissions and their externalities at the container terminal of Piraeus e Greece. Int. J. Environ. Res. 8, 1329e1340. https://doi.org/ 10.1016/j.atmosenv.2009.10.024.

Klepac P., Locatelli I., Korošec S., Künzli N., Kukec A., (2018), Ambient air pollution and pregnancy outcomes: A comprehensive review and identification of environmental public health challenges, Environmental Research, 167, 144-159.

Kulkarni PR, Singh SN, Seshadri V. Study of exhaust smoke ingress into GT intake on ships MAHY-06. In: Int conference on marine hydrodynamics, NSTL, Visakhapatnam (India), January 2006.

Kulkarni, P. R., Singh, S. N., & Seshadri, V. (2007). Parametric studies of exhaust smoke–superstructure interaction on a naval ship using CFD. Computers & fluids, 36(4), 794-816.

Kuzu, S. L., Bilgili, L., & Kiliç, A. (2020). Estimation and dispersion analysis of shipping emissions in Bandirma Port, Turkey. Environment, Development and Sustainability, 1-21.

Liu, H., Fu, M., Jin, X., Shang, Y., Shindell, D., Faluvegi, G., Shindell, C., He, K., 2016a. Health and climate impacts of ocean-going vessels in East Asia. Nat. Clim. Chang. 6 (11), 1037.

Liu, H.; Fu, M.; Jin, X.; Shang, Y.; Shindell, D.; Faluvegi, G.; Shindell, C.; He, K. Health and climate impacts of ocean-going vessels in East Asia. Nat. Clim. Chang. 2016, 6, 1037–1041.

Liu, Z., Lu, X., Feng, J., Fan, Q., Zhang, Y., Yang, X., 2016. Influence of ship emissions on urban air quality: a comprehensive study using highly time-resolved online measurements and numerical simulation in Shanghai. Environ. Sci. Technol. 51 (1), 202–211.

Lonati, G., Cernuschi, S., & Sidi, S. (2010). Air quality impact assessment of at-berth ship emissions: Case-study for the project of a new freight port. Science of the Total Environment, 409(1), 192-200.

Maragkogianni, A., Papaefthimiou, S., 2015. Evaluating the social cost of cruise ships air emissions in major ports of Greece. Transp. Res. D Transp. Environ. 36, 10–17.

Maragkogianni, A., Papaefthimiou, S., Zopounidis, C., 2016. Mitigating Shipping Emissions in European Ports: Social and Environmental Benefits, p. 1e9.

Marelle, L., Thomas, J. L., Raut, J. C., Law, K. S., Jalkanen, J. P., Johansson, L., ... & Weinzierl, B. (2016). Air quality and radiative impacts of Arctic shipping emissions in the summertime in northern Norway: from the local to the regional scale.

Menter F. R., and Egorov, Y., The scale-adaptive simulation method for unsteady turbulent flow predictions. Part I. Theory and model description, Flow, Turbul. Combust. 85, 113 (2010). https://doi.org/10.1007/s10494-010-9264-5.

Merico, E., Dinoi, A., & Contini, D. (2019). Development of an integrated modelling-measurement system for near-real-time estimates of harbour activity impact to

atmospheric pollution in coastal cities. Transportation Research Part D: Transport and Environment, 73, 108-119.

Merico, E., Donateo, A., Gambaro, A., Cesari, D., Gregoris, E., Barbaro, E., ... & Contini, D. (2016). Influence of in-port ships emissions to gaseous atmospheric pollutants and to particulate matter of different sizes in a Mediterranean harbour in Italy. Atmospheric environment, 139, 1-10.

Merico, E., Gambaro, A., Argiriou, A., Alebic-Juretic, A., Barbaro, E., Cesari, D., ... & Giannaros, C. (2017). Atmospheric impact of ship traffic in four Adriatic-Ionian port-cities: comparison and harmonization of different approaches. Transportation Research Part D: Transport and Environment, 50, 431-445.

MINENV, April 2009. Annual Inventory Submission under the Convention and the Kyoto Protocol for Greenhouse and Other Gases for the Years 1990-2007. http://unfccc.int/national_reports/annex_i_ghg_inventories/national_inventories_submissions/ite ms/4771.php.

Miola, A., Ciuffo, B., 2011. Estimating air emissions from ships: meta-analysis of modelling approaches and available data sources. Atmos. Environ. 45, 2242–2251.

Moreno-Gutierrez, J., Calderay, F., Saborido, N., Boile, M., Valero, R.R., Dur_an-Grados, V., 2015. Methodologies for estimating shipping emissions and energy consumption: a comparative analysis of current methods. Energy 86, 603–616.

Morris, R.E., Kessler, R.C., Douglas, S.G., Styles, K.R., Moore, G.E., 1988. Rocky Mountain Acid Deposition Model Assessment: Acid Rain Mountain Mesoscale Model (ARM3). Atmospheric Sciences Research Laboratory, San Rafael, CA.: Systems Applications, Inc., US EPA, Research Triangle Park, NC

Murena, F., Mele, B., & Toscano, D. (2018a). Using a CFD model to assess the impact of cruise ship emissions on the façades of waterfront buildings in Naples, Italy. WIT Transaction on Ecology and the Environment, 230, 189-197.

Murena, F., Mele, B., 2014. Effect of short-time variations of wind velocity on mass transfer rate between street canyons and the atmospheric boundary layer. Atmos. Pollut. Res. 5, 484e490

Murena, F., Mele, B., 2016. Effect of balconies on air quality in deep street canyons. Atmos. Pollut. Res. 7, 1004e1012.

Murena, F., Mocerino, L., Quaranta, F., & Toscano, D. (2018b). Impact on air quality of cruise ship emissions in Naples, Italy. Atmospheric Environment, 187, 70-83.

Murena, F., Prati, M. V., & Quaranta, F. (2018c). Assessment of the impact of ship emissions on the air quality in Naples. Soares, Guedes, Teixeira (Eds.), Maritime Transportation and Harvesting of Sea Resources. Taylor & Francis Group, London ISBN, 978-0.

Ng, S.K.W., Loh, C., Lin, C., Booth, V., Chan, J.W.M., Yip, A.C.K., Li, Y., Lau, A.K.H., 2013. Policy change driven by an AIS-assisted marine emission inventory in Hong Kong and the Pearl River Delta. Atmos. Environ. 76, 102e112. https://doi.org/ 10.1016/j.atmosenv.2012.07.070.

Nironi C, Salizzoni P, Marro M, Mejean P, Grosjean N, Soulhac L (2015) Dispersion of a passive scalar fluctuating plume in a turbulent boundary layer. Part I: velocity and concentration measurements. Boundary-Layer Meteorology 156(3):415-446.

Nunes, R. A., Alvim-Ferraz, M., Martins, F. G., Calderay-Cayetano, F., Durán-Grados, V., Moreno-Gutiérrez, J., ... & Sousa, S. I. (2020). Shipping emissions in the Iberian Peninsula and the impacts on air quality. Atmospheric Chemistry and Physics, 20(15), 9473-9489.

Nunes, R.A.O., Alvim-Ferraz, M.C.M., Martins, F.G., Sousa, S.I.V., 2017a. Assessment of shipping emissions on four ports of Portugal. Environ. Pollut. 231, 1370e1379.

Nunes, R.A.O., Alvim-Ferraz, M.C.M., Martins, F.G., Sousa, S.I.V., 2017b. The activity based methodology to assess ship emissions e a review. Environ. Pollut. 231, 87e103. https://doi.org/10.1016/j.envpol.2017.07.099.

Pallis, A.A., Vaggelas, G.K., 2018. Cruise shipping and green ports: a strategic challenge. In: Monios, J., Bergqvist, R. (Eds.), In Green Ports: Inland and Seaside Sustainable Transportation Strategies. Edward Elgar, Cheltenham, pp. 255–273.

Panofsky, H. A., Tennekes, H., Lenschow, D. H., & Wyngaard, J. C. (1977). The characteristics of turbulent velocity components in the surface layer under convective conditions. Boundary-Layer Meteorology, 11(3), 355-361.

Papaefthimiou, S., Maragkogianni, A., Andriosopoulos, K., 2016. Evaluation of cruiseships emissions in the Mediterranean basin: the case of Greek ports. Int. J. Sustain. Transp. https://doi.org/10.1080/15568318.2016.1185484,00e00, 8318.

Peisley, T., 2014. End of the beginning for cruising. Colchester: Seatrade Commun.

Perez, H.M., Chang, R., Billings, R., Kosub, T.L., 2009. Automatic identification systems (AIS) data use in marine vessel emission estimation. In: 18th Annual International Emission Inventory Conference, vol. 14, p. e17.

Poplawski, K., Setton, E., McEwen, B., Hrebenyk, D., Graham, M., & Keller, P. (2011). Impact of cruise ship emissions in Victoria, BC, Canada. Atmospheric Environment, 45(4), 824-833.

Prati, M. V., Costagliola, M. A., Quaranta, F., & Murena, F. (2015). Assessment of ambient air quality in the port of Naples. Journal of the Air & Waste Management Association, 65(8), 970-979.

Ramacher, M. O. P., Matthias, V., Aulinger, A., Quante, M., Bieser, J., & Karl, M. (2020). Contributions of traffic and shipping emissions to city-scale NOx and PM2. 5 exposure in Hamburg. Atmospheric Environment, 237, 117674.

Ramacher, M.O.P.; Tang, L.; Moldanová, J.; Matthias, V.; Karl, M.; Fridell, E.; Johansson, L. The impact of ship emissions on air quality and human health in the Gothenburg area—Part II: Scenarios for 2040. Atmos. Chem. Phys. Discuss. 2020, 20, 10667–10686.

RCP, 2016, Every breath we take: The lifelong impact of air pollution, Working Party Report, Royal College of Physicians, London (https://www.rcplondon.ac.uk/ projects/outputs/every-breath-we-take-lifelongimpact-air pollution)

Saraçoglu, H., Deniz, C., Kiliç, A., 2013. An investigation on the effects of ship sourced emissions in Izmir port, Turkey. Sci. World J. 2013 https://doi.org/10.1155/2013/ 218324.

Sarvi, A., Fogelholm, C.J., Zevenhoven, R., 2008. Emissions from large-scale mediumspeed diesel engines: 1. Influence of engine operation mode and turbo-charger. Fuel Process. Technol. 89, 510e519. https://doi.org/10.1016/j.fuproc.2007.10.006.

Sarvi, A., Fogelholm, C.J., Zevenhoven, R., 2008. Emissions from large-scale mediumspeed diesel engines: 2. Influence of fuel type and operating mode. Fuel Process. Technol. 89, 520e527. https://doi.org/10.1016/j.fuproc.2007.10.005.

Saxe, H., Larsen, T., 2004. Air pollution from ships in three Danish ports. Atmos. Environ. 38 (24), 4057–4067.

Scire, J. S., Strimaitis, D. G., & Yamartino, R. J. (2000). A user's guide for the CALPUFF dispersion model. Earth Tech, Inc, 521, 1-521.

Skjølsvik, K.O., Andersen, A.B., Corbett, J.J., Skjelvik, J.M., 2000. Study of Greenhouse Gas Emissions from Ships (Report to International Maritime Organization on the Outcome of the IMO Study on Greenhouse Gas Emissions from Ships), MEPC 45/8. MARINTEK Sintef Group/Carnegie Mellon Univ., Center for Economic Analysis/Det Norske Veritas, Trondheim, Norway.

Smith, T.W.P., Jalkanen, J.-P., Anderson, B.A., Corbett, J.J., Faber, J., Hanayama, S., O'Keeffe, E., Parker, S., Johansson, L., Aldous, L., Raucci, C., Traut, M., Ettinger, S., Nelissen, D., Lee, D.S., Ng, S., Agrawal, A., Winebrake, J.J., Hoen, M., Chesworth, S., Pandey, A., 2015. Third IMO GHG Study 2014. InternationalMaritime Organization (IMO), London, UK. Available from: http://www.imo.org/en/OurWork/Environme nt/PollutionPrevention/AirPollution/, 2014.

Sofiev, M.; Winebrake, J.J.; Johansson, L.; Carr, E.W.; Prank, M.; Soares, J.; Vira, J.; Kouznetsov, R.; Jalkanen, J.-P.; Corbett, J.J. Cleaner fuels for ships provide public health benefits with climate tradeoffs. Nat. Commun. 2018, 9, 406.

Song, S., 2014. Ship emissions inventory, social cost and eco-efficiency in Shanghai Yangshan port. Atmos. Environ. 82, 288e297. https://doi.org/10.1016/j. atmosenv.2013.10.006.

Sówka I., Nych A., Kobus D., Bezyk Y., Zathey M., editors., (2019), Analysis of exposure of inhabitants of Polish cities to air pollution with particulate matters with application of statistical and geostatistical tools, E3S Web of Conferences, 100, 00075.

Starcrest Consulting Group, 2005. Port of Log Angeles Inventory of Air Emissions (2005).

Starcrest Consulting Group, 2005. Port of Long Beach Air Emissions Inventory (2005).

Tang, L., Ramacher, M. O., Moldanová, J., Matthias, V., Karl, M., Johansson, L., ... & Gustafsson, M. (2020). The impact of ship emissions on air quality and human health in the Gothenburg area–Part 1: 2012 emissions. Atmospheric Chemistry and Physics, 20(12), 7509-7530.

Tennekes, H., & Lumley, J. L. (1972). A first course in turbulence MIT Press Cambridge.

Tichavska, M., Tovar, B., 2015a. port-city exhaust emission model: an application to cruise and ferry operations in Las Palmas port. Transp. Res. A Policy Pract. 78, 347–360.

Tichavska, M., Tovar, B., 2015b. Environmental cost and eco-efficiency from vessel emissions in Las Palmas Port. Transp. Res. Part E: Logist. Transp. Rev. 83, 126–140.

Tichavska, M., Tovar, B., Gritsenko, D., Johansson, L., Jalkanen, J.P., 2017. Air emissions from ships in port: does regulation make a difference? Transp. Policy. https://doi. org/10.1016/j.tranpol.2017.03.003 (in press).

Tominaga, Y., & Stathopoulos, T. (2016). Ten questions concerning modeling of near-field pollutant dispersion in the built environment. Building and Environment, 105, 390-402.

Tominaga, Y., Mochida, A., Yoshie, R., Kataoka, H., Nozu, T., Yoshikawa, M., & Shirasawa, T. (2008). AIJ guidelines for practical applications of CFD to pedestrian wind environment around buildings. Journal of wind engineering and industrial aerodynamics, 96(10-11), 1749-1761. https://doi.org/10.1016/j.jweia.2008.02.05

Toscano D., Marro M., Mele B., Murena F. and Salizzoni P. Physical and numerical models of atmospheric urban dispersion of pollutants. In: Proceedings of the 20th International Conference on Computational Science and Its Applications. ICCSA 2020- Lecture Notes in Computer Science, Springer

Toscano D., Mele B., Murena F. A CFD model to assess the impact of cruise ship emissions in the port of Naples. ITM 2019-37th International technical meeting on air pollution modelling and its application. 23-27 September 2019, Katholische Akademie, Hamburg, Germany.

Toscano, D., & Murena, F. (2019). Atmospheric ship emissions in ports: A review. Correlation with data of ship traffic. Atmospheric Environment: X, 4, 100050.

Trozzi, C., & De Lauretis, R. 2019. EMEP/EEA Air Pollutant Emission Inventory Guidebook 2019, European Environment Agency

Tzannatos, E., 2010. Ship emissions and their externalities for the port of Piraeus e Greece. Atmos. Environ. 44, 400e407.

UNCTAD, 2017. Review of Maritime Transport 2017.

UNCTAD, 2018. Review of Maritime Transport 2018. New York. October 2018. https://unctad.org/en/PublicationsLibrary/rmt2018_en.pdf.

Ünlügençoğlu, K., Yurtseven, A., & Alarçin, F. (2020). Shipping emission dispersions on the port of Ambarli via CFD modelling. Journal of Thermal Engineering, 6(2), 1-14.

van der Gon, H.D., Hulskotte, J., 2010. Methodologies for Estimating Shipping Emissions in the Netherlands Netherland Environmental Assessment Agency.

Viana, M.; Rizza, V.; Tobías, A.; Carr, E.; Corbett, J.; Sofiev, M.; Karanasiou, A.; Buonanno, G.; Fann, N. Estimated health impacts from maritime transport in the Mediterranean region and benefits from the use of cleaner fuels. Environ. Int. 2020, 138, 105670.

WHO, 2005, Effects of air pollution on children's health and development — A review of the evidence, World Health Organization, Regional Office for Europe, Copenhagen.

WHO, 2013a, Review of evidence on health aspects of air pollution — REVIHAAP Project, Technical Report, World Health Organization, Regional Office for Europe, Copenhagen.

WHO, 2014, Burden of disease from ambient air pollution for 2012 — Summary of results, World Health Organization(http://www.who.int/phe/health_topics/outdoorair/databases/AAP_BoD_results_March2014. pdf)

WHO, 2016, WHO expert consultation: Available evidence for the future update of the WHO Global air quality guidelines (AQGs), World Health Organisation Regional Office for Europe, Copenhagen, (http://www.euro.who.int/data/assets/pdffile/0013/301720/Evidencefuture-update-AQGs-mtg-report-Bonn-sept-oct-15.pdf?ua=1)

WHO, 2018a, 'WHO Global Ambient Air Quality Database (update 2018)', World Health Organization (https://www.who.int/airpollution/data/en/)

WHO, 2018b, Burden of disease from the joint effects of household and ambient air pollution for 2016, World Health Organization (http://www.who.int/airpollution/data/AP_joint_effect_BoD_results_May2018.pdf?ua=1)

Winebrake, J.J.; Corbett, J.J.; Green, E.H.; Lauer, A.; Eyring, V. Mitigating the health impacts of pollution from oceangoing shipping: An assessment of low-sulfur fuel mandates. Environ. Sci. Technol. 2009, 43, 4776–4782.

Winther, M., Christensen, J.H., Plejdrup, M.S., Ravn, E.S., Eriksson, Omar F., Kristensen, H.O., 2014. Emission inventories for ships in the arctic based on satellite sampled AIS data. Atmos. Environ. 91, 1e14. https://doi.org/10.1016/j. atmosenv.2014.03.006.

Wyngaard, J. C., Coté, O. R., & Rao, K. S. (1974). Modeling the atmospheric boundary layer. Advances in Geophysics, 18, 193-211.

Yang, D., Wu, L., Wang, S., Jia, H., & Li, K. X. (2019). How big data enriches maritime research–a critical review of automatic identification system (AIS) data applications. Transport Reviews, 39(6), 755-773.

Yau, P.S., Lee, S.C., Corbett, J.J., Wang, C., Cheng, Y., Ho, K.F., 2012. Estimation of exhaust emission from ocean-going vessels in Hong Kong. Sci. Total Environ. 431, 299e306.

Zetterdahl, M., Moldanova, J., Pei, X., Pathak, R.K., Demirdjian, B., 2016. Impact of the 0.1% fuel sulfur content limit in SECA on particle and gaseous emissions from marine vessels. Atmos. Environ. 145, 338–345.

Zhang, F., Chen, Y., Tian, C., Lou, D., Li, J., Zhang, G., Matthias, V., 2016. Emission factors for gaseous and particulate pollutants from offshore diesel engine vessels in China. Atmos. Chem. Phys. 16 (10), 6319–6334.

Zhang, Y., Yang, X., Brown, R., Yang, L., Morawska, L., Ristovski, Z., Fu, Q., Huang, C., 2017. Shipping emissions and their impacts on air quality in China. Sci. Total Environ. 581, 186–198.

Zhao, M., Zhang, Y., Ma, W., Fu, Q., Yang, X., Lia, C., Zhoua, B., Yua, Q., Chena, L., 2013. Characteristics and ship traffic source identification of air pollutants in China's largest port. Atmos. Environ. 64, 277–286.

Paper published in ISI Journals

Toscano, D., Marro, M., Mele, B., Murena, F., & Salizzoni, P. (2021). Assessment of the impact of gaseous ship emissions in ports using physical and numerical models: The case of Naples. Building and Environment, 107812.

Fattoruso, G., Nocerino, M., Toscano, D., Pariota, L., Sorrentino, G., Manna, V., ... & Di Francia, G. (2020). Site Suitability Analysis for Low Cost Sensor Networks for Urban Spatially Dense Air Pollution Monitoring. Atmosphere, 11(11), 1215.

Toscano, D., & Murena, F. (2020). The Effect on Air Quality of Lockdown Directives to Prevent the Spread of SARS-CoV-2 Pandemic in Campania Region—Italy: Indications for a Sustainable Development. Sustainability, 12(14), 5558.

Toscano, D., Marro, M., Mele, B., Murena, F., & Salizzoni, P. (2020, July). Physical and Numerical Models of Atmospheric Urban Dispersion of Pollutants. In International Conference on Computational Science and Its Applications (pp. 692-699). Springer, Cham.

Mocerino L., Murena F., Quaranta F., Toscano D. A methodology for the design of an effective air quality monitoring network in port areas. 2020. Scientific Reports 10 (1), 1-10

Toscano D., Murena F. Atmospheric ship emissions in ports: A review. Correlation with data of ship traffic. 2019. Atmospheric Environment: X 4, 100050

Murena F., Mocerino L., Quaranta F., Toscano D. Impact on air quality of cruise ship emissions in Naples, Italy. Atmospheric Environment Volume 187, August 2018, Pages 70-83.

Papers published in Conference Proceedings

Toscano, D., Murena, F., Salizzoni, P., & Marro, M. Impact of ship emissions on the urban pollution: An experimental study. 12th International Conference on Air Quality – Science and Application.

Toscano D., Mele B., Murena F., A CFD model to assess the impact of cruise ship emissions in the port of Naples. ITM 2019 - 37th International technical meeting on air pollution modelling and its application. 23 - 27 September 2019, Katholische Akademie, Hamburg, Germany.

Murena F., D'Ambrosio M.G.R., Toscano D. Assessment of air quality and analysis of representativeness of fixed stations from data of a regional air quality network. /th International Conference on Environmental Management, Engineering, Planning and Economics (CEMEPE 2019) and SECOTOX Conference.19 -24 May 2019. Mykonos, Greece.

Murena F., Mele B., Toscano D. A CFD model to assess the impact of cruise ship emissions on the facades of waterfront buildings in Naples. 26th International Conference on Modelling, Monitoring and Management of Air Pollution 19 - 21 June, 2018 Naples, Italy